

Distribution Agreement

In presenting this thesis or dissertation as a partial fulfillment of the requirements for an advanced degree from Emory University, I hereby grant to Emory University and its agents the non-exclusive license to archive, make accessible, and display my thesis or dissertation in whole or in part in all forms of media, now or hereafter known, including display on the world wide web. I understand that I may select some access restrictions as part of the online submission of this thesis or dissertation. I retain all ownership rights to the copyright of the thesis or dissertation. I also retain the right to use in future works (such as articles or books) all or part of this thesis or dissertation.

Signature:

Carlie Hoffman

Date

The synaptic vesicle glycoprotein 2C regulates vesicular dopamine transport

By

Carlie Anne Hoffman
Doctor of Philosophy

Graduate Division of Biological and Biomedical Science
Neuroscience

Dr. Gary Miller
Advisor

Dr. W. Michael Caudle
Committee Member

Dr. Victor Faundez
Committee Member

Dr. Ellen Hess
Committee Member

Dr. Malú Tansey
Committee Member

Accepted:

Lisa A. Tedesco, Ph.D.
Dean of the James T. Laney School of Graduate Studies

Date

The synaptic vesicle glycoprotein 2C regulates vesicular dopamine transport

By

Carlie Anne Hoffman
B.S., Florida State University, 2014

Advisor: Gary Wright Miller, PhD

An abstract of
A dissertation submitted to the Faculty of the
James T. Laney School of Graduate Studies of Emory University
in partial fulfillment of the requirements for the degree of
Doctor of Philosophy in
Graduate Division of Biological and Biomedical Science
Neuroscience
2018

Abstract

The synaptic vesicle glycoprotein 2C regulates vesicular dopamine transport

By Carlie Anne Hoffman

Regular packaging of dopamine into synaptic vesicles is required for the survival of dopamine neurons. Ineffective sequestration of dopamine leads to dopaminergic cell death and can contribute to neurodegenerative disease progression. Indeed, dopamine vesicle function is impaired in patients with Parkinson's disease (PD). Proper vesicle function relies on synaptic vesicle glycoprotein 2 (SV2), which facilitates responsiveness to Ca^{2+} and transports with synaptotagmin to the synapse. Further, the expression of one isoform in the SV2 family, SV2C, is enriched in dopaminergic brain regions and alterations in the expression of SV2C have been linked to PD. SV2C expression is disrupted in the basal ganglia of PD brain and variations in the human SV2C gene are correlated with responsiveness to levodopa and the protective effect of nicotine on PD risk. In the experiments described herein, I examined how alterations in SV2C expression mediate dopamine vesicle packaging. To this end, I developed a series of fluorescent *in vitro* assays to visualize vesicle packaging mediated by the dopamine-packaging protein the vesicular monoamine transporter 2 (VMAT2), and to measure changes in vesicle packaging arising from pharmacological, toxicological, and genetic manipulations. I first used a fluorescent plate reader assay to test a representative group of pharmacological compounds and environmental toxicants for their effect on vesicle function and dopamine packaging. I show significant reduction in vesicular storage of a dopamine analog after treatment with tetrabenazine, reserpine, methylphenidate, and methamphetamine, and modest reduction in vesicular storage after treatment with select pesticides and halogenated toxicants. Seeking to determine how SV2C affects dopamine vesicle function, I then used the plate reader assay to determine how SV2C expression affected vesicle packaging *in vitro*. I demonstrate SV2C expression leads to increased uptake of a dopamine analog. I then overexpressed SV2C in the substantia nigra of C57BL/6 mice and observed enhanced retention of dopamine over time and prolonged presence of dopamine in the synaptic cleft after electrically-stimulated release. These results identify SV2C as a mediator of dopamine vesicle packaging, retention, and release and indicate that SV2C represents an exciting target for further understanding and treating dopaminergic pathologies.

The synaptic vesicle glycoprotein 2C regulates vesicular dopamine transport

By

Carlie Anne Hoffman
B.S., Florida State University, 2014

Advisor: Gary Wright Miller, PhD

A dissertation submitted to the Faculty of the
James T. Laney School of Graduate Studies of Emory University
in partial fulfillment of the requirements for the degree of
Doctor of Philosophy in
Graduate Division of Biological and Biomedical Science
Neuroscience
2018

Acknowledgements

Getting a PhD is hard work. I knew that (at least I thought I knew that) as I started my PhD, but the full implications of how much work goes into getting a PhD has slowly sunk in over the last four and a half years. I definitely could not have completed this degree without tremendous help, love, and support. First and foremost, I want to thank God for getting me through graduate school. I could not have done this without His daily outpouring of grace, strength, and wisdom. My community of friends and mentors at my church have also been a continual source of encouragement, support, and prayer.

I want to thank my advisor, Dr. Gary Miller, for his mentorship during my time in his laboratory. The focus and direction of my thesis work changed numerous times before we finally settled on the story presented here, but Gary could always see the bigger picture (even when I couldn't) and strived to help me see what direction my research needed to move toward. I also want to thank my labmates for their companionship and always being willing and available to talk over my research (and my life in general): Rachel, you were my labmate and my roommate and I am so thankful for the laughter and fun you brought to my time in lab and for helping me edit this document; Amy and Kristen, you both set up this crazy project on SV2C that Gary decided I should pick up and I am thankful (though I wasn't when Gary first told me I needed to start researching SV2C) for all of the amazing work you both did to start figuring out what this protein does; Vrinda and Aimée, thank you for being willing to listen to me vent about my experiments and then calm me down after listening to my venting; and Kenny, we started our journey in the Miller lab together and I am glad that our research paths overlapped. I especially want to thank our lab manager, Josh Bradner, for his invaluable help in talking over research strategy and design, the spontaneous songs he would break into while in lab, and for being a good friend. Many thanks also go to our lab technician, Cheyenne Hurst, for the many, many hours she put into assisting me with surgeries and

slicing, staining, mounting, and imaging countless brains. I could not have gotten a good amount of this thesis work done without your help. I would also like to thank my committee members: Drs. Ellen Hess, Malú Tansey, Victor Faundez, and especially Michael Caudle, for their support, for helping me get back on track when I got lost in my experiments and missed the bigger picture of my thesis, and for being understanding as I navigated Gary's move to Columbia. I especially want to thank Mike for being willing to read my dissertation numerous times and for going above and beyond the typical committee member duties.

Last and definitely not least, I want to thank my family: mom, dad, Austin, and Spencer. I love you all so much and am so glad for the countless hours you have collectively spent listening to me talk over everything happening in lab. You have always been there for me through the many highs and lows of my time in the Miller lab and you have helped make me into the person I am today.

Table of Contents

Chapter 1- Introduction: Rationale, hypothesis, and scope	1
<i>Section I: Environmental and genetic contributors to Parkinson's disease</i>	
<i>pathogenesis</i>	<i>2</i>
Environmental exposures and Parkinson's disease	2
Genetic mutations and Parkinson's disease.....	3
Alpha-synuclein and Parkinson's disease pathology.....	5
<i>Section II: Vesicle handling and the dopamine system</i>	<i>6</i>
Synaptic vesicles: From vesicle pools to vesicle recycling.....	6
Monoamines, VMAT2, and dopamine handling	9
<i>Section III: The synaptic vesicle glycoprotein 2 C, dopamine, and</i>	
<i>Parkinson's disease</i>	<i>11</i>
Structure and function of the synaptic vesicle glycoprotein 2 (SV2).....	11
The synaptic vesicle glycoprotein 2 C (SV2C)	14
<i>Section IV: Rationale and hypothesis</i>	<i>15</i>
Rationale.....	15
Hypothesis and scope	15
Chapter 2- Assessing vesicular monoamine transport using false fluorescent	
neurotransmitters	21
<i>Abstract.....</i>	<i>22</i>
<i>Introduction</i>	<i>23</i>
<i>Materials and Methods</i>	<i>25</i>
<i>Results.....</i>	<i>28</i>
<i>Discussion.....</i>	<i>33</i>
Chapter 3- The role of SV2C in dopamine vesicle function	58
<i>Abstract.....</i>	<i>59</i>
<i>Introduction</i>	<i>60</i>
<i>Materials and Methods</i>	<i>62</i>
<i>Results.....</i>	<i>69</i>
<i>Discussion.....</i>	<i>74</i>
Chapter 4- Discussion, future directions, and concluding remarks.....	101
<i>Summary of findings</i>	<i>102</i>
<i>Working hypothesis of the mechanism of action of SV2C</i>	<i>103</i>
<i>Discussion of unexpected results</i>	<i>108</i>

<i>Future directions</i>	109
<i>Conclusion</i>	113
References	124
Appendix I- SV2C expression mediates alpha-synuclein pathology	150
<i>Abstract</i>	151
<i>Introduction</i>	152
<i>Materials and Methods</i>	154
<i>Results</i>	156
<i>Discussion</i>	159

List of Figures

Figure 1.1	Distribution of dopamine molecules in wildtype synaptic vesicles	18
Figure 1.2	Dopamine release in wildtype synaptic vesicles	20
Figure 2.1	FFN206 packaging is dependent on VMAT2 function and maintenance of the vesicular proton gradient	41
Figure 2.2	Quantification of FFN206 fluorescence	43
Figure 2.3	High-resolution imaging of FFN206 packaging	45
Figure 2.4	Real-time uptake of FFN206 in a single cell	47
Figure 2.5	Real-time uptake of FFN206	49
Figure 2.6	Determining optimal parameters for a FFN206 96-well plate assay	51
Figure 2.7	Validation of the optimal parameters for the FFN206 screening assay	53
Figure 2.8	Screening pharmacological inhibitors of VMAT2	55
Figure 2.9	Screening environmental toxicants for influence on VMAT2 function	57
Figure 3.1	Localization of in vitro expression of SV2C and pcDNA3.1	82
Figure 3.2	Validation of a quantifiable vesicular uptake assay under transfection with miniSOG-pcDNA	84
Figure 3.3	Validation of a quantifiable vesicular uptake assay under transfection with miniSOG-SV2C	86
Figure 3.4	In vitro overexpression of SV2C increases vesicle packaging	88
Figure 3.5	Immunofluorescent validation of viral injections of AAV2/9 mCherry	90
Figure 3.6	Immunofluorescent validation of viral injections of AAV2/9 miniSOG-SV2C	92
Figure 3.7	Overexpression of miniSOG-SV2C does not alter expression of other dopaminergic proteins	94

Figure 3.8	SV2C overexpression does not increase peak dopamine uptake	96
Figure 3.9	SV2C overexpression results in a trend toward increased vesicular retention of dopamine over time	98
Figure 3.10	SV2C overexpression does not affect the amount of dopamine released, but decreases the rate of dopamine clearance	100
Figure 4.1	Distribution of dopamine molecules in wildtype, SV2C-overexpressing, and SV2C-KO synaptic vesicles	116
Figure 4.2	Dopamine release in wildtype synaptic vesicles	118
Figure 4.3	Dopamine release in SV2C-overexpressing synaptic vesicles	120
Figure 4.4	Dopamine release in SV2C-KO animals	122
Table 4.1	SV2 expression and dopamine handling across genotypes	123
Figure A.1	Overexpression of SV2C in A53T-OE mice	165
Figure A.2	Overexpression of SV2C in A53T-OE mice reduces expression of total alpha-synuclein	167
Figure A.3	SV2C overexpression in A53T-OE mice decreases expression of total alpha-synuclein	169
Figure A.4	Overexpression of alpha-synuclein in SV2C-KO and SV2C-WT mice	171
Figure A.5	Overexpression of alpha-synuclein causes reduction in TH expression in SV2C-KO and SV2C-WT mice	173
Figure A.6	Quantification of protein expression resulting from overexpression of alpha-synuclein	175

Chapter 1- Introduction: Rationale, hypothesis, and scope

Section I: Environmental and genetic contributors to Parkinson's disease pathogenesis

Historically known as the shaking palsy, Parkinson's disease (PD) is characterized by resting tremors, bradykinesia, muscle stiffness, and a shortened, shuffling gait that arise from progressive degeneration of dopamine-producing neurons in the substantia nigra pars compacta (Lee and Gilbert 2016; Parkinson 1817; Shulman *et al.*, 2011). Currently, more than 10 million people worldwide have PD and approximately 60,000 Americans are diagnosed with PD each year. PD pathogenesis also includes the formation of Lewy bodies, aggregates of the protein alpha-synuclein (Spillantini *et al.*, 1997). PD symptomology includes a range of features that often predate the onset of motor symptoms, including olfactory deficits, sleep disturbances, gastrointestinal complications, and comorbidity with mood disorders such as depression and anxiety (Lee and Gilbert 2016; Rana *et al.*, 2015). PD was once thought to be caused exclusively by environmental factors; however, more recent research has identified there are also numerous genetic contributors to PD pathogenesis (Shulman *et al.*, 2011).

Environmental exposures and Parkinson's disease

Halogenated environmental chemicals such as polychlorinated biphenyls (PCBs), polybrominated biphenyls (PBBs), and polybrominated diphenyl ethers (PBDEs), have been associated with a variety of deleterious neurodevelopmental and neurodegenerative outcomes. Exposure to certain PBDE and PCB congeners disrupts the nigrostriatal dopamine system, potentially contributing to the development of PD (Caudle *et al.*, 2006; Hatcher-Martin *et al.*, 2012; Richardson and Miller 2004). Other environmental chemicals known to contribute to PD pathogenesis include exposure to heavy metals and pesticides such as manganese, dieldrin, rotenone, and paraquat (Ascherio *et al.*, 2006; Elbaz *et al.*, 2009; Freire and Koifman 2012; Goldman 2014; Nistico *et al.*, 2011; Richardson *et al.*, 2006; Semchuk *et al.*, 1992; Tanner *et al.*,

2011). Rotenone and paraquat exposures have been associated with PD in both humans and animal models (Bove and Perier 2012; Nistico *et al.*, 2011; Tanner *et al.*, 2011). Rotenone is a known inhibitor of mitochondrial complex I and exerts its toxicity by oxidizing mitochondrial proteins and causing oxidative stress that leads to cell death (Ramachandiran *et al.*, 2007; Sherer *et al.*, 2007). Similarly, paraquat exerts its toxicity predominantly through oxidative modification of cytosolic proteins, which causes oxidative stress and leads to cell death (Ramachandiran *et al.*, 2007; Wu *et al.*, 2017).

Alternately, caffeine consumption and cigarette smoking reduce risk for the development of PD. Caffeine consumption reduces PD risk by 30% and increased caffeine consumption decreases PD risk in a dose-dependent manner (Hernan *et al.*, 2002; Singh *et al.*, 2010). The neuroprotective effects of caffeine are thought to be driven by the interaction of caffeine with the A2a adenosine receptor and caffeine has been used in clinical trials for PD with modest success (Chen *et al.*, 2001; Postuma *et al.*, 2012). Smoking is the strongest environmental mediator of PD risk and reduces PD risk by approximately 50% (Godwin-Austen *et al.*, 1982; Grandinetti *et al.*, 1994). Nicotine is thought to be the agent underlying this neuroprotection: nicotine treatment attenuates dopaminergic cell loss resulting from treatment with 1-methyl-4-phenyl-1,2,3,6-tetrahydropyridine (MPTP) and 6-hydroxydopamine (Hernan *et al.*, 2001; Huang *et al.*, 2009; Parain *et al.*, 2003; Singh *et al.*, 2010).

Genetic mutations and Parkinson's disease

PD affects over 1% of the population above age 60, making aging the greatest risk factor for developing PD (Collier *et al.*, 2011; Driver *et al.*, 2009). However, 3-5% of patients with PD present with symptoms before the age of 60 and first-degree relatives of patients with PD have an increased risk of developing the disorder, underscoring the fact that PD risk and pathogenesis are

mediated by both environmental and genetic factors (Marder *et al.*, 2003; Reeve *et al.*, 2014). While a majority of PD cases are sporadic and have no distinct genetic underpinnings, approximately 10% of PD cases result from hereditary factors (Cannon and Greenamyre 2013; Shulman *et al.*, 2011). A little over two decades ago, a mutation associated with PD in a large Italian family was localized to *SNCA*, the gene encoding the protein alpha-synuclein (Polymeropoulos *et al.*, 1997). This finding represented the first indication of a genetic basis of PD. In the same year, alpha-synuclein was also identified as the main protein component in Lewy bodies, cytoplasmic neuronal aggregates associated with PD pathology and other related dementias (Spillantini *et al.*, 1997).

Mutations in alpha-synuclein may lead to PD development via gain-of-function mechanisms. The two most common and well-characterized alpha-synuclein mutations are A53T and E46K (Miraglia *et al.*, 2018). The A53T missense mutation was the first mutation in alpha-synuclein to be associated with familial PD and leads to a disruption in ubiquitin-dependent proteolysis and impaired lysosomal and mitochondrial function (Liu *et al.*, 2015; Miraglia *et al.*, 2018; Polymeropoulos *et al.*, 1997; Stefanis *et al.*, 2001). Both the A53T and E46K mutations lead to an increase in fibril formation (Fredenburg *et al.*, 2007). Wild-type alpha-synuclein gene dose has also been correlated to PD risk, with duplication or triplication of the *SNCA* gene being associated with onset of parkinsonism (Chartier-Harlin *et al.*, 2004; Ross *et al.*, 2008).

Other common genetic mutations that contribute to PD development create altered forms of the leucine-rich repeat kinase 2 protein (LRRK2; *PARK8*), the E3 ubiquitin ligase *Parkin*, the glucocerebrosidase gene (*GBA*), and the microtubule-associated protein tau gene (*MAPT*). Mutations in these genes and their associated proteins have been associated with altered mitochondrial function and oxidative stress, alpha-synuclein fibrilization, and the early onset of PD (Cannon and Greenamyre 2013; Lubbe and Morris 2014; Shulman *et al.*, 2011). More recently,

expression of the synaptic vesicle glycoprotein 2C (SV2C) was found to be disrupted in the basal ganglia of PD brain (Dunn *et al.*, 2017b) and variations in the human SV2C gene are correlated with responsiveness to levodopa, the frontline treatment therapy for PD (Altmann *et al.*, 2016).

Alpha-synuclein and Parkinson's disease pathology

Alpha-synuclein is expressed at the presynaptic terminal in the central nervous system and exists in a dynamic equilibrium between cytoplasmic and membrane-bound states. Alpha-synuclein associates with membranes of synaptic vesicles, the endoplasmic reticulum and golgi apparatus, and mitochondria, and these associations contribute to both healthy and pathological activities of alpha-synuclein (Iwai *et al.*, 1995; Miraglia *et al.*, 2018). Alpha-synuclein acts as a protein chaperone and mediates soluble N-ethylmaleimide-sensitive factor attachment protein receptor (SNARE) complex assembly (see a more detailed discussion of SNARE proteins and the vesicle cycle in Section II). Mutations in alpha-synuclein lead to alterations in SNARE protein associations (Burre *et al.*, 2010; Garcia-Reitböck *et al.*, 2010). Alpha-synuclein is also associated with neurotransmitter release and synaptic plasticity, as it facilitates vesicular trafficking, recycling, clustering, and docking (Diao *et al.*, 2013; Miraglia *et al.*, 2018; Nemani *et al.*, 2010; Wang *et al.*, 2014).

Alpha-synuclein is able to adopt a wide range of conformations, including soluble, unfolded monomers, membrane-bound multimers, protofibrillar oligomers, and insoluble fibrils (Ghiglieri *et al.*, 2018; Miraglia *et al.*, 2018; Theillet *et al.*, 2016). The toxicity of alpha-synuclein is dependent on its conformation. Soluble alpha-synuclein monomers become mature, insoluble fibrils through several intermediate protofibril stages (Goldberg and Lansbury 2000). Amyloid alpha-synuclein fibrils are comprised of beta-sheets and combine to form Lewy bodies (Serpell *et al.*, 2000). Evidence indicates that formation of amyloid fibrils is neuroprotective (Caughey and

Lansbury 2003; Winner *et al.*, 2011) and protofibrils are the pathogenic species of alpha-synuclein (Caughey and Lansbury 2003; Volles and Lansbury 2003; Winner *et al.*, 2011), though there is still debate over which conformation of alpha-synuclein is pathogenic (Ghiglieri *et al.*, 2018; Miraglia *et al.*, 2018).

Alpha-synuclein has a unique relationship with dopamine and dopamine neurons. Alpha-synuclein modulates the trafficking of the dopamine transporter (DAT) to the synaptic terminal and influences its activity (Butler *et al.*, 2015; Lee *et al.*, 2001). Complete knock-out of alpha-synuclein results in altered dopamine release, suggesting that alpha-synuclein regulates dopamine transmission (Abeliovich *et al.*, 2000). Dopamine and norepinephrine have also been shown to inhibit the formation of alpha-synuclein fibrils and to break down existing fibrils, thus producing more of the toxic, oligomeric form of alpha-synuclein (Fischer and Matera 2015; Mor *et al.*, 2017). Dopamine also stabilizes the toxic oligomers of alpha-synuclein and induces their formation (Fischer and Matera 2015). Oxidation of dopamine and norepinephrine increases their effectiveness at inhibiting alpha-synuclein fibrilization and stabilizing toxic oligomers (Conway *et al.*, 2001; Li *et al.*, 2004). Thus, as dopamine neurotransmission is disrupted in PD, the resulting increase in cytoplasmic oxidized dopamine contributes to alpha-synuclein-mediated neurotoxicity.

Section II: Vesicle handling and the dopamine system

Synaptic vesicles: From vesicle pools to vesicle recycling

Synaptic vesicles are concentrated in presynaptic nerve terminals and store neurotransmitter until their action potential-dependent fusion with the presynaptic membrane, resulting in the release of stored neurotransmitter into the synaptic cleft. Synaptic vesicles are thought to reside in three pools within the presynaptic terminal: the readily releasable pool, the recycling pool, and the reserve pool. Vesicles in the readily releasable pool represent

approximately one to two percent of all vesicles in the presynaptic terminal and are immediately released upon electrical stimulation. Vesicles in the readily releasable pool are docked and primed for release at the active zone, a specialized region of the presynaptic membrane that contains a high density of proteins involved in vesicle exocytosis, including voltage-gated ion channels and SNARE proteins. Vesicles in the recycling pool represent approximately 10-20% of all vesicles in the presynaptic terminal and are released upon moderate electrical stimulation, moving from the recycling pool into the readily releasable pool as needed. The final pool of vesicles is the reserve pool, which represents 80-90% of all presynaptic vesicles. Vesicles in the reserve pool are recruited upon high frequency electrical stimulation after the recycling pool is depleted. In this three-pool model, vesicles are thought to move from the recycling pool into the readily releasable pool or into the reserve pool, and the protein synapsin is thought to cross-link vesicles, thus stabilizing and immobilizing them. There is debate over the number and nature of the vesicle pools, with some groups advocating a model with spatial intermixing of all three vesicle pools; the presence of a surface pool of fused vesicles ready for endocytosis; or the presence of a super pool of vesicles that freely move between synaptic boutons and the synaptic terminal (Denker and Rizzoli 2010; Harlow *et al.*, 2001; Harlow *et al.*, 2013; Jung *et al.*, 2016; Rizzoli 2014; Rosenmund and Stevens 1996; Szule *et al.*, 2015; Xu-Friedman *et al.*, 2001).

Synaptic vesicles contain over 80 different integral membrane proteins, including synaptotagmin, which is crucial for calcium-sensing and neurotransmitter release; a neurotransmitter transporter, such as VMAT2; a synaptic vesicular glycoprotein (SV2), which is thought to be the structural scaffold onto which other vesicular proteins are anchored; and synaptophysin and synaptobrevin, which are crucial for SNARE-mediated exocytosis (Takamori *et al.*, 2006). Vesicle release, or exocytosis, occurs via SNARE proteins. There are 36 SNARE proteins in humans that are associated with either the vesicular membrane, such as synaptobrevin,

or with the presynaptic membrane, such as syntaxin and SNAP-25. As stated above, vesicles in the readily releasable pool are docked and primed for SNARE-mediated exocytosis. Vesicle priming entails the partial formation of the SNARE complex: synaptobrevin, syntaxin, and SNAP-25 form a four-helix bundle that wrenches the vesicle membrane and the presynaptic membrane within close proximity of each other. When an action potential reaches the presynaptic terminal, voltage-gated calcium channels are opened and the increase in concentration of Ca^{2+} is detected by synaptotagmin. Ca^{2+} binding causes synaptotagmin to change conformation, thus twisting the four-helix SNARE complex and forcing the vesicle membrane and the plasma membrane to fuse and neurotransmitter to be released (Bennett *et al.*, 1992; Bombardier and Munson 2015; Kumar *et al.*, 2015).

There are multiple models that explain how a vesicle could undergo exocytosis and then be endocytosed back into the presynaptic terminal. The first is the kiss-and-run model, in which vesicles transiently fuse and form a small fusion pore through which some neurotransmitter is exocytosed into the synaptic cleft. In this model, endocytosis occurs when the vesicle detaches from the presynaptic membrane following neurotransmitter release, as the vesicle membrane did not fully collapse into the presynaptic membrane. The second model is full fusion, in which the vesicle membrane fully fuses and incorporates into the plasma membrane, allowing for complete release of neurotransmitter. In this model, the vesicle is recycled via clathrin-mediated endocytosis in which the to-be vesicle membrane is covered with a coat of clathrin triskelia, groups of three heavy and three light chains of the clathrin molecule (Denker and Rizzoli 2010). Alternate models of vesicle endocytosis include endosomal recycling and bulk endocytosis. In endosomal recycling, vesicles fully fuse with the plasma membrane and then are endocytosed and fuse with an endosome in the presynaptic terminal. The vesicle membranes and the contents of the endocytosed vesicles are sorted in the endosome and new vesicles bud off of the endosome. Alternately, bulk

endocytosis occurs after vesicles fully fuse with the plasma membrane and are endocytosed through large membrane invaginations. New vesicles then bud off of this large infolding (Denker and Rizzoli 2010; Rahamimoff and Fernandez 1997; Rizzoli 2014).

Monoamines, VMAT2, and dopamine handling

Dopamine, serotonin, norepinephrine, epinephrine, and histamine are monoamine neurotransmitters that are packaged into synaptic vesicles by VMAT2 (*SLC18A2*). Within the class of monoamine neurotransmitters, dopamine, norepinephrine, and epinephrine are considered members of the sub-group catecholamines due to the presence of a catechol group comprised of a benzene ring with two hydroxyl groups. Catecholamines are synthesized in the cytoplasm by tyrosine hydroxylase (TH), which converts tyrosine into L-dihydroxyphenylalanine (L-DOPA); L-DOPA is then converted into dopamine by DOPA decarboxylase; dopamine is converted into norepinephrine by dopamine beta hydroxylase within the vesicular lumen; and norepinephrine is converted into epinephrine by phenylethanolamine-N-methyltransferase. Once synthesized, dopamine is transported from the cytoplasm and into the vesicular lumen by VMAT2. VMAT2 exchanges two hydrogen ions for one dopamine molecule and is powered by a luminal proton gradient established by the V-type ATPase, which actively transports protons from the cytosol into the vesicular lumen. After release, dopamine is removed from the synaptic space through 1) degradation by catechol-O-methyltransferase (COMT) or monoamine oxidase (MAO), 2) reabsorption into the presynaptic terminal by the dopamine transporter (DAT), or 3) diffusion away from the synaptic cleft (Burke *et al.*, 2004).

Proper presynaptic dopamine storage is essential for the survival of dopamine neurons, as cytosolic dopamine is toxic to the nerve terminal. Excess levels of dopamine in the cytosol results in auto-oxidation, enzymatic deamination, oxidative stress, and subsequent cell death (Chen *et al.*,

2008; Graham *et al.*, 1978). Normal packaging of dopamine into synaptic vesicles removes dopamine from the cytosol and thus reduces potential dopaminergic toxicity; conversely, decreased packaging of dopamine into synaptic vesicles results in increased neurotoxicity (Bradner *et al.*, 2013; Burke *et al.*, 2004; Caudle *et al.*, 2007; Chen *et al.*, 2008; Fumagalli *et al.*, 1999; Gainetdinov *et al.*, 1998; Guillot and Miller 2009; Guillot *et al.*, 2008; Lohr *et al.*, 2014; Lohr *et al.*, 2016; Lohr *et al.*, 2015; Wang *et al.*, 1997). Regular activity of VMAT2 not only sequesters dopamine, but also transports toxicants into synaptic vesicles. Treatment with 1-methyl-4-phenyl-1,2,3,6-tetrahydropyridine (MPTP) results in immediate onset of parkinsonism (Langston *et al.*, 1983) and VMAT2 is known to sequester 1-methyl-4-phenylpyridinium (MPP⁺), the active metabolite of MPTP, thus preventing its accumulation in the cytosol and diminishing its neurotoxic effect (Guillot and Miller 2009; Liu and Edwards 1997).

Alterations in expression and function of VMAT2 also affect neuronal vulnerability and vesicle function. While genetic deletion of VMAT2 is neonatal lethal, mice with 5% functional expression of VMAT2 (VMAT2-LO mice), 50% functional expression of VMAT2 (VMAT2-HET), or 200% functional expression of VMAT2 (VMAT2-HI mice) are viable (Caudle *et al.*, 2007; Fon *et al.*, 1997; Fumagalli *et al.*, 1999; Lohr *et al.*, 2014; Mooslehner *et al.*, 2001; Takahashi *et al.*, 1997; Wang *et al.*, 1997). These genetic modifications of VMAT2 expression result in differential neuronal vulnerability: VMAT2-LO and VMAT2-HET mice exhibit progressive neurodegeneration and increased cell death upon exposure to methamphetamine and MPTP (Caudle *et al.*, 2007; Fumagalli *et al.*, 1999; Gainetdinov *et al.*, 1998; Guillot *et al.*, 2008; Lohr *et al.*, 2016; Wang *et al.*, 1997); whereas VMAT2-HI mice exhibit protection from toxic insult with methamphetamine and MPTP (Lohr *et al.*, 2014; Lohr *et al.*, 2016; Lohr *et al.*, 2015).

Pharmacological reduction in VMAT2 function can be achieved through treatment with tetrabenazine or reserpine, drugs that inhibit VMAT2. Tetrabenazine is used to treat hyperkinetic

movement disorders including levodopa-induced dyskinesia in PD (Brusa *et al.*, 2013), chorea in Huntington's disease (Scott 2011), and Tourette's syndrome (Porta *et al.*, 2008); and reserpine was introduced as one of the first antipsychotic drugs in the 1950s (Nur and Adams 2016).

Alterations in *SLC18A2*, the gene encoding VMAT2 have also been associated with PD pathogenesis. Mutations in VMAT2 lead to infantile parkinsonism (Rilstone *et al.*, 2013) and genetic reduction of VMAT2 expression results in progressive nigrostriatal neurodegeneration as well as development of olfactory deficits, depressive behavior, and altered sleep latency in mice—symptoms that mirror both the motor and non-motor symptoms of PD (Alter *et al.*, 2016; Caudle *et al.*, 2007; Taylor *et al.*, 2011; Taylor *et al.*, 2009). Alternatively, increased expression of VMAT2 is associated with decreased risk for PD (Brighina *et al.*, 2013; Glatt *et al.*, 2006). VMAT2 transport deficits have also been observed in vesicles isolated from striata of human patients who died with PD, thus suggesting that PD is a vesicular dopamine storage disorder (Pifl *et al.*, 2014). This finding, coupled with the known role of alpha-synuclein in vesicle trafficking and dopamine release and the association of alpha-synuclein mutations in PD suggests that disruption of vesicular function contributes to PD development.

Section III: The synaptic vesicle glycoprotein 2 C, dopamine, and Parkinson's disease

Structure and function of the synaptic vesicle glycoprotein 2 (SV2)

The synaptic vesicle glycoprotein 2 (SV2) family of 12-transmembrane glycoproteins is a member of the major facilitator superfamily and is known to be involved in synaptic vesicle function. An isoform of SV2 is found on all neurosecretory vesicles in the body (Feany *et al.*, 1992) and there are three proteins within the SV2 family: SV2A, SV2B, and SV2C. Each family member differs in its expression pattern; SV2A and SV2B are ubiquitously expressed throughout the brain, while SV2C expression is highly enriched in dopaminergic brain regions (Bajjalieh *et*

al., 1994; Dardou *et al.*, 2011; Dunn *et al.*, 2017a; Janz *et al.*, 1999). Neurons can express more than one SV2 isoform (Bajjalieh *et al.*, 1994) and five copies of SV2 localize to each synaptic vesicle (Mutch *et al.*, 2011). Furthermore, SV2A contains the binding site for the antiepileptic drug levetiracetam (Lynch *et al.*, 2004), while SV2C contains the binding site for select botulinum neurotoxin serotypes (Mahrhold *et al.*, 2006). Although the sequence, location, and distribution of SV2 proteins are clearly understood, the actual function of SV2 proteins is an area of active investigation.

SV2s have been implicated in several aspects of vesicular function. SV2s modulate vesicle release by altering the size of the readily releasable pool of vesicles and affecting vesicle fusion, with deletion of SV2A resulting in the delayed recovery of readily releasable pool size following stimulus-dependent depletion (Wan *et al.*, 2010), a reduction in the number of fusion-competent vesicles present at the presynaptic membrane, and decreased SNARE complex formation (Xu and Bajjalieh 2001). Furthermore, the loss of SV2C results in impaired recruitment of granules for exocytosis in adrenal chromaffin cells (Iezzi *et al.*, 2005). SV2s have also been posited to play a crucial role in the maturation and priming of vesicles for release as they render synaptic vesicles responsive to Ca^{2+} (Chang and Sudhof 2009; Custer *et al.*, 2006) and bind to and travel with synaptotagmin to the synapse. Proper regulation of the SV2-synaptotagmin interaction is required for normal neurotransmission (Nowack *et al.*, 2010; Schivell *et al.*, 2005; Yao *et al.*, 2010).

It is possible that SV2s also act as the master regulator of vesicle structure, anchoring all other trans-vesicular proteins into their appropriate orientation to enable efficient association with vesicular fusion machinery. Over 80 integral membrane proteins reside on the synaptic vesicle membrane and the transmembrane domains of these proteins occupy 25% of the overall vesicle membrane surface (Takamori *et al.*, 2006). These vesicular proteins interact to form a large protein complex comprised of SV2, synaptotagmin, synaptophysin, vesicle-associated membrane protein

(VAMP), and the vacuolar proton pump (Baldwin and Barbieri 2007; Baldwin and Barbieri 2009; Bennett *et al.*, 1992). Reconstructed images of the frog neuromuscular junction obtained via electron tomography indicate that luminal macromolecules occupy 10% of the vesicle's volume (Harlow *et al.*, 2001; Harlow *et al.*, 2013). This luminal assembly has a bilateral shape consisting of four arms radiating out from a central focal point and is found, nearly identically, in all synaptic vesicles. The points at which the density contacts the luminal membrane are associated with the macromolecules that regulate fusion to the active zone, and as the vesicle travels to the active zone its orientation is brought into precise and consistent alignment (Harlow *et al.*, 2013). While it has been posited that the assembly of macromolecules within the vesicle lumen is made up of the intravesicular domains of proteins such as SV2, synaptobrevin, and synaptotagmin (Harlow *et al.*, 2013), SV2 has been proposed to be the mainstay of the luminal assembly due to the length of its luminal domain being greater than the diameter of the vesicle lumen. The large size of the SV2 luminal domain further supports the notion that luminal domains of vesicular proteins attach to a backbone within the vesicle lumen that is comprised of SV2 proteins (Harlow *et al.*, 2013; Szule *et al.*, 2015).

SV2s also contain a large, heavily glycosylated intravesicular loop that is theorized to form a gel matrix that absorbs neurotransmitter molecules within the vesicle, thus decreasing the amount of free-floating neurotransmitter inside the vesicle lumen and reducing the neurotransmitter concentration gradient present across the vesicle membrane (Nowack *et al.*, 2010; Reigada *et al.*, 2003; Vautrin 2009). This effect may regulate both the loading of neurotransmitter into vesicles and the quantity of neurotransmitter released upon vesicle fusion (Figures 1.1 and 1.2).

The synaptic vesicle glycoprotein 2 C (SV2C)

SV2C expression is enriched in the ventral pallidum, substantia nigra, nucleus accumbens, striatum, globus pallidus, ventral tegmental area, and olfactory bulb (Bajjalieh *et al.*, 1994; Dardou *et al.*, 2011; Dunn *et al.*, 2017a; Janz *et al.*, 1999). SV2C expression colocalizes with TH-positive cell bodies in midbrain dopamine neurons and in GABAergic medium spiny neurons in the striatum (Dunn *et al.*, 2017a). 70% of dopamine neurons in the midbrain express SV2C (Dardou *et al.*, 2011; Dardou *et al.*, 2013; Dunn *et al.*, 2017b; Janz and Sudhof 1999). In addition to its localization to the dopamine system, we recently identified SV2C as a modulator of dopamine release. Mice with a genetic deletion of SV2C (SV2C-KO) mirror the motor disturbances and deficits in gait seen in human PD patients, displaying decreased total locomotor activity and a reduction in stride length (Dunn *et al.*, 2017b). SV2C-KO mice also have decreased striatal dopamine release compared to wildtype (WT) littermate controls, as measured by fast scan cyclic voltammetry (Dunn *et al.*, 2017b).

Furthermore, SV2C is associated with PD pathogenesis: SV2C expression is disrupted in the basal ganglia of PD brain (Dunn *et al.*, 2017b) and variations in the human SV2C gene are correlated with responsiveness to levodopa, the frontline treatment therapy for PD (Altmann *et al.*, 2016). Two single nucleotide polymorphisms (SNPs) upstream from the SV2C gene were recently identified as genetic mediators of one of the most robust environmental modulators of PD risk: nicotine/smoking use, which is strongly protective against PD (Hill-Burns *et al.*, 2013). Smokers homozygous for the major SV2C SNPs had a 56% decreased risk of developing PD, while smokers homozygous for the minor SV2C SNPs had a threefold increased PD risk (Hill-Burns *et al.*, 2013). Several lines of evidence also suggest a connection between SV2C and alpha-synuclein: there is aggregated SV2C in mice that overexpress the A53T variant of alpha-synuclein, and immunoprecipitation of SV2C pulls down alpha-synuclein (Dunn *et al.*, 2017b).

SV2C expression is associated with the dopamine system and with PD risk and pathogenesis. Thus far, our lab has examined the function of SV2C through the creation of SV2C-KO mice and by measuring the effects of this deletion on the dopamine system. The functions of SV2C when it is normally expressed or overexpressed as well as the mechanism through which altered SV2C expression contributes to PD pathogenesis will be examined herein.

Section IV: Rationale and hypothesis

Rationale

Vesicular dysfunction in the dopamine system contributes to the progression of PD. SV2C has recently been associated with both the dopamine system and PD: SV2C is a modulator of dopamine neurotransmission, SV2C expression is disrupted in human PD, and genetic deletion of SV2C results in the development of motor symptoms of PD and dopaminergic neurodegeneration. This evidence suggests that SV2C mediates dopamine vesicle function and susceptibility to dopaminergic neurodegeneration. This dissertation further explores these connections and investigates the mechanism of action of SV2C in dopamine vesicle packaging and release.

Hypothesis and scope

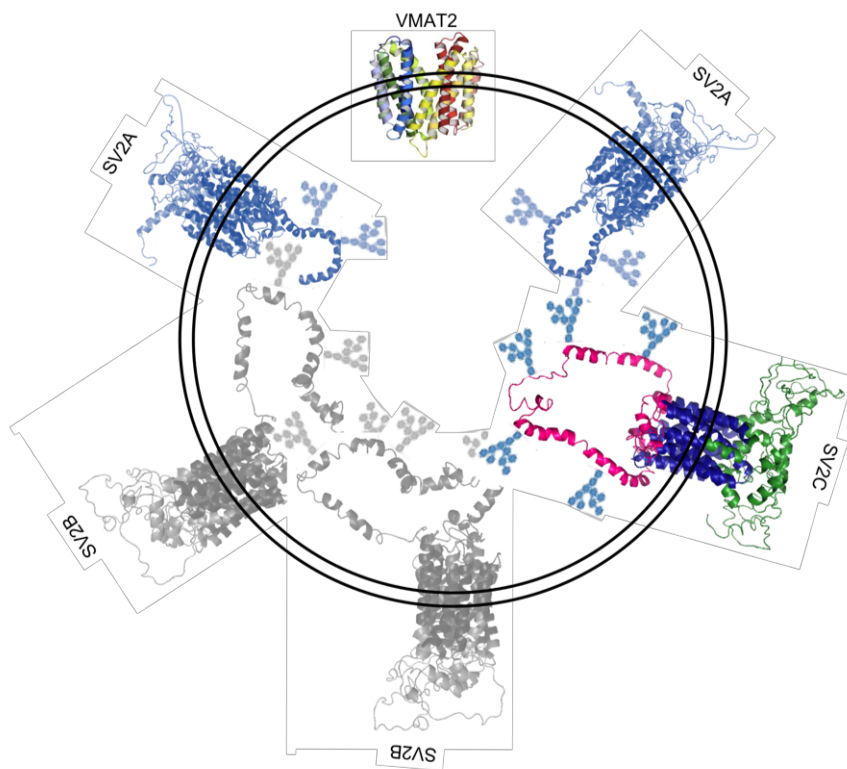
I hypothesize that SV2C mediates the packaging and retention of dopamine over time such that increased expression of SV2C allows synaptic vesicles to better retain dopamine. To this end, my objectives in this dissertation were to 1) develop a series of *in vitro* techniques to examine the effect of SV2C on dopamine packaging and retention, and 2) characterize the effects of overexpression of SV2C on dopamine packaging and retention both *in vitro* and *in vivo*.

In my first aim (Chapter 2), I use the fluorescent false neurotransmitter 206 (FFN206) to investigate VMAT2-mediated vesicle uptake at high resolution and in real-time, and I optimize a 96-well plate reader assay to visualize VMAT2-mediated vesicle packaging and to measure changes in vesicle function arising from pharmacological, toxicological, and genetic manipulations. I then used this assay to assess VMAT2 function and the dynamics of vesicle loading under physiological conditions, during treatment with pharmacological inhibitors, and during treatment with select pesticides and halogenated compounds.

In my second aim (Chapter 3), I seek to identify the mechanism of action of SV2C by overexpressing SV2C *in vitro* and using the VMAT2-mediated vesicle uptake assay developed in Chapter 2 to characterize the effect of SV2C expression on the packaging of FFN206. I then overexpress SV2C *in vivo* and characterize the effect of this overexpression on dopamine vesicle packaging, retention, and release, as measured by fast scan cyclic voltammetry and radioactive dopamine uptake.

The data from these experiments shed light on the function of SV2C within the dopamine system and will be useful for better understanding and treating dopaminergic disorders such as PD.

A



B

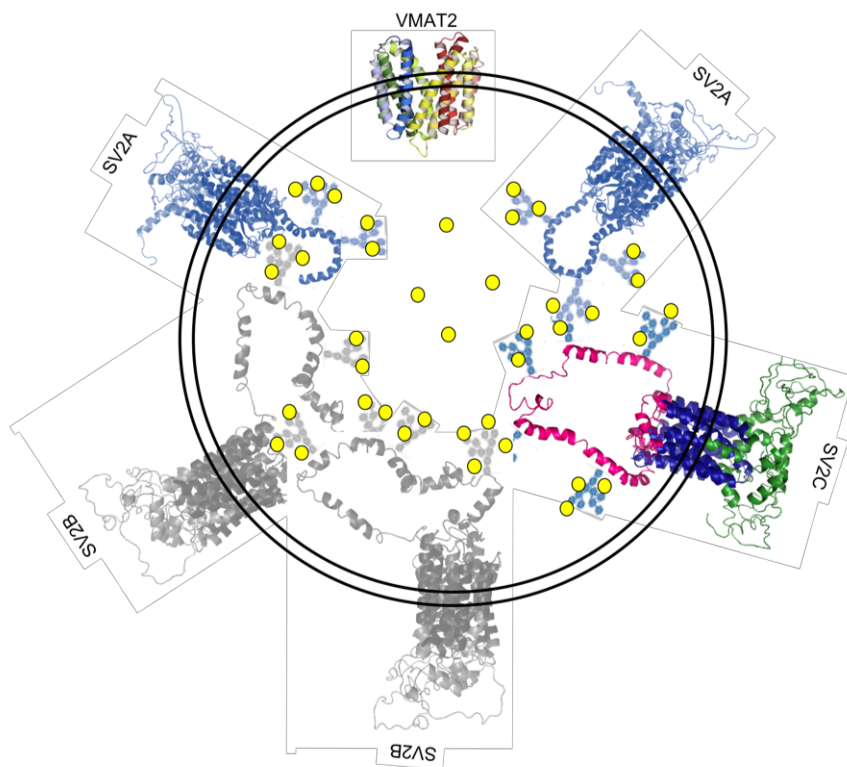


Figure 1.1. Distribution of dopamine molecules in wildtype synaptic vesicles. A) Wildtype synaptic vesicles contain five copies of SV2 protein. The vesicle shown here is expressing one VMAT2 molecule (located at the top of the vesicle) as well as two SV2A proteins (blue), two SV2B proteins (gray), and one SV2C protein (green, blue, and pink). B) Representation of distribution of dopamine molecules (yellow dots) within a wildtype vesicle. Out of 40 dopamine molecules, four (10%) are free-floating within the cytosol and 36 (90%) are bound up in the glycosylated intravesicular loops of the SV2 proteins.

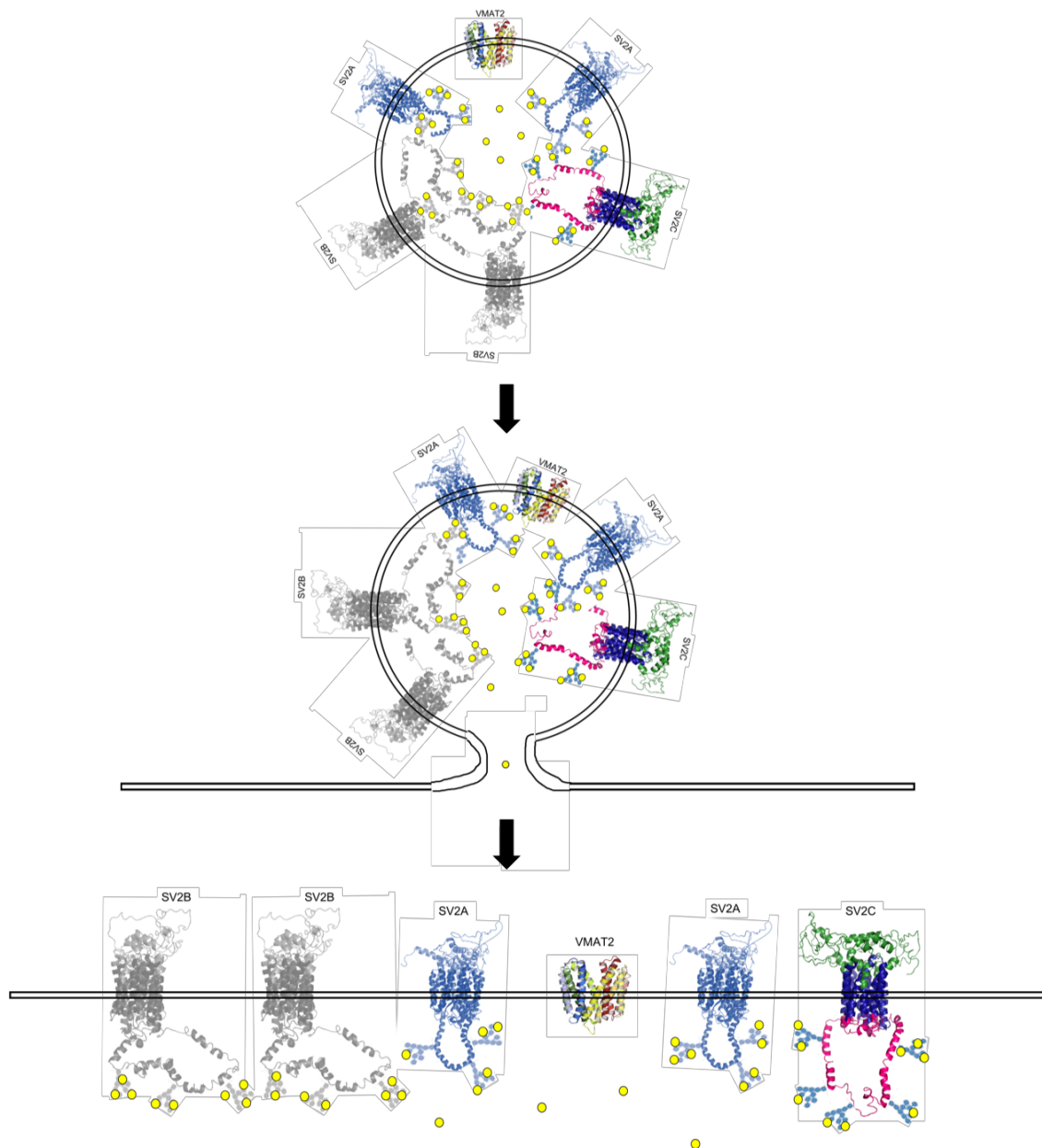


Figure 1.2. Dopamine release in wildtype synaptic vesicles. Dopamine release in a wildtype synaptic vesicle after full fusion exocytosis. The vesicle shown at the top is expressing one VMAT2 molecule (located at the top of the vesicle) as well as two SV2A proteins (blue), two SV2B proteins (gray), and one SV2C protein (green, blue, and pink) and is loaded with dopamine molecules (yellow dots). This hypothetical representation of a wildtype dopamine vesicle contains 40 molecules of dopamine. Out of 40 dopamine molecules, four (10%) are free-floating within the cytosol and 36 (90%) are bound up in the glycosylated intravesicular loops of the SV2 proteins. After formation of a fusion pore (middle image) followed by full collapse of the vesicle membrane into the plasma membrane (bottom image), the intravesicular lumen becomes exposed to the extracellular space. This allows the four previously free-floating dopamine molecules to diffuse away from the plasma membrane, while the 36 remaining dopamine molecules continue to be bound to the glycosylated loops of the SV2 proteins until they dissociate from the glycosylated moieties through ion-exchange.

Chapter 2- Assessing vesicular monoamine transport using false fluorescent neurotransmitters

This chapter is adapted from a manuscript in final preparation for submission as:

Hoffman CA, Jonas L, Igarza K, Miller GW. Assessing effects of toxicants on vesicular monoamine transport using false fluorescent neurotransmitters.

Abstract

Improper vesicular storage of dopamine results in increased levels of cytoplasmic dopamine. In the cytosol, dopamine can undergo enzymatic degradation or auto-oxidation to form toxic dopamine intermediates that contribute to cell death. Perturbations in the expression and function of the vesicular monoamine transporter 2 (VMAT2), which transports monoamines from the cytosol into the vesicle, result in altered dopamine packaging. Here, we developed a series of assays using the fluorescent false neurotransmitter 206 (FFN206) to visualize VMAT2-mediated vesicle packaging and to measure changes in vesicle function arising from pharmacological, toxicological, and genetic manipulations. In this chapter, we tested several known pharmacological inhibitors of VMAT2 as well as a representative group of toxicants for their effect on vesicle storage. We found significant reduction in vesicular storage after treatment with reserpine (IC₅₀: 0.0149 μM), tetrabenazine (IC₅₀: 0.0338 μM), methamphetamine (IC₅₀: 2.085 μM), and methylphenidate (IC₅₀: 3322.8 μM), and we found modest reduction in vesicular storage after treatment with paraquat (IC₅₀: 3.067 μM), rotenone (IC₅₀: 93.2 μM), unichlor (IC₅₀: 55830.2 μM), perfluorooctanesulfonic acid (IC₅₀: 1823.5 μM), Paroil (IC₅₀: 1688.8 μM), Aroclor 1260 (IC₅₀: 14.07 μM), and hexabromocyclododecane (IC₅₀: 2046 μM). The methods of assessing vesicle function discussed here can be used to determine how pharmacological compounds and environmental toxicants exert their effects at the level of the vesicle and can elucidate how exposure to such factors alter dopamine packaging and thus contribute to the progression of monoaminergic diseases such as Parkinson's disease. Furthermore, these assays can be used to assess how genetic manipulation, such as SV2C expression (discussed in the next chapter), alters vesicle packaging.

Introduction

The synaptic vesicle is a vulnerable target for toxicity. The dopamine system presents a prime example of this vulnerability: unpackaged dopamine left in the cytosol is toxic to dopaminergic neurons. Excess levels of cytosolic dopamine lead to autoxidation, enzymatic deamination, oxidative stress, and subsequent cell death (Alter *et al.*, 2013; Chen *et al.*, 2008; Graham *et al.*, 1978).

Cytosolic monoamines, including dopamine, are packaged into vesicles by the vesicular monoamine transporter 2 (VMAT2; SLC18A2). VMAT2 sequesters dopamine as well as 1-methyl-4-phenylpyridinium (MPP⁺), the toxic active metabolite of 1-methyl-4-phenyl-1,2,3,6-tetrahydropyridine (MPTP), into synaptic vesicles, thus reducing their neurotoxic effects (Chen *et al.*, 2005; Guillot and Miller 2009; Liu *et al.*, 1992; Staal and Sonsalla 2000; Takahashi *et al.*, 1997). Alterations in the expression and function of VMAT2 affect neuronal vulnerability and vesicle function. While genetic deletion of VMAT2 is neonatal lethal, mice with 5% functional expression of VMAT2 (VMAT2-LO mice), 50% functional expression of VMAT2 (VMAT2-HET), or 200% functional expression of VMAT2 (VMAT2-HI mice) are viable (Caudle *et al.*, 2007; Fon *et al.*, 1997; Fumagalli *et al.*, 1999; Lohr *et al.*, 2014; Mooslehner *et al.*, 2001; Takahashi *et al.*, 1997; Wang *et al.*, 1997). These genetic modifications of VMAT2 expression result in differential neuronal vulnerability: VMAT2-LO and VMAT2-HET mice exhibit progressive neurodegeneration and increased cell death upon exposure to methamphetamine and MPTP (Caudle *et al.*, 2007; Fumagalli *et al.*, 1999; Gainetdinov *et al.*, 1998; Guillot *et al.*, 2008; Lohr *et al.*, 2016; Wang *et al.*, 1997); whereas VMAT2-HI mice exhibit protection from toxic insult with methamphetamine and MPTP (Lohr *et al.*, 2014; Lohr *et al.*, 2016; Lohr *et al.*, 2015). This direct relationship between vesicle function and neuronal vulnerability reiterates that the vesicle is a vulnerable target for toxicity.

Further, genetic, pharmacological, and toxicant-induced perturbations in VMAT2 function have been associated with disease progression and treatment. Genetic reduction of VMAT2 expression results in progressive nigrostriatal neurodegeneration as well as development of olfactory deficits, depressive behavior, and altered sleep latency in mice—symptoms that mimic both the motor and non-motor symptoms of Parkinson’s disease (PD) (Alter *et al.*, 2016; Caudle *et al.*, 2007; Taylor *et al.*, 2011; Taylor *et al.*, 2009). VMAT2 transport deficits have also been observed in vesicles isolated from striata of human patients who died with PD (Pifl *et al.*, 2014). Pharmacological reduction in VMAT2 function can be achieved through treatment with tetrabenazine or reserpine, drugs that inhibit VMAT2. Tetrabenazine is used to treat hyperkinetic movement disorders including levodopa-induced dyskinesia in PD (Brusa *et al.*, 2013), chorea in Huntington’s disease (Scott 2011), and Tourette’s syndrome (Porta *et al.*, 2008); and reserpine was introduced as one of the first antipsychotic drugs in the 1950s (Nur and Adams 2016). As mentioned above, VMAT2 can also package toxicants in addition to dopamine. Treatment with MPTP results in immediate onset of parkinsonism (Langston *et al.*, 1983) and VMAT2 is known to sequester MPP⁺, the active metabolite of MPTP. This ability of VMAT2 to package MPP⁺ prevents its accumulation in the cytosol and diminishes its neurotoxic effect (Guillot and Miller 2009; Liu and Edwards 1997). Other environmental toxicants have also been associated with the dopamine system and PD development, including exposure to manganese and pesticides such as rotenone and dieldrin (Ascherio *et al.*, 2006; Caudle *et al.*, 2006; Elbaz *et al.*, 2009; Richardson *et al.*, 2006; Semchuk *et al.*, 1992). The mechanisms of action of these toxicants are not known in their entirety (Bemis and Seegal 2004; Miller *et al.*, 1999), and the relationship between VMAT2 and PD suggests that these toxicants exert their neurotoxicity in part by affecting VMAT2 function. Developing novel tools to study VMAT2-mediated vesicle function will allow for visualization of

vesicle packaging as well as identification of changes in vesicle function arising from pharmacological, toxicological, and genetic manipulations.

One tool that has been developed to investigate VMAT2 function is the fluorescent false neurotransmitter 206 (FFN206) reported by Sames and Sulzer in 2013. FFN206 is a monoamine analog and a substrate of VMAT2 that fluoresces in acidic compartments such as the vesicle lumen (Hu *et al.*, 2013). Here, we use FFN206 to investigate VMAT2-mediated vesicle uptake at high resolution and in real-time, and we optimize a 96-well plate reader-based screening assay to assess VMAT2 function and the dynamics of vesicle loading 1) under physiological conditions, 2) during treatment with pharmacological inhibitors of VMAT2, and 3) during treatment with select pesticides and halogenated compounds. We found significant reduction in vesicle packaging after treatment with tetrabenazine, reserpine, methylphenidate, and methamphetamine and modest reduction in vesicle packaging after treatment with paraquat, rotenone, unichlor, perfluorooctanesulfonic acid, Paroil, Aroclor 1260, and hexabromocyclododecane. The methods of assessing vesicle function developed here can be used to identify additional pharmacological, toxicological, and genetic factors, including SV2C expression, that alter vesicular storage and can elucidate how exposure to such factors contributes to the progression of monoaminergic diseases such as PD.

Materials and Methods

Cell culture. Human embryonic kidney cells (HEK293, ATCC) were cultured at 37°C with 5% CO₂ in media comprised of Dulbecco's Modified Eagle Medium (DMEM, Corning), 10% Fetal Bovine Serum (FBS, Atlanta Biologicals), and 1% Penicillin-Streptomycin (Pen Strep, Corning). HEK293 cells stably expressing human VMAT2 (HEK+VMAT2) or mCherry-tagged human VMAT2 (HEK+mCherry-VMAT2) were cultured at 37°C with 5% CO₂ in selection media comprised of DMEM (Corning), 10% FBS (Atlanta Biologicals), 1% Pen Strep (Corning), and

zeocin (100 $\mu\text{g}/\text{mL}$, InvivoGen). All human VMAT2-containing constructs were made in pcDNA3.1 vectors (Life Technologies) containing a zeocin resistance gene. Plasmids were transfected into HEK293 cells with Lipofectamine 2000 using the manufacturer protocol and stable cell lines were generated by repetitive rounds of limiting dilutions in selection media. Experimental media used to optimize the 96-well plate screening assay and to screen pharmacological inhibitors of VMAT2 and environmental toxicants was comprised of DMEM without phenol red (Corning), 1% Pen Strep (Corning), and 1% L-glutamine (Gibco).

Live-cell total internal reflection fluorescence (TIRF) microscopy. HEK+VMAT2 cells were seeded at 60,000 cells per well on laminin-coated glass-bottom 8-well chamber dishes (LabTek) and maintained in selection media until they reached 60% confluence. Upon reaching confluence, the selection media was aspirated and replaced with experimental media containing 1 μM FFN206 (Abcam). Cells incubated with FFN206 for 1 hour at 37°C with 5% CO₂ before the FFN206-containing media was aspirated and replaced with experimental media. Cells were then imaged at 37°C with 5% CO₂ on the GE Delta Vision OMX total internal reflection fluorescence (TIRF) microscope (FFN206 peak excitation = 369 nm; peak emission = 464 nm).

Real-time uptake with confocal microscopy. HEK+VMAT2 cells or HEK+mCherry-VMAT2 cells were seeded at 100,000 cells per plate in laminin-coated glass-bottom round 35 mm dishes (ThermoFisher) and maintained in selection media until they reached 80% confluency. Upon reaching confluency, selection media was aspirated and replaced with experimental media. Cells were imaged on a Nikon A1R TE2000 confocal microscope at 37°C with 5% CO₂. Cells were imaged for a 30 second baseline before the addition of FFN206 to a final concentration of 20 μM . Imaging lasted for a duration of 5 minutes or 1000 seconds (16.67 minutes; FFN206 peak excitation = 369 nm; peak emission = 464 nm; mCherry peak excitation = 587 nm; peak emission = 610 nm).

96-well plate screening assay. We adapted the protocol utilized by Hu and colleagues (Hu *et al.*, 2013) for use in a 96-well plate reader. HEK+VMAT2 cells were seeded at 40,000 cells per well in half volume, black-walled, laminin-coated 96-well plates (Grenier Bio One) and maintained in selection media at 37°C with 5% CO₂ until 90-100% confluent (approximately 24 hours). Upon reaching confluency, selection media was aspirated and replaced with 90 µL of either experimental media or experimental media containing the desired pharmacological compounds or environmental toxicants. Plates were incubated with the pharmacological compounds and/or environmental toxicants for 30 minutes at 37°C with 5% CO₂ before FFN206 (Abcam) was diluted in experimental media and added to the appropriate wells to produce a final concentration of 1 µM FFN206 per well. Plates were incubated with FFN206 for 60 minutes at 37°C with 5% CO₂. Wells were then washed with sterile phosphate-buffered saline (PBS, Gibco) and imaged in PBS on a BioTek Synergy H1 multi-mode plate reader (FFN206 peak excitation = 369 nm; peak emission = 464 nm).

Concentrations of pharmacological compounds and environmental toxicants. Tetrabenazine (Sigma) was diluted in experimental media to a final concentration of 10 µM per well/plate for the negative control group and to concentrations of 0.0001, 0.001, 0.01, 0.1, 1, and 10 µM to produce a dose response curve. Bafilomycin (InvivoGen) was diluted in experimental media to a final concentration of 1 µM per well/plate. Reserpine was diluted in experimental media to final concentrations of 0.0001, 0.001, 0.01, 0.1, 1, and 10 µM. Methamphetamine and methylphenidate were diluted in experimental media to final concentrations of 0.01, 0.1, 1, 10, and 100 µM. Stock concentrations of rotenone, paraquat, chlorpyrifos, unichlor, PFOS, Paroil, HBCDD, and Aroclor 1260 were dissolved in dimethyl sulfoxide (DMSO, Fisher) and then diluted in experimental media into a 200 µM working stock. From this working stock, each compound was diluted in experimental media to final concentrations of 0.01, 0.1, 1, 10 and 100 µM.

Statistical analysis. The data were analyzed by t-test, ANOVA, and z factor analysis as appropriate using GraphPad Prism software. All 96-well plate experiments were conducted in three replicate plates with at least four replicate wells per plate per condition. The z factor is commonly used in the design of protocols for high-throughput screens and incorporates the positive control mean (μ_+), the positive control standard deviation (σ_+), the negative control mean (μ_-), and the negative control standard deviation (σ_-) (Hu *et al.*, 2013).

$$Z = 1 - \frac{(3\sigma_+ + 3\sigma_-)}{|\mu_+ - \mu_-|}$$

Results

FFN206 packaging is dependent on VMAT2 function and maintenance of the vesicular proton gradient. We first sought to confirm that FFN206 fluorescence was a reliable representation of VMAT2-mediated vesicular uptake. To this end, we treated HEK cells stably transfected with mCherry-tagged human VMAT2 (HEK+mCherry-VMAT2) with 1 μ M FFN206 and FFN206 fluorescence was recorded after one hour of incubation. FFN206 fluorescence was observed to overlap with VMAT2 fluorescence (Figure 2.1A), thus confirming that FFN206 was loaded into VMAT2-containing cells. To further confirm that FFN206 was loaded via VMAT2 into vesicular compartments, we treated HEK cells stably transfected with human VMAT2 (HEK+VMAT2) with 10 μ M tetrabenazine or 1 μ M bafilomycin. Tetrabenazine is a pharmacological inhibitor of VMAT2 and bafilomycin inhibits the vesicular H⁺ ATPase that maintains the proton gradient present across the vesicular membrane. Treatment with tetrabenazine and bafilomycin resulted in almost total loss of FFN206 fluorescence (Figure 2.1B and 2.2A), indicating that VMAT2 function and vesicle function must be maintained in order to observe FFN206 fluorescence. To further confirm that FFN206 fluorescence is dependent on VMAT2 function, we treated HEK cells not expressing VMAT2 with FFN206 and observed no

FFN206 uptake (Figure 2.1C and 2.2B), again establishing that FFN206 loading is dependent on VMAT2 function.

High resolution imaging of FFN206 packaging. After confirming the dependence of FFN206 fluorescence on normal VMAT2 function and vesicle function, we sought to observe the localization of FFN206 fluorescence to vesicular compartments. To this end, we grew HEK+VMAT2 cells in a glass-bottom 8-chamber dish and observed the cells after incubation with 1 μ M FFN206 using a GE Delta Vision OMX Blaze TIRF microscope, which allows for high resolution (60x magnification) imaging of live cells. At this resolution, we observed the localization of FFN206 fluorescence to the small vesicle-like compartments present in a single HEK+VMAT2 cell (Figure 2.3).

Real-time VMAT2-mediated uptake of FFN206. After examining FFN206 packaging in high-resolution in a live cell, we sought to observe the dynamic packaging of FFN206 in living cells in real-time. To that end, we grew HEK+mCherry-VMAT2 cells in glass-bottom round dishes and recorded a baseline of mCherry and background fluorescence for 30 seconds. Cells were then treated with 20 μ M FFN206 and fluorescence was recorded for 5 minutes (Figure 2.4). We observed the gradual appearance of FFN206 fluorescence and its co-localization with the VMAT2-containing vesicles. We then sought to examine how perturbations in VMAT2 function and vesicle function affected real-time uptake and retention of FFN206. Uptake was recorded under four conditions and FFN206 fluorescence was recorded for 1000 seconds in each condition (16.67 minutes, Figure 2.5A).

In the first condition, HEK+VMAT2 cells were recorded for a 30 second baseline before being treated with 20 μ M FFN206. In this condition, FFN206 fluorescence started at a low intensity and then exhibited a rapid period of increase from 100 seconds to 500 seconds, at which point the fluorescence intensity continued to increase but at a lesser rate until the time-course

ended. This pattern of fluorescence supports the notion that FFN206 is loaded and retained in VMAT2-containing compartments (Figure 2.5A, HEK+VMAT2 line).

In the second condition, HEK cells not expressing VMAT2 were recorded for a 30 second baseline before being treated with 20 μ M FFN206. In this condition, FFN206 fluorescence started low and then rapidly increased for a duration of approximately 100 seconds. FFN206 fluorescence plateaued from 100 seconds until around 500 seconds, after which point the fluorescence intensity gradually declined until the time-course ended (Figure 2.5A, HEK line).

In the third condition, HEK+VMAT2 cells were incubated with tetrabenazine for 30 minutes before being recorded for a 30 second baseline and then being treated with 20 μ M FFN206. Similar to the third condition, in this condition FFN206 fluorescence started at a low intensity and then experienced a period of gradual increase in FFN206 fluorescence from 100 seconds until around 350 seconds. After reaching peak intensity, FFN206 fluorescence then gradually decreased until the time-course ended (Figure 2.5A, HEK+VMAT2+TBZ line).

In the fourth condition, HEK+VMAT2 cells were incubated with 20 μ M FFN206 for 1 hour before being recorded for a 30 second baseline and then being treated with 1 μ M bafilomycin. In this condition, FFN206 fluorescence started high and then gradually dissipated over time after treatment with bafilomycin. This pattern of fluorescence indicates the loss of FFN206 over time as the pH gradient within the vesicle-like compartments dissipated (Figure 2.5A, HEK+VMAT2+BAF line).

FFN206 fluorescence stabilized in the final 100 seconds of the time-course, thus FFN206 fluorescence in the last 20 seconds of the 1000 second uptake time-course was averaged and compared for each of the four conditions (Figure 2.5B). HEK+VMAT2 cells displayed significantly greater fluorescence than HEK cells and HEK+VMAT2 cells treated with tetrabenazine or bafilomycin ($p < 0.0001$, $\alpha=0.05$ as determined by a one-way ANOVA).

Optimizing parameters for a 96-well plate assay. We adapted the protocol utilized by Hu and colleagues (2013) for use in our 96-well plate assay. In developing this protocol, we first determined which concentration of FFN206 would produce a dynamic range of fluorescence in the HEK+VMAT2 cell line. To this end, we treated HEK+VMAT2 cells with FFN206 at 0.0001, 0.001, 0.01, 0.1, 1, and 10 μM concentrations (Figure 2.6A and Figure 2.7A). We observed a positive relationship between fluorescence and FFN206 concentration; however, variability in FFN206 fluorescence scaled with the increase in signal strength. Furthermore, the fluorescence emitted by 10 μM FFN206 approached the peak signal that can be detected by the 96-well plate reader, thus making detection of subtle alterations in FFN206 fluorescence at this concentration unrealistic. Therefore, a midlevel dose of 1 μM FFN206 was chosen for use in further experiments to ensure the assay had the dynamic range necessary to detect both potential decreases and increases in VMAT2 function.

The Hu (2013) protocol utilized tetrabenazine as a negative control; thus, we performed a dose response of tetrabenazine-suppressed FFN206 fluorescence to determine the appropriate tetrabenazine dose to utilize in our cell line. We treated HEK+VMAT2 cells with tetrabenazine at 0, 0.0001, 0.001, 0.01, 0.1, 1, and 10 μM concentrations (Figure 2.6B and Figure 2.7B). In selecting the tetrabenazine dose, we desired that the assay have a good dynamic range and for a high degree of FFN206 fluorescence to be suppressed with the selected tetrabenazine concentration. We observed decreased FFN206 fluorescence with increasing tetrabenazine concentration and recorded the greatest suppression in FFN206 fluorescence at 10 μM tetrabenazine; we thus chose this dose for use in our assay.

High-throughput assays require a high degree of accuracy and sensitivity, and therefore demand a wide dynamic range and minimal variability within the datasets. The z factor is commonly used in the design of protocols for high throughput screens and incorporates the positive

control mean (μ_+), the positive control standard deviation (σ_+), the negative control mean (μ_-), and the negative control standard deviation (σ_-) (Zhang *et al.*, 1999).

$$Z = 1 - \frac{(3\sigma_+ + 3\sigma_-)}{|\mu_+ - \mu_-|}$$

Z factor calculation ensures that assays with favorable z values (as close to 1 as possible) will have a large band of separation between the distributions of the data for the positive and negative control. A z factor above 0.5 represents a suitable assay. For the FFN206 assay, the positive control was represented by HEK+VMAT2 cells treated with 1 μ M FFN206 and 0 μ M tetrabenazine, while the negative control was represented by HEK+VMAT2 cells treated with 1 μ M FFN206 and 10 μ M tetrabenazine. After performing iterative experiments to optimize cell density, incubation time, and reaction volume, a z factor of 0.76 was consistently achieved, indicating that the protocol is suitable for high-throughput screening (Figure 2.7C).

Pharmacological inhibitors of VMAT2. After optimizing the 96-well plate protocol, the assay was used to test a variety of pharmacological VMAT2 inhibitors to demonstrate the utility and accuracy of the assay. Dose-dependent VMAT2 inhibition was observed in HEK+VMAT2 cells treated with reserpine, tetrabenazine, methamphetamine, and methylphenidate (Figure 2.8). HEK+VMAT2 cells treated with 0.0001, 0.001, 0.01, 0.1, 1, and 10 μ M of tetrabenazine yielded an IC_{50} of 0.0338 μ M and showed essentially complete inhibition at 1 μ M. HEK+VMAT2 cells treated with 0.0001, 0.001, 0.01, 0.1, 1, and 10 μ M of reserpine yielded an IC_{50} of 0.0149 μ M and showed essentially complete inhibition at 0.1 μ M. HEK+VMAT2 cells treated with 0.01, 0.1, 1, 10, and 100 μ M of methamphetamine yielded an IC_{50} of 2.085 μ M and showed essentially complete inhibition at 10 μ M and total inhibition by 100 μ M. HEK+VMAT2 cells treated with 0.01, 0.1, 1, 10, and 100 μ M of methylphenidate yielded an IC_{50} of 3322.8 μ M and reached 50% inhibition at 100 μ M.

Environmental toxicants and VMAT2 function. The optimized assay was then used to test a variety of pesticides (Figure 2.9A) and halogenated environmental toxicants (Figure 2.9B) of interest. Dose-dependent VMAT2 inhibition was observed in HEK+VMAT2 cells treated with rotenone and paraquat (Figure 2.9A), as well as with unichlor, PFOS, Paroil, HBCDD, and Aroclor 1260 (Figure 2.9B). All compounds were tested at concentrations of 0.01, 0.1, 1, 10 and 100 μM . We found a 42.1% reduction in VMAT2 function at 100 μM of rotenone (IC_{50} 93.2 μM), and a 61.7% reduction in VMAT2 function at 10 μM and a 67.4% reduction at 100 μM of paraquat (IC_{50} 3.067 μM). We found no significant reduction in VMAT2 function at any of the tested doses of chlorpyrifos. We found a 12.75% reduction in VMAT2 function at 1 μM and a 30% reduction at 100 μM of unichlor (IC_{50} 55830.2 μM), and a 13.4% reduction in VMAT2 function at 0.01 μM , a 15.2% reduction at 0.1 μM , a 15.1% reduction at 1 μM , a 16.5% reduction at 10 μM , and a 26.9% reduction at 100 μM of perfluorooctanesulfonic acid (PFOS, IC_{50} 1823.5 μM). We found a 17.6% reduction in VMAT2 function at 1 μM , a 21.9% reduction at 10 μM , and a 59.7% reduction at 100 μM of Paroil (IC_{50} 1688.8 μM), and a 51.4% reduction in VMAT2 function at 100 μM of Aroclor 1260 (IC_{50} 14.07 μM). We found a 12.7% reduction in VMAT2 function at 0.1 μM , 11.2% reduction at 1 μM , a 13.1% reduction at 10 μM , and a 38.3% reduction at 100 μM of hexabromocyclododecane (HBCDD, IC_{50} 2046 μM).

Discussion

Here, we used FFN206 to examine VMAT2 function and the dynamics of vesicle packaging at high resolution and in real-time. We optimized a fluorescent 96-well plate assay with a dynamic range that allows for detection of pharmacological, environmental, and genetic factors that alter VMAT2-mediated vesicular uptake and is amenable to high-throughput screening. Using these techniques, we investigated VMAT2-mediated vesicle uptake under physiological

conditions, during treatment with pharmacological inhibitors of VMAT2, and during treatment with select environmental toxicants. In an attempt to create a platform to measure VMAT2 function, we previously developed an assay to spatially resolve VMAT2-mediated packaging of dopamine utilizing high-content imaging with a fluorescent dye and mCherry-tagged VMAT2, but this assay required time-intensive image analysis to obtain suitable results (Bernstein *et al.*, 2012). The development of FFN206 allowed us to adapt our assay to a fluorescent plate reader format and to visualize monoamine transport with an ease and in a real-time manner that was previously inaccessible. Further, the methods developed here can be used to assess how any pharmacological, environmental, and genetic manipulations affect vesicle function and can contribute to monoaminergic disease progression.

Several fluorescent false neurotransmitters have been utilized to visualize monoamine uptake and release, including FFN206 as well as FFN200, FFN511 and FFN102 (Gubernator *et al.*, 2009; Hu *et al.*, 2013; Lau *et al.*, 2015; Pereira *et al.*, 2016; Rodriguez *et al.*, 2013; Zhang *et al.*, 2009). FFN206 is a substrate of VMAT2 that has been used as an analog of dopamine uptake in HEK cells stably transfected with rat VMAT2 (Hu *et al.*, 2013) and as an analog of histamine exocytosis in mast cells (Kiyoi *et al.*, 2018). Here, we used FFN206 in HEK cells stably transfected with human VMAT2 and demonstrated the utility of FFN206 to investigate the dynamic process of vesicle packaging and to assess the effect of pharmacological compounds and environmental toxicants on VMAT2 function.

We first demonstrated the utility of FFN206 fluorescence as a representation of VMAT2-mediated vesicle uptake and show that FFN206 fluorescence overlapped with mCherry-tagged VMAT2 fluorescence, indicating that FFN206 is loaded into VMAT2-containing cells. Furthermore, treatment with tetrabenazine and bafilomycin resulted in almost total loss of FFN206 fluorescence, indicating that VMAT2 function and the vesicular pH gradient must be maintained

in order to observe FFN206 fluorescence. With TIRF-level resolution of FFN206 packaging, we observed the localization of FFN206 fluorescence to the small vesicle-like compartments present in a single HEK+VMAT2 cell. We also show real-time VMAT2-mediated monoamine uptake. This real-time uptake assay can be used to assess the effects of pharmacological compounds and environmental toxicants on the active process of vesicle packaging and leak. FFN206 uptake was recorded under four conditions: HEK+VMAT2 cells treated with FFN206, HEK cells not expressing VMAT2 treated with FFN206, HEK+VMAT2 cells incubated with tetrabenazine and then treated with FFN206, and HEK+VMAT2 cells incubated with FFN206 for 1 hour before being treated with bafilomycin. Together, these four conditions depict a dynamic process of monoamine packaging, leak, and retention over time that mimics the dynamic equilibrium seen in monoamine vesicles.

Synaptic vesicles are inherently leaky, meaning neurotransmitter levels in the vesicle will decline unless neurotransmitter is continually loaded from the cytosol into the vesicle (Floor *et al.*, 1982; Takami *et al.*, 2017). We show that FFN206 leaks out of vesicles over time if it is not continually reloaded into the vesicle by VMAT2, as evidenced by the decrease in FFN206 fluorescence in conditions where there is no VMAT2 (HEK cells) or inactive VMAT2 (HEK+VMAT2 cells treated with tetrabenazine). This corroborates the recent finding from Kiyoi *et al.* (Kiyoi *et al.*, 2018), which reported FFN206 leak in mast cells. Similarly, we show the retention of FFN206 over time and the maintenance of FFN206 fluorescence in conditions where there is continual loading of FFN206 via VMAT2 (HEK+VMAT2 cells). While cells treated with bafilomycin also exhibit a decline in FFN206 fluorescence over time, this loss of fluorescence is caused by a different mechanism. Bafilomycin inhibits the vacuolar H⁺ ATPase present on vesicles, leading to the dissipation of the vesicular proton gradient present across the vesicular membrane. As the proton gradient dissipates, the physiological state of the vesicle is disrupted,

and vesicular homeostasis cannot be maintained despite the continued normal function of VMAT2. Overall, our results suggest that FFN206 fluorescence initially occurs in a non-VMAT2-dependent manner, but maintenance of FFN206 fluorescence within vesicles is VMAT2-dependent and is reliant on continual VMAT2 activity.

We adapted the protocol utilized by Hu and colleagues (Hu *et al.*, 2013) for use in our 96-well plate assay. We chose concentrations of 1 μ M FFN206 and 10 μ M tetrabenazine to ensure the assay had the dynamic range necessary to detect both decreases and increases in VMAT2 function. Iterative experiments were conducted to refine the protocol until a z score above 0.70 was consistently achieved. We further verified the reliability of the assay by screening pharmacological compounds known to inhibit VMAT2: tetrabenazine, methamphetamine, methylphenidate, and reserpine, and observed dose-dependent VMAT2 inhibition that aligned with previously published results (Hu *et al.*, 2013).

After confirming the reliability of the FFN206 assay, we treated HEK+VMAT2 cells with select pesticides and halogenated environmental toxicants. There is an association between exposure to environmental toxicants and PD and it has long been established that exposure to heavy metals and pesticides such as manganese, permethrin, dieldrin, rotenone, and paraquat contribute to PD risk (Ascherio *et al.*, 2006; Cannon and Greenamyre 2013; Elbaz *et al.*, 2009; Freire and Koifman 2012; Goldman 2014; Nistico *et al.*, 2011; Richardson *et al.*, 2006; Semchuk *et al.*, 1992; Tanner *et al.*, 2011). The extent to which altered VMAT2 function mediates the toxicity of exposure to these environmental toxicants has not been extensively studied. As a result, we tested representative pesticides and halogenated environmental toxicants including rotenone, paraquat, chlorpyrifos, unichlor, PFOS, Paroil, HBCDD, and Aroclor 1260 for their effect on VMAT2 function. Of these compounds, exposures to rotenone and paraquat have been most extensively linked with PD and VMAT2: rotenone and paraquat exposures have been associated

with PD in both humans and animal models (Bove and Perier 2012; Nistico *et al.*, 2011; Tanner *et al.*, 2011) and VMAT2 functional deficits have been observed in vesicles isolated from striata of human patients who had PD (Pifl *et al.*, 2014).

Rotenone is a known inhibitor of mitochondrial complex I and exerts its toxicity by oxidizing mitochondrial proteins and causing oxidative stress that leads to cell death (Ramachandiran *et al.*, 2007; Sherer *et al.*, 2007). Similarly, paraquat exerts its toxicity predominantly through oxidative modification of cytosolic proteins, which causes oxidative stress and leads to cell death (Bove and Perier 2012; Ramachandiran *et al.*, 2007; Wu *et al.*, 2017). Here, we detected a reduction in VMAT2 function with administration of 100 μ M of rotenone and with 10 μ M and 100 μ M of paraquat, though this reduced VMAT2 activity occurred at such high doses as to be physiologically irrelevant. Previous studies examining rotenone and paraquat toxicity have observed 70-80% cell death resulting from mitochondrial complex I inhibition with doses of 100 nM rotenone and 200 μ M paraquat (Nistico *et al.*, 2011; Ramachandiran *et al.*, 2007; Wu *et al.*, 2017). The present study differs from these studies in several respects, the first of which being the length of exposure. We exposed cells to each toxicant for a total of 90 minutes (30-minute incubation with the toxicant followed by a 60-minute incubation with FFN206), while previous studies examined toxicity after 48 hours. We also screened for VMAT2 function and not cell death. We did not assess cell death in our assay because the amount of cell death imposed by a 90-minute length of exposure is minimal. Finally, given the high IC₅₀ values we determined for paraquat and rotenone exposures, the mild inhibition of VMAT2 caused by exposures to these toxicants is not likely to be mediated by mitochondrial complex I inhibition.

We also observed reduction in VMAT2 function with 1 and 100 μ M of unichlor; 0.01, 0.1, 1, 10, and 100 μ M of PFOS; 1, 10, and 100 μ M of Paroil; 100 μ M of Aroclor 1260; and 0.1, 1, 10, and 100 μ M of HBCDD, but did not see any effect of chlorpyrifos treatment on VMAT2 function.

These findings align with previous literature indicating exposure to PFOS (Salgado *et al.*, 2016), Aroclor 1260 (Bradner *et al.*, 2013), and HBCDD (Genskow *et al.*, 2015) exerts toxicity on the dopamine system. While these results indicate that unichlor, PFOS, Paroil, Aroclor 1260, and HBCDD are weak inhibitors of VMAT2 over the course of a short-term exposure, it is unlikely that these compounds affect VMAT2 function at environmentally and physiologically relevant concentrations.

In conclusion, we have used FFN206 to investigate VMAT2-mediated vesicle uptake at high resolution and in real-time, we optimized a 96-well plate assay that has a dynamic range and is amenable to a high throughput format, and we used this assay to assess VMAT2 function and the dynamics of vesicle loading upon exposure to pharmacological and environmental compounds. We observed a robust reduction in VMAT2 function after exposure to tetrabenazine, reserpine, methamphetamine, and methylphenidate, and observed a modest reduction in VMAT2 function after short-term exposure to high concentrations of rotenone, paraquat, unichlor, PFOS, Paroil, Aroclor 1260, and HBCDD, though inhibition of VMAT2 is unlikely to contribute to the mechanism of action of these compounds at physiologically and environmentally relevant concentrations. The methods of assessing vesicle function discussed here can be used to assess how other pharmacological and environmental compounds exert their toxicity at the level of the vesicle as well as how genetic manipulations, such as SV2C expression, affect vesicle function. These assays can also elucidate how exposure to such manipulations contributes to the progression of monoaminergic diseases such as PD. In the next chapter, we use the FFN206 96-well plate assay to explore the influence of SV2C expression on vesicle uptake.

Funding Information

This work was supported by NIEHS R01ES023839, NIEHS P30ES019776, and the Lewis Dickey Memorial Fund to G.W.M.; and T32ES012870 to C.A.H.

Acknowledgements

We would like to acknowledge Bethany Wilson for her assistance in the initial stages of method development for the 96-well plate assay. This research project was also supported in part by the Emory University Integrated Cellular Imaging Microscopy Core.

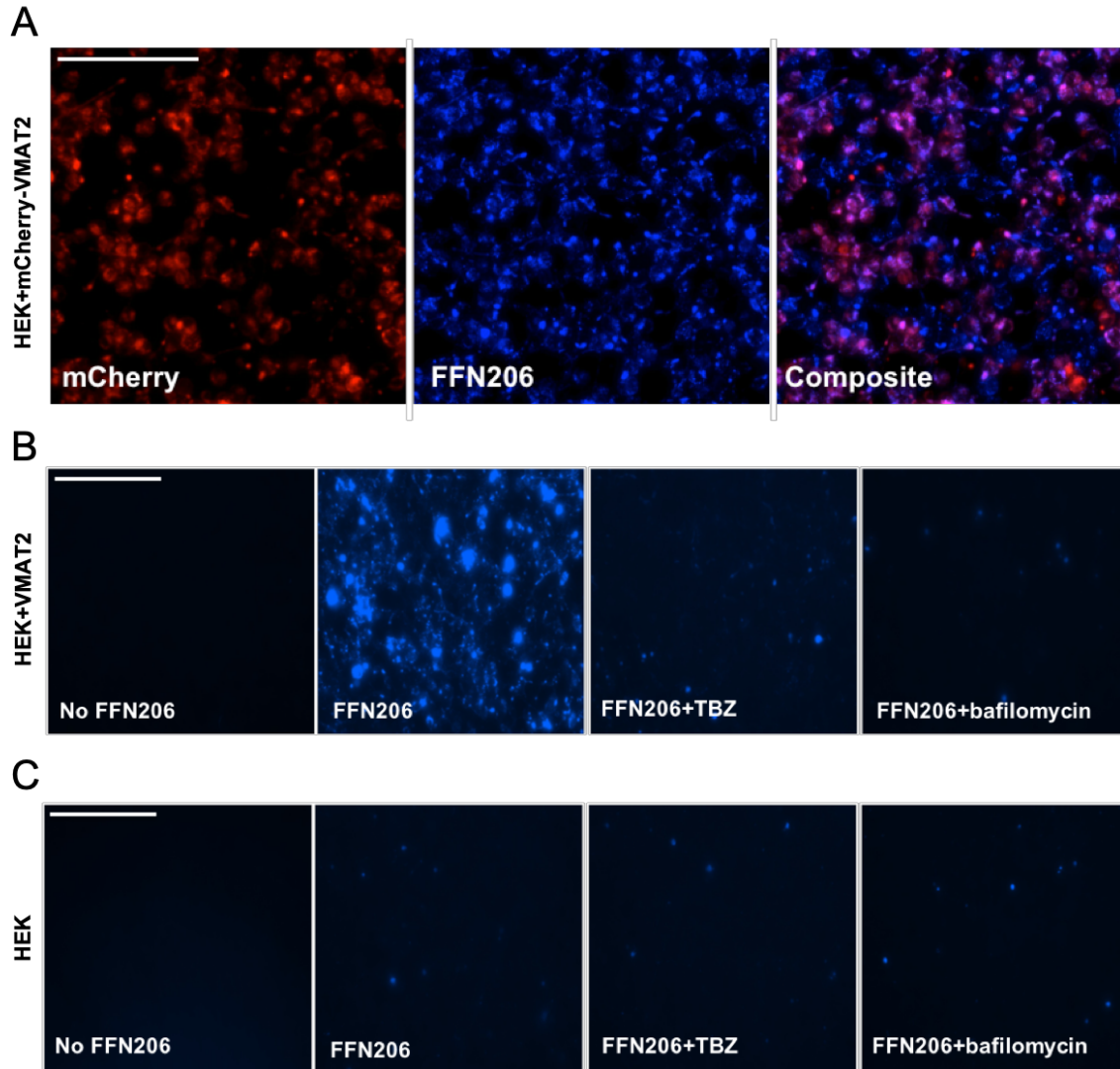
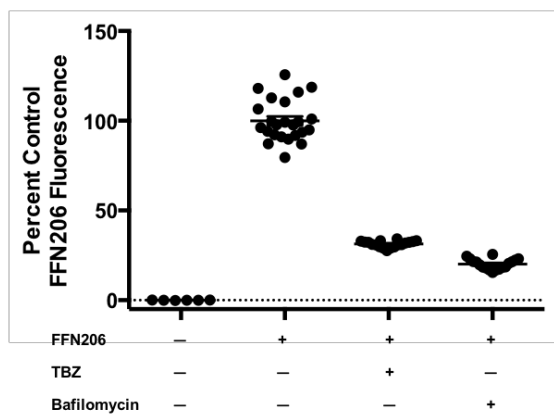


Figure 2.1. FFN206 packaging is dependent on VMAT2 function and maintenance of the vesicular proton gradient. A) FFN206 is loaded into VMAT2-containing cells. A population of HEK cells stably transfected with mCherry-tagged VMAT2 (HEK+mCherry-VMAT2, left image) were treated with FFN206 (center image) and FFN206 fluorescence was observed to overlap with VMAT2 fluorescence (purple, right image). Image taken with an array scan at 10x magnification. B) FFN206 loading is dependent on VMAT2 function and maintenance of the vesicular proton gradient. In the absence of FFN206, no background fluorescence is observed in HEK+VMAT2 cells (left image). HEK+VMAT2 cells treated with FFN206 exhibit robust fluorescence (second from left image). FFN206 uptake is diminished in HEK+VMAT2 cells when VMAT2 function is inhibited by treatment with 10 μ M tetrabenazine (second from right image). FFN206 uptake is diminished in HEK+VMAT2 cells when the vesicular proton gradient is dissipated by treatment with bafilomycin (right image). C) FFN206 loading is minimal in cells not containing VMAT2. In the absence of FFN206, no background fluorescence is observed in HEK cells (left image). HEK cells treated with FFN206 exhibit minimal fluorescence (second from left image). FFN206 uptake is unchanged and minimal in HEK cells when VMAT2 function is inhibited by treatment with 10 μ M tetrabenazine (second from right image). FFN206 uptake is unchanged and minimal in HEK cells when the vesicular proton gradient is dissipated by treatment with bafilomycin (right image). Scale bar = 400 μ M.

A



B

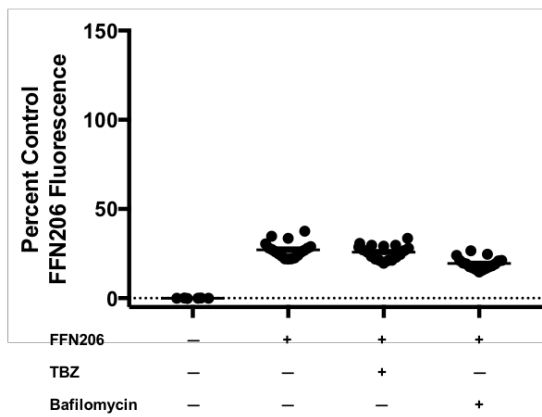
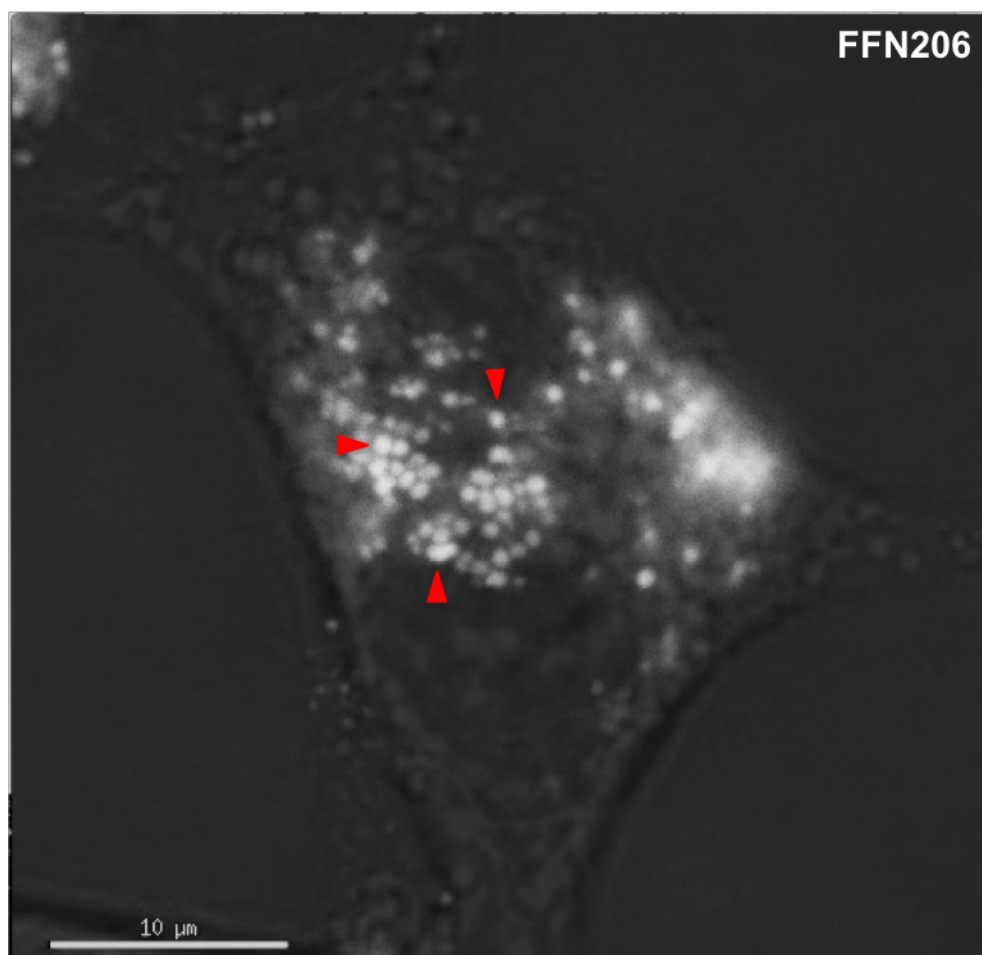
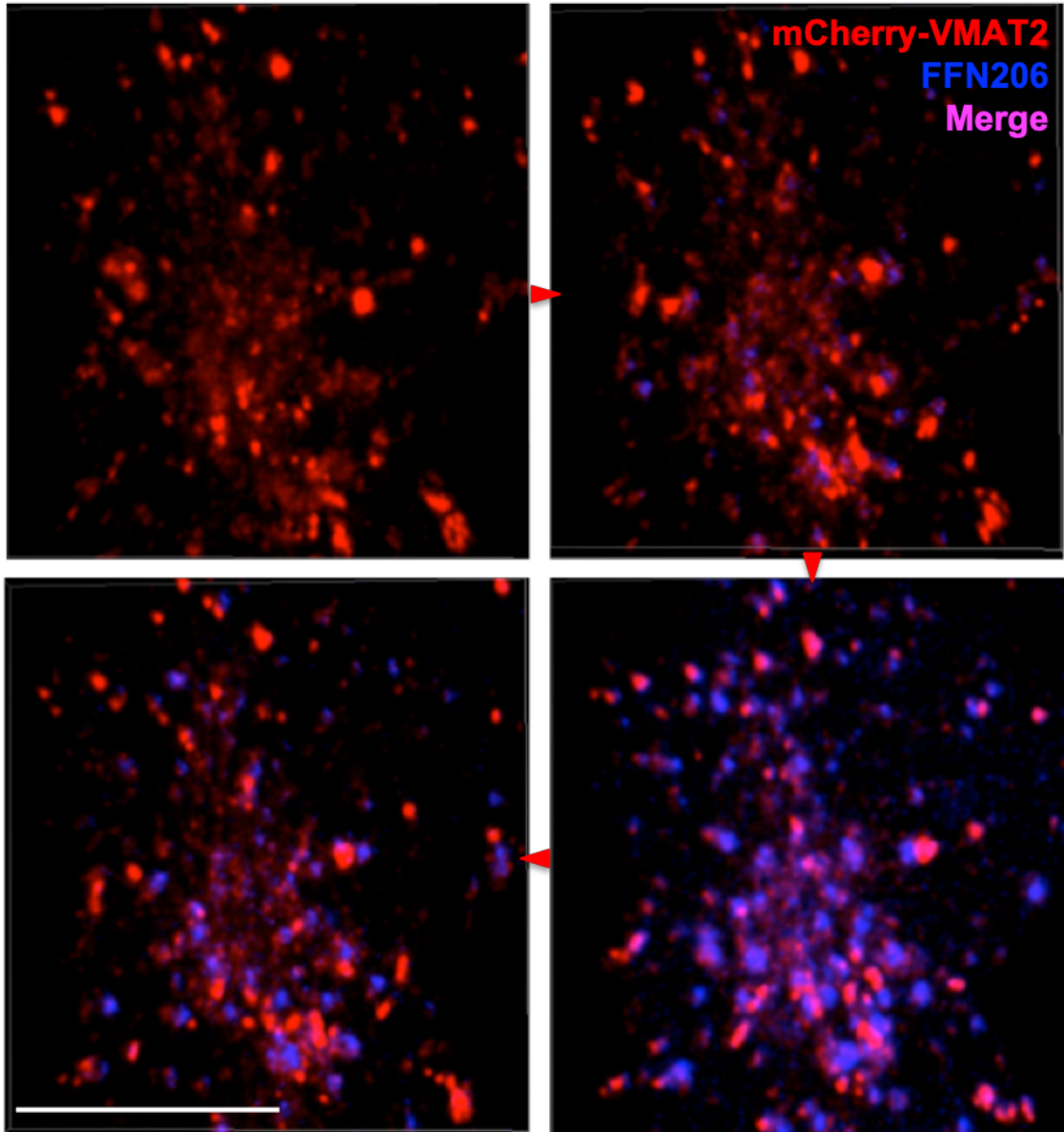


Figure 2.2. Quantification of FFN206 fluorescence. A) Quantification of FFN206 fluorescence observed in Figure 2.1B. In the absence of FFN206, no background fluorescence is observed in HEK+VMAT2 cells. HEK+VMAT2 cells treated with FFN206 exhibit robust fluorescence. FFN206 uptake is diminished in HEK+VMAT2 cells when VMAT2 function is inhibited by treatment with 10 μ M tetrabenazine. FFN206 uptake is diminished in HEK+VMAT2 cells when the vesicular proton gradient is dissipated by treatment with bafilomycin. B) Quantification of FFN206 fluorescence observed in Figure 2.1C. In the absence of FFN206, no background fluorescence is observed in HEK cells. HEK cells treated with FFN206 exhibit minimal fluorescence. FFN206 uptake is unchanged and minimal in HEK cells when VMAT2 function is inhibited by treatment with 10 μ M tetrabenazine. FFN206 uptake is unchanged and minimal in HEK cells when the vesicular proton gradient is dissipated by treatment with bafilomycin. Graphs displayed as percent control mean and standard error of the mean, with the control group being HEK+VMAT2 cells incubated with FFN206. Each point represents one well of cells from a 96-well plate.



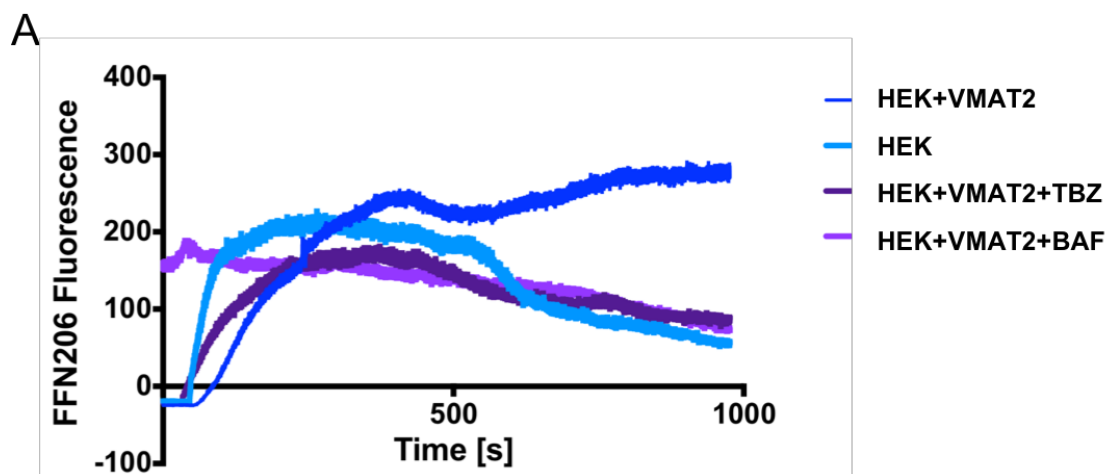
HEK+VMAT2 cell

Figure 2.3. High-resolution imaging of FFN206 packaging. A single HEK cell stably transfected with VMAT2 (HEK+VMAT2) was treated with FFN206. FFN206 fluorescence was localized to the vesicle-like compartments within the cell, as denoted by red arrows. Image taken with a TIRF microscope at 60x magnification. Scale bar = 10 μ M.



HEK+mCherry-VMAT2 cell

Figure 2.4. Real-time uptake of FFN206 in a single cell. Sequential stills taken from a video of FFN206 uptake (blue fluorescence) into the vesicle-like compartments of a single HEK cell stably transfected with mCherry-tagged VMAT2 (red fluorescence). The accelerated time-course video represents 5 minutes of uptake. Still photos taken at 0.93s, 3.18s, 3.94s, and 5.94s into the accelerated video. Scale bar = 10 μ M.



B

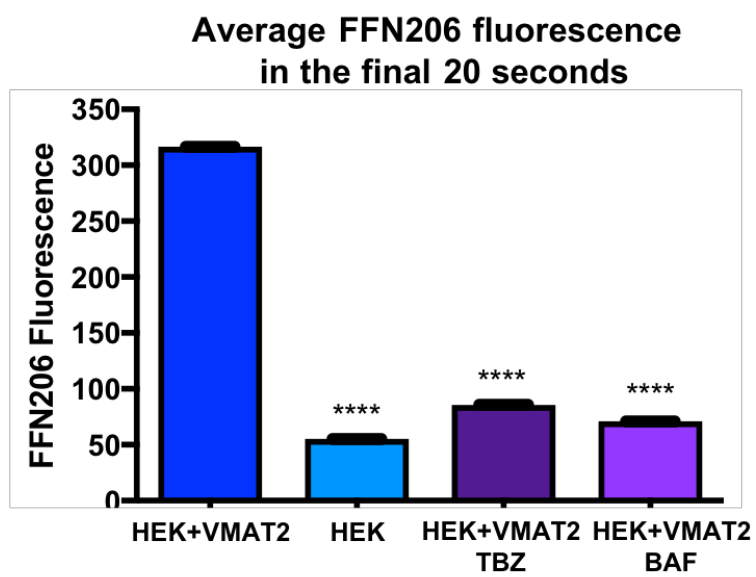


Figure 2.5. Real-time uptake of FFN206. A) Real-time uptake of FFN206 over 1000 seconds (16.67 minutes). Uptake was recorded under four conditions. In the first condition, HEK cells stably transfected with VMAT2 (HEK+VMAT2) were recorded for a 30 second baseline before being treated with FFN206. In the second condition, HEK cells were recorded for a 30 second baseline before being treated with FFN206. In the third condition, HEK+VMAT2 cells were incubated with tetrabenazine (TBZ) for 30 minutes before being recorded for a 30 second baseline and then being treated with FFN206. In the fourth condition, HEK+VMAT2 cells were incubated with FFN206 for 1 hour before being recorded for a 30 second baseline and then being treated with bafilomycin (BAF). Curves represent averaged fluorescence from 7 to 21 cells and are displayed as mean without error. B) Comparison of peak FFN206 fluorescence in the final 20 seconds of 1000 total seconds of uptake. HEK+VMAT2 cells display significantly greater fluorescence than HEK cells and HEK+VMAT2 cells treated with tetrabenazine or bafilomycin. Bars are displayed as mean and standard error of the mean; $p < 0.0001$, $\alpha = 0.05$ as determined by a one-way ANOVA.

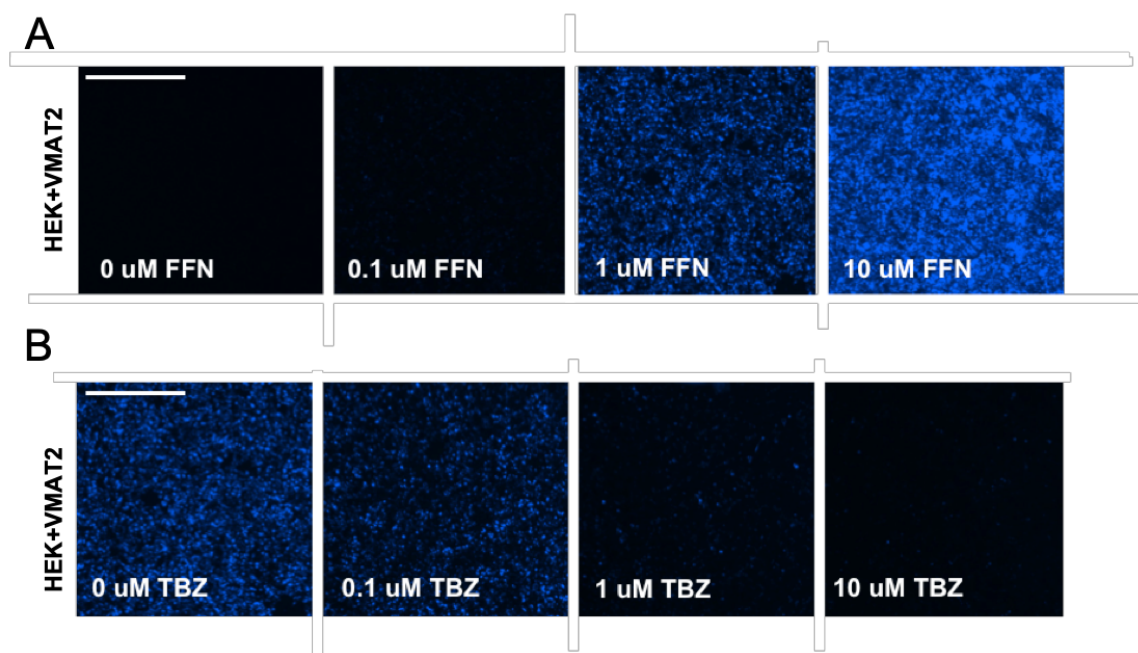


Figure 2.6. Determining optimal parameters for a FFN206 96-well plate assay. A) Representative images of HEK+VMAT2 cells treated with 0, 0.1, 1, or 10 μM of FFN206. Although the highest amount of FFN206 fluorescence was observed at 10 μM , a midlevel dose of FFN206 was chosen for use in the screening assay (1 μM) to ensure the assay had the dynamic range necessary to detect both decreases and increases in VMAT2 function. Cells imaged at 10x magnification. B) Representative images of HEK+VMAT2 cells treated with 0, 0.1, 1, and 10 μM of tetrabenazine (TBZ) and 1 μM FFN206. The greatest TBZ-suppressed FFN206 fluorescence occurred at 10 μM TBZ; therefore, the 10 μM dose was selected for use as a negative control in the screening assay. Cells imaged by EVOS system at 10x magnification. Scale bar = 400 μM .

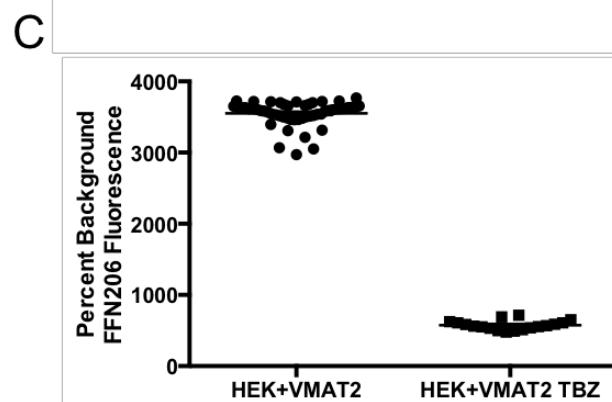
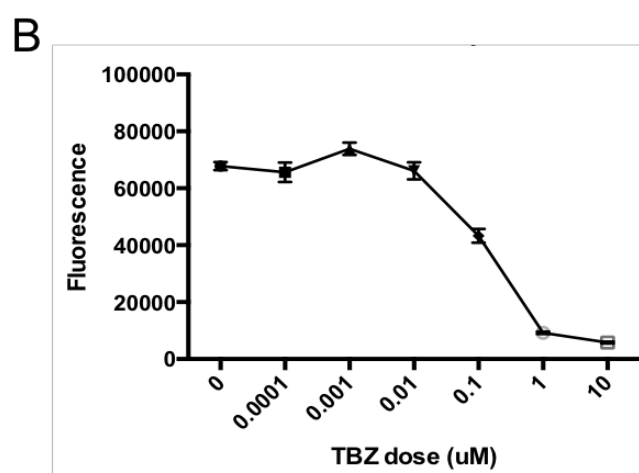
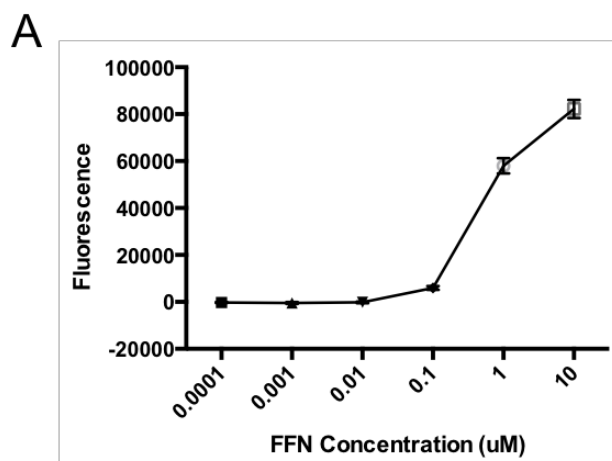


Figure 2.7. Validation of the optimal parameters for the FFN206 screening assay. A) Quantification of FFN206 dose response depicted in Figure 2.6A. FFN206 fluorescence increases as FFN206 dose increases. B) Quantification of tetrabenazine (TBZ)-suppressed FFN206 fluorescence depicted in Figure 2.6B. FFN206 fluorescence decreases as TBZ dose increases. Graphs in A and B depict mean and standard error of the mean. C) The optimized concentrations of FFN206 and TBZ produce positive (cells treated with 1 μ M FFN206 and 0 μ M TBZ) and negative (cells treated with 1 μ M FFN206 and 10 μ M TBZ) control groups with a large separation. The z factor calculated from this data, which incorporates the mean and standard deviation of the positive control and the negative control, was 0.7621, indicating this assay has a dynamic screening range. Each point represents the fluorescence measured for one well of a 96-well plate.

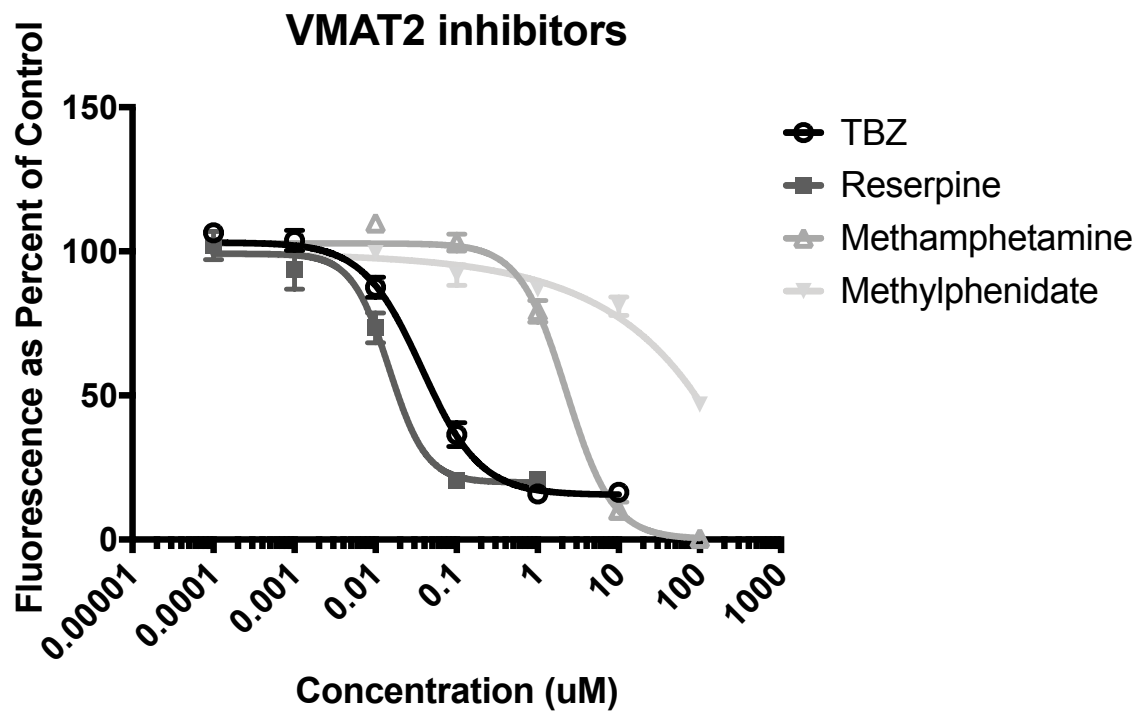
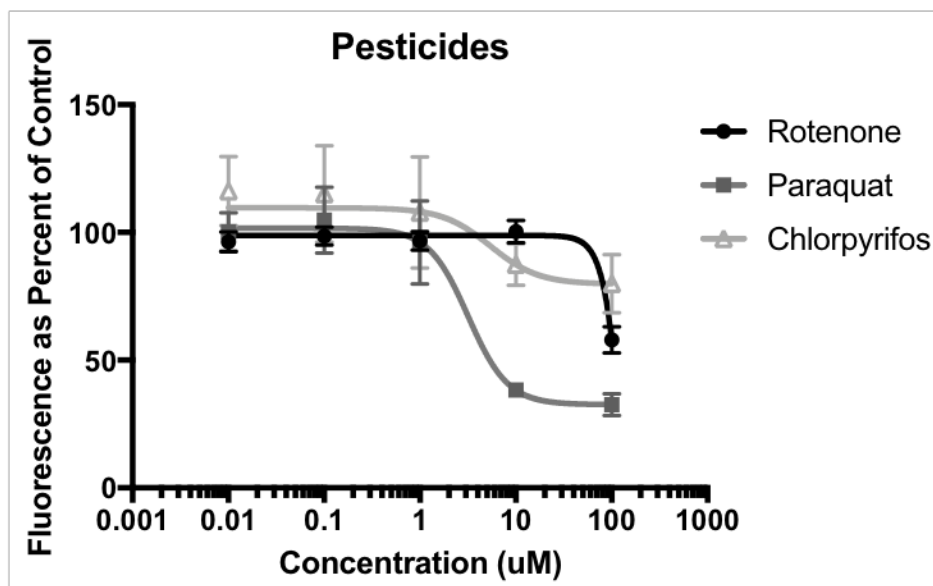


Figure 2.8. Screening pharmacological inhibitors of VMAT2. HEK+VMAT2 cells were treated with either 0.0001, 0.001, 0.01, 0.1, 1, and 10 μM of tetrabenazine (TBZ); 0.0001, 0.001, 0.01, 0.1, 1, and 10 μM of reserpine; 0.01, 0.1, 1, 10, and 100 μM of methamphetamine; or 0.01, 0.1, 1, 10, and 100 μM of methylphenidate. FFN206 fluorescence represented as percent of control (HEK+VMAT2 cells treated with 0 μM drug). Graphs depict mean and standard error of the mean and curves represent non-linear regressions.

A



B

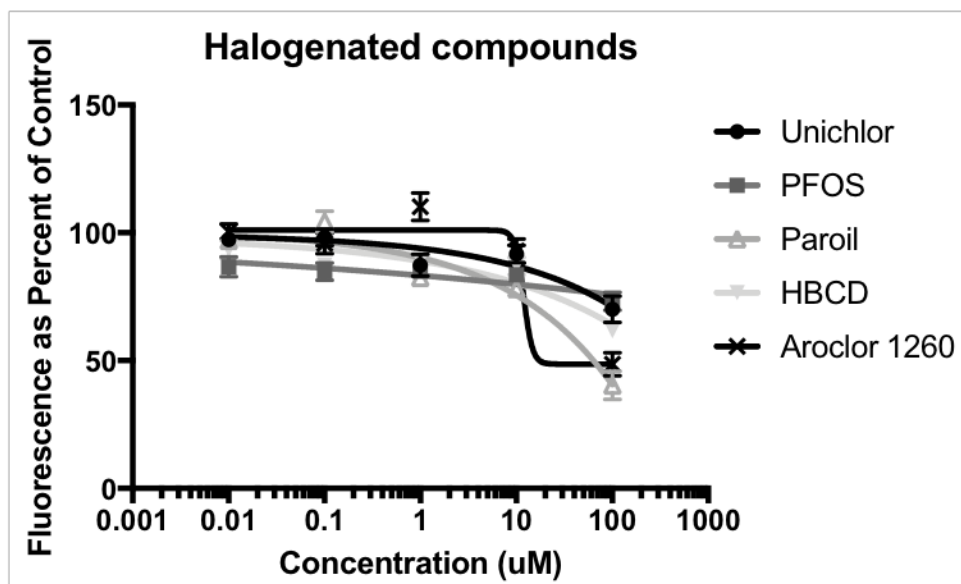


Figure 2.9. Screening environmental toxicants for influence on VMAT2 function. A) HEK+VMAT2 cells were treated with 0.01, 0.1, 1, 10 and 100 μM of the pesticides rotenone, paraquat, or chlorpyrifos. B) HEK+VMAT2 cells were treated with 0.01, 0.1, 1, 10 and 100 μM of the halogenated compounds unichlor, PFOS, Paroil, HBCDD, or Aroclor 1260. FFN206 fluorescence represented as percent of control (HEK+VMAT2 cells treated with 0 μM drug). Graphs depict mean and standard error of the mean and curves represent non-linear regressions.

Chapter 3- The role of SV2C in dopamine vesicle function

Abstract

Synaptic vesicles within the dopaminergic nigrostriatal pathway package neurotransmitter for release and ineffective sequestration of dopamine can contribute to neurodegenerative disease progression. Indeed, dopamine vesicle function is impaired in patients with Parkinson's disease (PD). Proteins within the synaptic vesicle glycoprotein 2 (SV2) family positively modulate vesicle function and one SV2 variant, SV2C, was recently associated with PD risk. Further, SV2C expression is disrupted in the basal ganglia of PD brain and several lines of evidence suggest a connection between SV2C and alpha-synuclein, a protein known to be involved in the pathogenesis of PD. We sought to investigate the role of SV2C in dopamine vesicle handling and to determine how SV2C affects dopamine packaging. To these ends, we overexpressed SV2C *in vitro* through transient transfection and demonstrate that SV2C overexpression leads to increased uptake of a dopamine analog. We then overexpressed SV2C *in vivo* through injection of AAV2/9 vectors in the substantia nigra of C57BL/6 mice. We show enhanced retention of dopamine in the synaptic vesicle over time and prolonged presence of dopamine in the synaptic cleft after electrically-stimulated dopamine release in C57BL/6 mice. These results identify SV2C as a mediator of dopamine vesicle packaging, retention, and release.

Introduction

Synaptic vesicles within the dopaminergic nigrostriatal pathway package transmitter for release and sequester intracellular toxicants such as cytosolic dopamine. Ineffective sequestration of dopamine via the vesicular monoamine transporter 2 (VMAT2) leads to the production of reactive oxygen species and dopamine quinones that contribute to cell death and neurodegenerative disease progression (Caudle *et al.*, 2007; Chen *et al.*, 2005; Chen *et al.*, 2008; Gainetdinov *et al.*, 1998; Graham *et al.*, 1978; Guillot *et al.*, 2008; Lohr *et al.*, 2016; Staal and Sonsalla 2000). Indeed, dopamine vesicle function is impaired in patients with Parkinson's disease (PD): vesicles isolated from striata of human patients who had PD exhibit VMAT2 functional deficits (Pifl *et al.*, 2014). Mutations in the gene encoding VMAT2 also lead to infantile parkinsonism (Rilstone *et al.*, 2013) and increased expression of VMAT2 is associated with decreased risk for PD (Brighina *et al.*, 2013; Glatt *et al.*, 2006).

Mutations and alterations in the expression of another vesicular-associated protein, the synaptic vesicular glycoprotein 2 C (SV2C), have also been linked to PD. Recently, two single nucleotide polymorphisms (SNPs) upstream from the SV2C gene were found to underlie the protective effect of nicotine on PD risk: smokers homozygous for the major SV2C SNPs had a 56% decreased risk of developing PD, while smokers homozygous for the minor SV2C SNPs had a threefold increased risk of developing PD (Hill-Burns *et al.*, 2013). Further, variations in the human SV2C gene are correlated with responsiveness to levodopa, the frontline treatment therapy for PD (Altmann *et al.*, 2016), and SV2C expression is disrupted in the basal ganglia of PD brain (Dunn *et al.*, 2017b). Several lines of evidence also suggest a connection between SV2C and alpha-synuclein, a protein whose involvement in PD pathogenesis has been extensively researched: there is aggregated SV2C in mice overexpressing the A53T mutant of alpha-synuclein and immunoprecipitation of SV2C pulls down alpha-synuclein (Dunn *et al.*, 2017b). Mice lacking

SV2C expression (SV2C-KO) also exhibit increased expression of higher molecular weight forms of alpha-synuclein (Dunn *et al.*, 2017b).

SV2C is a variant of the SV2 family, 12-transmembrane glycoproteins that are found throughout the brain; indeed, an isoform of SV2 is found on all neurosecretory vesicles in the body (Feany *et al.*, 1992). There are three isoforms within the SV2 family, SV2A, SV2B, and SV2C. SV2C expression is enriched in dopaminergic regions of the brain, with 70% of dopamine neurons expressing SV2C (Dardou *et al.*, 2011; Dardou *et al.*, 2013; Dunn *et al.*, 2017a; Janz and Sudhof 1999). SV2s have also been implicated in several aspects of vesicular function. SV2s modulate vesicle release by affecting vesicle fusion: deletion of SV2A results in a reduction in the number of fusion-competent vesicles present at the presynaptic membrane and decreased SNARE complex formation (Xu and Bajjalieh 2001). SV2s have also been posited to play a crucial role in the maturation and priming of vesicles for release as they render synaptic vesicles responsive to Ca^{2+} (Chang and Sudhof 2009; Custer *et al.*, 2006) and bind to and traffic with synaptotagmin at the synapse (Iezzi *et al.*, 2005; Nowack *et al.*, 2010; Schivell *et al.*, 2005; Yao *et al.*, 2010). SV2s contain a large, heavily glycosylated intravesicular loop that is thought to regulate both the loading of neurotransmitter into vesicles and the quantity of neurotransmitter released upon vesicle fusion (Nowack *et al.*, 2010; Reigada *et al.*, 2003; Vautrin 2009). SV2s may also act as a master regulator of vesicle structure, anchoring all other trans-vesicular proteins into their appropriate orientation to enable efficient association with vesicular fusion machinery (Baldwin and Barbieri 2007; Baldwin and Barbieri 2009; Bennett *et al.*, 1992; Harlow *et al.*, 2001; Harlow *et al.*, 2013; Szule *et al.*, 2015; Takamori *et al.*, 2006).

We recently identified a role for SV2C in the dopamine system, reporting a decrease in electrically-stimulated striatal dopamine release and total dopamine content in mice with a pan-neuronal genetic deletion of SV2C (Dunn *et al.*, 2017b). Here, we sought to further investigate

the role of SV2C in dopamine vesicle handling and to determine how overexpression of SV2C affects dopamine packaging. To these ends, we overexpressed SV2C *in vitro* and *in vivo* and characterized the effect of this overexpression on the dopamine system. We demonstrate successful overexpression and localization of SV2C to vesicles within cells and in mouse midbrain and striatum. We show SV2C overexpression leads to increased uptake of a dopamine analog *in vitro* as well as enhanced retention of dopamine in the synaptic vesicle over time and prolonged presence of dopamine in the synaptic cleft after electrically-stimulated dopamine release in C57BL/6 mice. These results identify SV2C as a mediator of dopamine vesicle packaging, retention, and release.

Materials and Methods

Cell culture. Human embryonic kidney cells (HEK293) stably expressing human VMAT2 (HEK+VMAT2) were cultured at 37°C with 5% CO₂ in selection media comprised of Dulbecco's Modified Eagle Medium (DMEM, Corning), 10% Fetal Bovine Serum (FBS, Atlanta Biologicals), and 1% Penicillin-Streptomycin (Pen Strep, Corning), and zeocin (100 µg/mL, InvivoGen). All human VMAT2-containing constructs were made in pcDNA3.1 vectors (Life Technologies) containing a zeocin resistance gene. Plasmids were transfected into HEK293 cells with Lipofectamine 2000 using the manufacturer protocol and stable cell lines were generated by repetitive rounds of limiting dilutions in selection media. Experimental media used for imaging was comprised of DMEM without phenol red (Corning), 1% Pen Strep (Corning), and 1% L-glutamine (Gibco).

Transfection. HEK+VMAT2 cells were seeded at 10,000 cells per well in half volume, black-walled, laminin-coated 96-well plates (Grenier Bio One) or at 60,000 cells per well on laminin-coated glass-bottom 8 well chamber dishes (LakTek) in selection media. Twenty-four

hours after seeding, selection media was removed and replaced with transfection media [DMEM (Corning) with 10% FBS (Atlanta Biologicals)] and cells were transiently transfected with either miniSOG-tagged pcDNA 3.1 vector or miniSOG-tagged human SV2C vector (2 μ g DNA) and Lipofectamine 2000 (Thermo Fisher). The miniSOG vector was provided by Dr. Roger Tsien's laboratory (Shu *et al.*, 2011). Cells were allowed to incubate at 37°C with 5% CO₂ with the Lipofectamine/DNA complexes for 4-6 hours before media was aspirated and replaced with fresh transfection media. Cells incubated overnight at 37°C with 5% CO₂ and were used the following day for the FFN206 assay or TIRF imaging.

Fluorescent false neurotransmitter 206 (FFN206) assay. HEK+VMAT2 cells were seeded at 40,000 cells per well in half volume, black-walled, laminin-coated 96-well plates (Grenier Bio One) and maintained in selection media at 37°C with 5% CO₂ until 90-100% confluent (approximately 24 hours). Upon reaching confluency, selection media was aspirated and replaced with 90 μ L of either experimental media or experimental media containing tetrabenazine or bafilomycin. Plates were incubated with tetrabenazine or bafilomycin for 30 minutes at 37°C with 5% CO₂ before FFN206 (Abcam) was diluted in experimental media and added to the appropriate wells to produce a final concentration of 1 μ M FFN206 per well. Plates were incubated with FFN206 for 60 minutes at 37°C with 5% CO₂. Wells were then washed with sterile phosphate-buffered saline (PBS, Gibco) and imaged in PBS on a BioTek Synergy H1 multi-mode plate reader (FFN206 peak excitation = 369 nm; peak emission = 464 nm).

Live-cell total internal reflection fluorescence microscopy. HEK+VMAT2 cells transiently transfected with either miniSOG-tagged pcDNA3.1 vector or miniSOG-tagged hSV2C, as described above, were incubated with experimental media containing 1 μ M FFN206 (Abcam) for 1 hour at 37°C with 5% CO₂. The FFN206-containing media was aspirated and replaced with fresh experimental media. Cells were then imaged at 37°C with 5% CO₂ on the GE Delta Vision

OMX total internal reflection fluorescence (TIRF) microscope (FFN206 peak excitation = 369 nm; peak emission = 464 nm).

Mice. Male and female wildtype C57BL/6 mice (2 months of age) were purchased from Charles River Laboratories. Mice were group-housed in a 12-hour light cycled room with food and water *ad libitum*. SV2C knockout mice (SV2C-KO) were generated as previously described (Dunn *et al.*, 2017b). Briefly, C57BL/6 embryonic stem cells from the European Conditional Mouse Mutagenesis Program containing the SV2C “knockout-first construct” (Skarnes *et al.*, 2011) were implanted into female C57BL/6 mice. Heterozygous knockout-first (KOF) mice were then bred with FLP homozygous mice (Charles River) to excise the LacZ/neo cassette and restore a functional gene, with exon 2 flanked by loxP sites. Heterozygous SV2C-floxed mice positive for FLP were crossed with nestin-CRE mice (Charles River), then bred to homozygosity to generate global neuronal knockout of SV2C. Mice were separated into individual cages with food and water *ad libitum* one day prior to collecting tissue for immunohistochemistry or radioactive dopamine uptake. All procedures were carried out in accordance with NIH guidelines and the Institutional Animal Care and Use Committee at Emory University.

Stereotactic injections. C57BL/6 mice were anesthetized with vaporized isoflurane 1-4% (Piramal Healthcare) and placed into a stereotaxic frame with nose cone. Anesthesia was maintained using 1-2% isoflurane for the duration of surgery. An incision was made along the midline of the scalp. Thirty percent hydrogen peroxide was used to clean the skull and to better visualize lambda and bregma and ensure that the head was level. A hole was drilled through the skull above the left substantia nigra and AAV 2/9 vectors containing either mCherry or miniSOG-tagged SV2C were injected at a rate of 0.5 μ L per minute (2 μ L vector; AP -3.2 mm, ML -1.2 mm, DV -4.5 mm from surface of the brain). After each injection, the needle (pulled glass needle attached to a Hamilton syringe) was left in place for five minutes and then was slowly withdrawn.

The skin was glued back together (3M Vetbond) and neomycin antibiotic ointment (Waterjel) and lidocaine cream (Aspercreme) were placed on the incision. Animals were allowed to recover in their home cage on a heating pad for one-hour post-surgery. Buprenorphine injections were given once within this hour of recovery for post-operative pain relief (Buprenex, McKesson, dose 0.05 mg/kg body weight) and again the morning after surgery. Animals were monitored daily for three days post-surgery and were sacrificed for tissue collection 8 weeks post-surgery.

Western blotting. C57BL/6 mice injected with AAV2/9 mCherry or AAV2/9 miniSOG-SV2C (n = 2 per group) were decapitated and dissected striata were flash-frozen in liquid nitrogen. The frozen tissue was homogenized in homogenization buffer (HB; 4 mM HEPES, 0.32 M sucrose, pH 7.4) and protease inhibitors (1:1000) using an immersion homogenizer (Tissue Tearor) for 15 seconds. This homogenate was centrifuged at 1150 x g for 5 minutes at 4 °C and the resultant supernatant was centrifuged at 18,407 x g for 45 minutes at 4 °C. The pellet was resuspended in HB plus protease inhibitors and protein content was determined by BCA assay. Samples (9 µg of protein) were subjected to gel electrophoresis on 4-12% bis-tris gels (NuPAGE) before being transferred onto a polyvinylidene difluoride (PVDF) membrane at 4 °C, blocked with 7.5% nonfat dry milk for one hour at room temperature, and incubated with appropriate primary antibody overnight at 4 °C with gentle agitation (rabbit anti-TH was purchased from Millipore (AB152); rat anti-DAT was purchased from Millipore (MAB369); polyclonal rabbit anti-mSV2C antibodies were designed by our lab and custom-produced by Covance as described previously (Dunn *et al.*, 2017a); mouse anti-alpha-synuclein was purchased from BD Transduction Laboratories; mouse anti-actin was purchased from Sigma). The following day, blots were incubated at room temperature for 1 hour with the appropriate secondary antibody (HRP-conjugated). Signal was amplified using chemiluminescence (Thermo) and visualized using a BioRad UV imager. Densitometry was conducted using Image Lab software (Bio Rad).

Fluorescent immunohistochemistry. Mice injected with AAV2/9 mCherry or AAV2/9 miniSOG-SV2C were killed by rapid decapitation or transcardial perfusion. Brains were removed and placed in 4% paraformaldehyde for fixation followed by storage in 30% (wt/vol) sucrose. Brains were sectioned to 40 μm . As fluorescence was conferred by successful injection and expression of mCherry or miniSOG-SV2C AAV 2/9 vectors, slices were not incubated with any primary or secondary antibodies. Slices were mounted and slides were treated with hard-set mounting medium (Vector Laboratories) before being coverslipped.

Radioactive dopamine uptake and leak. Mice were decapitated and striatal dissections (n = 3-8 mice per group) were homogenized with 15 up-and-down strokes by hand in glass/Teflon homogenizers containing 5 mL HB. Glass tubes were rinsed with 5 mL HB, the contents of the tubes were centrifuged at 1000 x g for 10 minutes at 4 °C, and the resulting supernatants were centrifuged at 20,000 x g for 20 minutes at 4 °C. The resulting pellets were resuspended in 1.6 mL HB by pipetting up and down 30 times before they were transferred to a glass/Teflon homogenizer containing 6.4 mL cold water. The resuspended pellets were subjected to 20 up-and-down strokes by hand before being transferred to tubes containing 1 mL of 250 mM HEPES (0.250 M HEPES, pH 7.5) and 1 mL of 1 M potassium tartrate (1.039 M potassium tartrate, pH 7.5). Tubes were centrifuged at 20,000 x g for 20 minutes at 4 °C, and the resulting supernatants were placed in ultracentrifuge tubes and centrifuged at 120,000 x g at 4 °C for 2 hours. The resulting pellets (vesicles) were resuspended in complete assay buffer (100 mM potassium tartrate, 25 mM HEPES, 0.1 mM EDTA, 0.05 mM EGTA, 1.7 mM ascorbate, 2 mM ATP, pH 7.4) and then passed through a 27-gauge needle to fully suspend the vesicles. Uptake assays used 50 μL of vesicle solution, 175 μL of complete buffer +/- tetrabenazine (TBZ; 10 μM TBZ (Sigma) in complete buffer), and 25 μL [^3H] dopamine solution (0.876% [^3H] dopamine and 0.1% cold dopamine in complete buffer) per replicate (three specific replicates and one nonspecific replicate per animal). Samples were

incubated in complete buffer +/- TBZ for 10 minutes at 30 °C before the addition of [³H] dopamine and further incubation for 3 minutes at 30 °C. The assay was terminated by filtration through 0.5% polyethylenamine-soaked Whatman GF/F filters (Brandel). To measure radioactive dopamine leak, samples were incubated in complete buffer +/- TBZ for 10 minutes at 30 °C, [³H] dopamine was added and samples incubated for 3 minutes at 30 °C, and radioactive dopamine loading was halted by placing samples on ice and adding 175 µL of complete buffer + TBZ to each sample. This addition effectively halted the activity of VMAT2, preventing additional uptake of radiolabeled dopamine. Samples then incubated on ice for 2.5, 5, or 7.5 minutes before each assay was terminated by filtration through 0.5% polyethylenamine-soaked Whatman GF/F filters (Brandel). Filters were placed in scintillation fluid and counted using a Beckman LS6500 (Beckman Instruments, Fullerton, CA). Dopamine specific uptake was determined by subtracting counts from VMAT2-inhibited (10 µM tetrabenazine) reactions at each data point. Counts were normalized to a [³H] radioactivity standard and to total protein, as determined by a bovine serum albumin assay (Pierce). Two-tailed, unpaired t-tests and one-way ANOVAs with Dunnett's multiple comparisons test were performed as appropriate to determine differences between groups.

Fast scan cyclic voltammetry (FSCV). Slice FSCV was performed in the lateral dorsal striatum of male and female mice (4 months of age, n = 3-8 mice per group) injected with AAV 2/9 vectors containing either mCherry or miniSOG-SV2C. Mice were decapitated and the brain was rapidly removed and placed in ice-cold oxygenated (95% O₂ / 5% CO₂) sucrose artificial cerebral spinal fluid (aCSF; 193 mM sucrose, 11 mM d-glucose, 1.2 mM dihydrous CaCl₂, 4.5 mM KCl, 25 mM NaHCO₃, 20.5 mM NaCl, 1.2 mM NaH₂PO₄ monobasic, 2.6 mM MgCl₂, pH 7.4). Brains were then sliced coronally at 300 µm using a vibratome (Leica VT1000 S). Striatal slices were selected and bathed in oxygenated HEPES aCSF (19.7 mM HEPES, 11 mM d-glucose, 2.4 mM dihydrous CaCl₂, 25 mM NaHCO₃, 126.4 mM NaCl, 2.5 mM KCl, 1.2 mM monobasic

NaH₂PO₄, 2.6 mM MgCl₂, pH 7.4) at 20 °C for 30 mins prior to recording. For recording, a slice was superfused in 30 °C HEPES aCSF for the duration of the experiment. The cylindrical carbon-fiber (6 μm diameter, Thornel) recording microelectrodes were fabricated in-house by aspirating a single carbon fiber (7 μm radius, A-M Systems, Inc.) into a glass capillary. Filled glass capillaries were sealed and cut such that the length of the exposed carbon-fiber was approximately 65 μm from the end of the seal. Recording microelectrodes were backfilled with 150 mM potassium chloride using a spinal needle and a 4.5 in Kynal UL 1422 28/1 g wire was inserted into the open end of the capillary tube. A bipolar tungsten stimulating electrode (MicroProbes) and the recording electrode were placed on the surface of the slice in the striatum, forming an equilateral triangle. Stimulation was applied via the stimulating electrode (monophasic, 60 Hz, 2.31 V to produce a 700 μA stimulation) and stimulations were separated by five minutes. Dopamine release was averaged from five sites surveying the unilateral dorsal striatum, with five recordings at each site. Application of waveform, stimulus, and current monitoring was controlled by TarHeel CV (University of North Carolina) using a custom potentiostat (UEI, UNC Electronics Shop). The waveform for dopamine detection consisted of a -0.4 holding potential versus an Ag/AgCl (World Precision Instruments, Inc.) reference electrode. The applied cyclic voltage ramp went from -0.4 V to 1.0 V at a rate of 600 V/s at 60 Hz. The current at the peak oxidation potential for dopamine (0.6 vs Ag/AgCl) was used to evaluate dopamine concentration changes with time, and electrode sensitivity was calibrated to known dopamine standards in HEPES aCSF solution following the experiment. Primary outcome measures were peak dopamine release and tau. Peak dopamine release was evaluated by calculating the maximum current and dividing it by the calibration constant for that electrode, while tau was evaluated by determining the speed with which the dopamine signal was terminated. Nonlinear regression analysis was conducted to calculate the kinetic constant tau, which was defined as the amount of time in seconds needed to return to 66.6%

of baseline. Two-tailed t-tests were performed to determine differences in peak stimulated dopamine release and dopamine clearance between groups.

Statistical analyses. Data were analyzed by two-tailed t-test or one-way ANOVA with post hoc analyses as appropriate. All analyses were performed using GraphPad Prism software.

Results

Localization of in vitro expression of SV2C and pcDNA3.1. To evaluate how SV2C affects dopamine handling, we first transiently transfected miniSOG-tagged pcDNA3.1 or miniSOG-tagged SV2C into human embryonic kidney cells (HEK293) stably transfected with the human vesicular monoamine transporter 2 (hVMAT2; HEK+VMAT2 cells; pcDNA3.1 transfected cells: HEK+VMAT2+pcDNA3.1; SV2C-transfected cells: HEK+VMAT2+SV2C). To confirm the proper expression and localization of our transfected miniSOG-pcDNA3.1 vector and miniSOG-SV2C protein within the cell, we imaged single HEK+VMAT2+pcDNA3.1 and HEK+VMAT2+SV2C cells at high resolution on a GE Delta Vision OMX total internal reflection fluorescence (TIRF) microscope (Figure 3.1). We observed diffuse miniSOG fluorescence throughout the cytosol and the vesicle-like compartments of HEK+VMAT2+pcDNA3.1 cells (Figure 3.1, top left), while miniSOG fluorescence was punctate and compartmentalized to the vesicle-like compartments in HEK+VMAT2+SV2C cells (Figure 3.1, bottom left). The diffuse fluorescence in pcDNA transfected cells compared to the punctate fluorescence in SV2C transfected cells indicates that miniSOG-tagged SV2C was expressed on the vesicle-like compartments of HEK+VMAT2+SV2C cells.

SV2C overexpression increases vesicle packaging. To first confirm that our transfection protocol did not disrupt the function of the stably expressed VMAT2 protein on the vesicle-like compartments of HEK+VMAT2 cells, we incubated HEK+VMAT2+pcDNA3.1 and

HEK+VMAT2+SV2C expressing cells with FFN206, a monoamine analog and a substrate of VMAT2 (Hu *et al.*, 2013). FFN206 fluoresces in low pH environments, such as the acidic lumen of the vesicle-like compartments in HEK cells. As such, measuring FFN206 fluorescence is a proxy for VMAT2 function and vesicle loading. We observed FFN206 fluorescence within both a single HEK+VMAT2+pcDNA3.1 cell (Figure 3.1, top center) and a population of HEK+VMAT2+pcDNA3.1 cells (Figure 3.2A, second from right). FFN206 fluorescence was localized to the VMAT2-containing vesicle-like compartments in HEK+VMAT2+pcDNA cells (Figure 3.1, top right). We also observed FFN206 fluorescence in a single HEK+VMAT2+SV2C cell (Figure 3.1, bottom center) and in a population of HEK+VMAT2+SV2C cells (Figure 3.3A, second from right). FFN206 fluorescence was again localized to the VMAT2-containing vesicle-like compartments in HEK+VMAT2+SV2C cells (Figure 3.1, bottom right). This punctate pattern of FFN206 fluorescence indicates that the transfection protocol did not affect VMAT2 function. To further confirm that the transfection did not affect VMAT2 function or the maintenance of the proton gradient present across the vesicular membrane, we treated HEK+VMAT2+pcDNA3.1 and HEK+VMAT2+SV2C cells with 10 μ M tetrabenazine or 1 μ M bafilomycin. Tetrabenazine is a pharmacological inhibitor of VMAT2 and bafilomycin inhibits the vacuolar H⁺ ATPase that maintains the vesicular proton gradient. As anticipated, treatment with tetrabenazine and bafilomycin resulted in almost total loss of FFN206 fluorescence in both HEK+VMAT2+pcDNA3.1 cells (Figure 3.2A center and right; quantified in 3.2B) and HEK+VMAT2+SV2C cells (Figure 3.3A center and right; quantified in 3.3B). This suggests that our transfection does not disrupt normal vesicle function. After confirming that our transfection protocol did not alter normal vesicle function, we sought to determine whether the presence of SV2C differentially affected vesicle packaging *in vitro*. We observed significantly increased FFN206 fluorescence in HEK+VMAT2+SV2C cells incubated with 1 μ M FFN206 for one hour

as compared to HEK+VMAT2+pcDNA cells incubated with 1 μ M FFN206 for one hour (Figure 3.4, $p = 0.0026$).

Establishment of AAV2/9 virus expression protocol. After successful addition of SV2C in an *in vitro* system, we sought to recapitulate these results in an *in vivo* system with intact neuronal pathways. To this end, we adapted a rat stereotactic injection protocol for use in mouse substantia nigra (Reimsnider *et al.*, 2007). We infused either AAV2/9 mCherry or AAV2/9 miniSOG-SV2C vectors into the left substantia nigra (AP -3.2 , ML -1.2 , DV -4.5 from surface of the brain) of 2-month old male and female C57BL/6 mice. Eight weeks post-surgery, we harvested tissue from the injected mice and checked for viral expression in both the midbrain and striatum of both the injected (left) and the un-injected (right) hemispheres. As the laboratory had not previously performed this injection protocol and SV2C had not been overexpressed *in vivo*, we validated the viral injection protocol via fluorescent immunohistochemistry (IHC) and western blotting before performing assays assessing functional repercussions of SV2C overexpression.

Fluorescent immunohistochemistry. We first validated the viral injection protocol through fluorescent immunohistochemistry (Figures 3.5 and 3.6). In the mCherry-injected mice, we observed robust mCherry fluorescence in the midbrain of the injected hemisphere with an absence of fluorescence in the un-injected hemisphere (Figure 3.5A), as well as visible mCherry labeling of the striatum in the injected hemisphere and no labeling in the un-injected hemisphere (Figure 3.5B). In the miniSOG-SV2C injected mice, we observed miniSOG-SV2C fluorescence in the region known to be populated with nigrostriatal dopamine neurons in the injected hemisphere and an absence of fluorescence in the un-injected hemisphere (Figure 3.6).

Western blotting. Immunoblot analyses were performed on midbrain and striatal homogenates isolated from mice injected with either mCherry or miniSOG-SV2C ($n = 2$ per group, Figure 3.7). SV2C injection resulted in an increase in SV2C expression in the midbrain and

striatum of SV2C-injected mice as compared to mCherry-injected mice (Figure 3.7). Injection of SV2C did not lead to a significant alteration in expression of tyrosine hydroxylase (TH) or the dopamine transporter (DAT) in the midbrain or striatum of SV2C-injected mice (Figure 3.7).

SV2C overexpression does not increase vesicle packaging. After confirming that we were able to overexpress SV2C in nigrostriatal dopamine neurons, we sought to determine whether this increase in expression led to functional consequences in dopamine neurotransmission. We first assessed the influence of SV2C on dopamine packaging through radioactive dopamine uptake. Striatal vesicles from mice injected with mCherry (WT, n = 3) and from mice injected with SV2C (SV2C-OE, n = 8) were isolated through differential centrifugation and incubated with radioactive dopamine for three minutes, after which time vesicle loading was arrested by filtration. Peak VMAT2-specific radioactive dopamine uptake was normalized according to protein concentration and a radioactive dopamine standard. There was no difference in peak dopamine uptake between WT and SV2C-OE vesicles ($p = 0.2270$, unpaired two-tailed t-test, $\alpha = 0.05$, Figure 3.8), though SV2C-OE vesicles exhibited greater variance in dopamine uptake than WT vesicles.

SV2C overexpression increases vesicular retention of dopamine over time. After observing that the overexpression of SV2C did not lead to an increase in the peak amount of dopamine the vesicle could hold, we then sought to determine whether SV2C was involved in the dynamic process of dopamine handling. To this end, we measured retention of dopamine over time (Figure 3.9). Dopamine is actively loaded into vesicles via VMAT2; however, if the activity of VMAT2 is arrested or inhibited, dopamine will leak out of the vesicle over time. To measure the effect of SV2C expression on dopamine leak, isolated vesicles from un-injected WT mice and WT mice injected with mCherry (n = 6-7), SV2C-OE (n = 3), and mice with a pan-neuronal deletion of SV2C (SV2C-KO, n = 3-4) were incubated with radioactive dopamine for three minutes before vesicle loading was arrested by addition of tetrabenazine, a pharmacological inhibitor of VMAT2.

Because there was no difference in uptake recorded from un-injected WT mice and mCherry-injected WT mice, these samples were collapsed into one WT group. Samples were then incubated on ice for either 2.5, 5, or 7.5 minutes before dopamine leak was arrested through filtration. Because the peak amount of dopamine packaged into WT and SV2C-OE vesicles varied, residual dopamine present in the vesicles at each time point was represented as a percentage of the peak dopamine uptake for each group. SV2C-OE mice exhibited a strong trend toward decreased dopamine leak, or increased retention of dopamine, as compared to WT mice after 2.5 minutes ($p = 0.0559$), 5 minutes ($p = 0.0734$), and 7.5 minutes ($p = 0.0559$). SV2C-KO mice exhibited a general trend toward increased dopamine leak, or decreased retention of dopamine, as compared to WT mice (2.5 min.: $p = 0.4044$, 5 min.: $p = 0.3898$, 7.5 min.: $p = 0.0610$, one-way ANOVA with Dunnett's multiple comparisons test, Figure 3.9).

SV2C overexpression does not affect the amount of dopamine released, but decreases the rate of dopamine clearance. We next assessed the influence of SV2C on dopamine release and removal from the synapse through fast scan cyclic voltammetry. Mice injected with mCherry ($n = 3$) or SV2C ($n = 8$) were decapitated and striatal slices were isolated and kept in oxygenated HEPES aCSF. Dopamine release was stimulated by a single electrical pulse in the dorsal striatum and was averaged across five sites per mouse. There was no difference in peak dopamine release in mCherry-injected and SV2C-injected mice ($p = 0.4194$, two-tailed t-test, Figure 3.10 A&B), though DAT-mediated dopamine clearance rate was diminished in SV2C-injected mice as evidenced by increased tau in mice overexpressing SV2C ($p < 0.0001$, two-tailed t-test, Figure 3.10 C&D).

Discussion

The goal of the present study was to determine the role of SV2C in dopamine vesicle handling. We overexpressed SV2C *in vitro* and show this overexpression results in increased uptake of a dopamine analog. Overexpressing SV2C *in vivo* resulted in enhanced retention of dopamine in the vesicle and prolonged presence of dopamine in the synaptic cleft following electrically-stimulated dopamine release in C57BL/6 mice. These results indicate that SV2C expression affects dopamine vesicle packaging and retention.

We utilized miniSOG-tagged SV2C constructs to overexpress SV2C in both cells and mice. MiniSOG is a mini Singlet Oxygen Generator tag that was developed for electron microscopy. MiniSOG generates singlet oxygen when illuminated by blue light and fluoresces in the green range (Shu *et al.*, 2011). We first overexpressed miniSOG-SV2C and miniSOG-pcDNA3.1 vectors in HEK cells stably expressing VMAT2. Though HEK293 cells are not neuronal cells, they are derived from the same precursor cell line as neurons and possess vesicle-like compartments, causing them to often be utilized as a model for neural function (Thomas and Smart 2005). In addition, HEK293 cells do not express SV2 proteins and are easily transfected, making them an ideal model for investigating SV2C function. High resolution imaging of single cells confirmed proper differential localization of miniSOG-SV2C and miniSOG-pcDNA3.1: miniSOG-SV2C was confined to the vesicle-like compartments of the HEK+VMAT2 cells with minimal to no miniSOG fluorescence in the cytoplasm, while miniSOG-pcDNA3.1 fluorescence was visible throughout the cytosol with some punctate staining in the vesicle-like compartments. This differential pattern of miniSOG fluorescence indicates that transfected SV2C was properly localized to the vesicular membrane.

We also confirmed the proper localization of SV2C on vesicles by measuring the colocalization of miniSOG fluorescence and FFN206 fluorescence. As described in chapter 2, the

fluorescent false neurotransmitter 206 (FFN206) is a monoamine analog and a substrate of VMAT2 that fluoresces in acidic compartments such as the vesicle lumen (Hu *et al.*, 2013). FFN206 fluorescence is confined to VMAT2-containing compartments; therefore, the high degree of overlap of miniSOG-SV2C and FFN206 fluorescence indicates that SV2C is located on VMAT2-containing compartments. We then confirmed that our transfection protocol did not disrupt VMAT2 function or normal vesicle function by incubating a population of cells transfected with SV2C or pcDNA3.1 with FFN206 with tetrabenazine or bafilomycin. Tetrabenazine is a pharmacological inhibitor of VMAT2 and bafilomycin inhibits the vesicular H⁺ ATPase that maintains the vesicular proton gradient. Disruption of VMAT2 function via tetrabenazine inhibition should result in a loss of VMAT2-mediated FFN206 loading and thus decreased FFN206 fluorescence, while disruption of the vesicular proton gradient via treatment with bafilomycin should result in a loss of FFN206 fluorescence as the vesicle lumen is de-acidified. As anticipated, treatment with tetrabenazine and bafilomycin resulted in almost total loss of FFN206 fluorescence in both SV2C-transfected pcDNA3.1-transfected cells, indicating that our transfection protocol did not disrupt VMAT2 or normal vesicle function.

After confirming that we had produced an *in vitro* system that overexpressed SV2C without compromising normal vesicle function, we were then able to assess the effect of SV2C overexpression on vesicle handling. To that end, we again treated populations of cells transfected with either SV2C or pcDNA3.1 with FFN206 and compared the FFN206 fluorescence intensity after one hour of incubation. We observed a significant increase in fluorescence in cells transfected with SV2C compared to cells transfected with pcDNA3.1, indicating that the addition of SV2C allowed cells to package more FFN206 into their vesicle-like compartments. It is possible that the increase in capacity for FFN206 loading derives from the formation of an intravesicular glycomatrix within the SV2C-containing vesicles. In 2003, Reigada and colleagues reported that

only 5% of neurotransmitters in synaptic vesicles are in solution within the vesicular lumen, with the remaining 95% of transmitter being absorbed into a proteoglycan matrix that is predominantly comprised of SV2 (Reigada *et al.*, 2003). They further proposed that the intravesicular matrix acts as a smart gel, absorbing neurotransmitter molecules within the vesicle and thus decreasing the amount neurotransmitter in solution inside the vesicle lumen and reducing the neurotransmitter concentration gradient present across the vesicle membrane. This effect is thought to regulate both the loading of neurotransmitter into vesicles and the quantity of neurotransmitter released upon vesicle fusion (Nowack *et al.*, 2010; Reigada *et al.*, 2003; Vautrin 2009). Taken together, the increase in FFN206 fluorescence in cells containing SV2C could support that SV2C produces an intravesicular gel matrix that absorbs neurotransmitter molecules, with a greater amount of SV2C allowing for greater absorption of transmitter.

After successful addition of SV2C in an *in vitro* system, we sought to recapitulate these results in an *in vivo* system with intact neural pathways. To this end, we adapted a rat stereotactic injection protocol (Reimnsider *et al.*, 2007) to infuse either AAV2/9 mCherry or AAV2/9 miniSOG-SV2C vectors produced by Dr. Fredric Manfredsson into the left substantia nigra of two month old male and female C57BL/6 mice. We validated the viral injection protocol via fluorescent IHC and western blotting and show that we were able to overexpress SV2C in midbrain neurons in the region of the substantia nigra. We then performed assays assessing functional repercussions of this SV2C overexpression. We first assessed the influence of SV2C on dopamine packaging and retention through radioactive dopamine uptake and show that synaptic vesicles isolated from the striatum of mice injected with SV2C exhibited no difference in dopamine loading as compared to vesicles isolated from WT mice. The lack of increased dopamine loading in the SV2C overexpressing vesicles was unexpected, given the significant increase in FFN206 packaging that was measured in cells overexpressing SV2C *in vitro*.

We next assessed whether SV2C expression affected the dynamic process of dopamine handling instead of increasing the peak amount of dopamine packaged into the vesicle. To this end, we measured dopamine leak, or the retention of dopamine within the vesicle over time. Synaptic vesicles are inherently leaky, meaning neurotransmitter levels in the vesicle will decline unless neurotransmitter is continually loaded from the cytosol into the vesicle (Floor *et al.*, 1982; Takami *et al.*, 2017). Isolated vesicles from WT and SV2C overexpressing mice were incubated with radioactive dopamine for three minutes before vesicle loading was arrested by addition of tetrabenazine. Samples were then incubated on ice for either 2.5, 5, or 7.5 minutes before dopamine leak was arrested through filtration. SV2C overexpressing mice exhibited a strong trend toward decreased dopamine leak, or increased retention of dopamine, as compared to WT mice after 2.5 minutes, 5 minutes, and 7.5 minutes. This leak time course was compared to vesicle leak in mice with a pan-neuronal deletion of SV2C (SV2C-KO), thus producing a spectrum of SV2C expression. While SV2C-KO mice did not significantly differ in their retention of dopamine as compared to WT mice at any of the time points measured, SV2C-KO mice exhibited a general trend toward increased dopamine leak. Taken together, these results indicate that SV2C expression mediates dopamine retention, with increased expression of SV2C leading to increased retention of dopamine over time and decreased expression of SV2C leading to decreased retention of dopamine over time (Figure 3.9).

We then assessed the influence of SV2C on dopamine release and removal from the synapse through fast scan cyclic voltammetry. We observed no difference in peak dopamine release in mCherry-injected and SV2C-injected mice, which aligns with our above finding that there is no difference in peak dopamine uptake in mCherry-injected and SV2C-injected mice. We further show that the dopamine clearance rate was diminished in SV2C-injected mice as evidenced by increased tau in mice overexpressing SV2C. Dopamine clearance is mediated by DAT and a

decrease in dopamine clearance rate can be caused by a decrease in DAT expression or impaired DAT function. Immunoblot analyses on midbrain and striatal homogenates indicated that injection of SV2C did not lead to a significant alteration in expression of TH or DAT. This lack of compensatory alteration in dopaminergic proteins as a result of SV2C overexpression suggests that increasing SV2C expression does not have a drastic enough effect on the dopamine system to downregulate the production or reuptake of dopamine, and also indicates that the decrease in dopamine clearance rate observed in SV2C overexpressing mice results from a gain of function from SV2C expression and not from altered DAT expression.

Taken together, SV2C overexpression leads to increased retention of vesicular dopamine over time and a decrease in dopamine clearance rate *in vivo*. As indicated in the above discussion of our *in vitro* data, these findings could be explained by the presence of an intravesicular gel matrix formed in part by SV2C that mediates neurotransmitter loading and release (Nowack *et al.*, 2010; Reigada *et al.*, 2003; Vautrin 2009).

Vesicular proteins interact to form a large protein complex comprised of SV2, synaptotagmin, synaptophysin, vesicle-associated membrane protein, and the vacuolar proton pump (Baldwin and Barbieri 2007; Baldwin and Barbieri 2009; Bennett *et al.*, 1992). The intravesicular domains of these proteins form an intraluminal assembly with a uniform shape that is found in all synaptic vesicles. It has been proposed that SV2 is the mainstay of this luminal assembly and acts as a backbone to which other vesicular proteins attach (Harlow *et al.*, 2013; Szule *et al.*, 2015). In 2003, Reigada and colleagues proposed that this luminal assembly also acts as a gel matrix within the vesicle, finding that a majority of neurotransmitter in synaptic vesicles is absorbed into a proteoglycan matrix (Reigada *et al.*, 2003). By examining cholinergic vesicles isolated from *Torpedo* electric organ nerve terminals and measuring co-release of acetylcholine and ATP, Reigada and coworkers proposed that the intravesicular matrix acts as a smart gel that

regulates the loading of neurotransmitter into vesicles, the quantity of neurotransmitter released upon vesicle fusion, and the rate of neurotransmitter release, as neurotransmitter bound within the gel matrix requires ion-exchange in order to be released (Nowack *et al.*, 2010; Reigada *et al.*, 2003; Vautrin 2009).

The intravesicular loop of SV2A and SV2B contains three conserved sites for N-glycosylation; however, SV2C contains five predicted glycosylation sites (Bajjalieh *et al.*, 1994; Janz and Sudhof 1999), thus suggesting the potential for formation of a denser gel matrix with a higher proportion of glycosyl residues per unit in vesicles containing higher copy numbers of SV2C. Previous studies further indicate that glycosylation mediates normal SV2 function: mutation of the glycosylation sites of SV2A disrupts normal protein folding and trafficking (Chang and Sudhof 2009) and glycosylation mediates the binding of SV2C to botulinum neurotoxin A (Mahrhold *et al.*, 2016; Yao *et al.*, 2016). While an increase in the expression of SV2C does not increase the peak amount of dopamine loaded into the vesicle *in vivo*, excess SV2C on the vesicle could still create a denser vesicular gel matrix that shifts the distribution of dopamine within the vesicle and thus alters the rate at which dopamine is released upon vesicle fusion. This hypothesis is further expanded upon in Chapter 4.

Overall, in this chapter we sought to investigate the role of SV2C in the dopamine system. To this end, we overexpressed SV2C *in vitro* and *in vivo* and characterized the effect of this overexpression on dopamine vesicle handling and dopamine neuron vulnerability. We demonstrate *in vitro* and *in vivo* overexpression of SV2C and show that this overexpression leads to increased uptake of a dopamine analog *in vitro* as well as enhanced retention of dopamine in the vesicle over time and prolonged presence of dopamine in the synaptic cleft after electrically-stimulated dopamine release *in vivo*. These results indicate that SV2C mediates the retention of

dopamine within the vesicle and the release of dopamine from the vesicle during exocytosis and thus identify SV2C as a mediator of dopamine vesicle packaging, retention, and release.

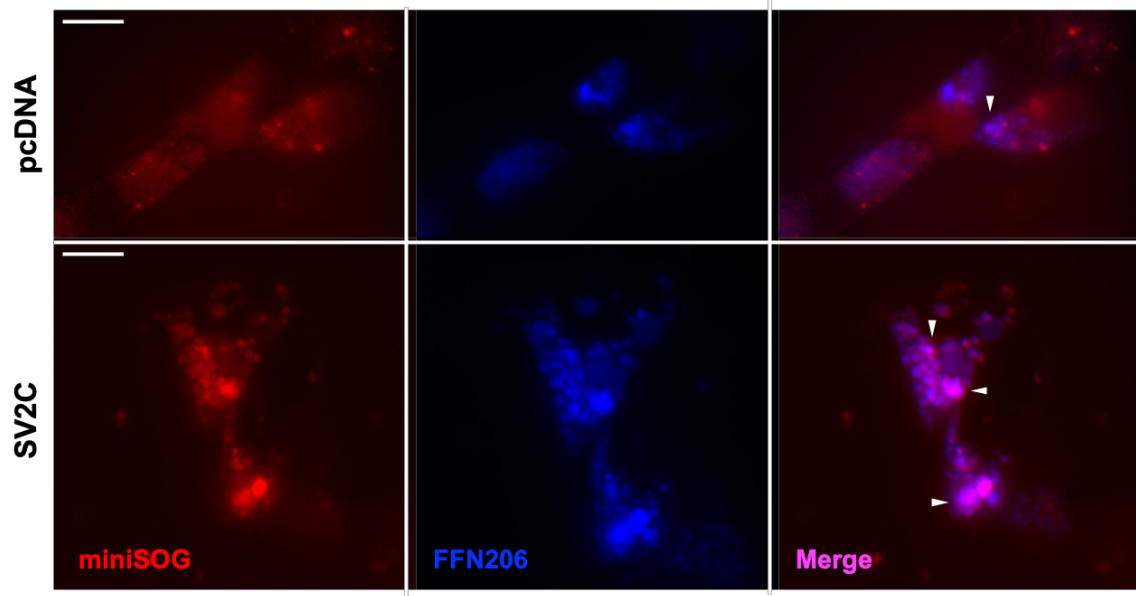


Figure 3.1. Localization of in vitro expression of SV2C and pcDNA3.1. HEK cells stably transfected with VMAT2 and transiently transfected with miniSOG-tagged pcDNA3.1 (top) or miniSOG-tagged SV2C (bottom) were then treated with FFN206. MiniSOG-pcDNA3.1 and miniSOG-SV2C fluorescence colocalized with VMAT2-dependent FFN206 fluorescence (FFN206: center; merge: right and denoted by arrows). MiniSOG-pcDNA3.1 and miniSOG-SV2C expression were pseudocolored red to enhance the visualization of colocalization with FFN206 fluorescence. Images taken with a GE Delta Vision OMX TIRF microscope at 60x magnification. Scale bar = 10 μ M.

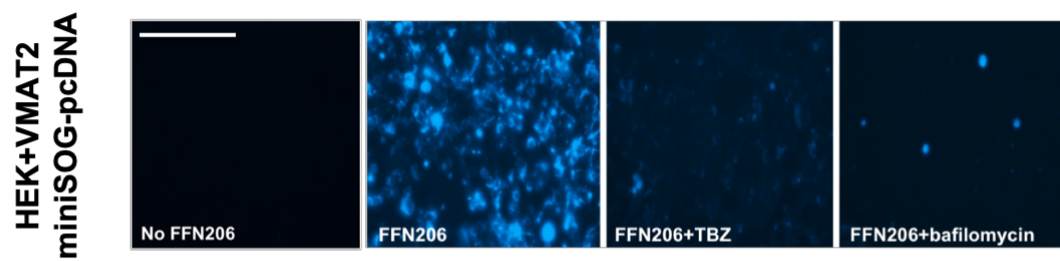
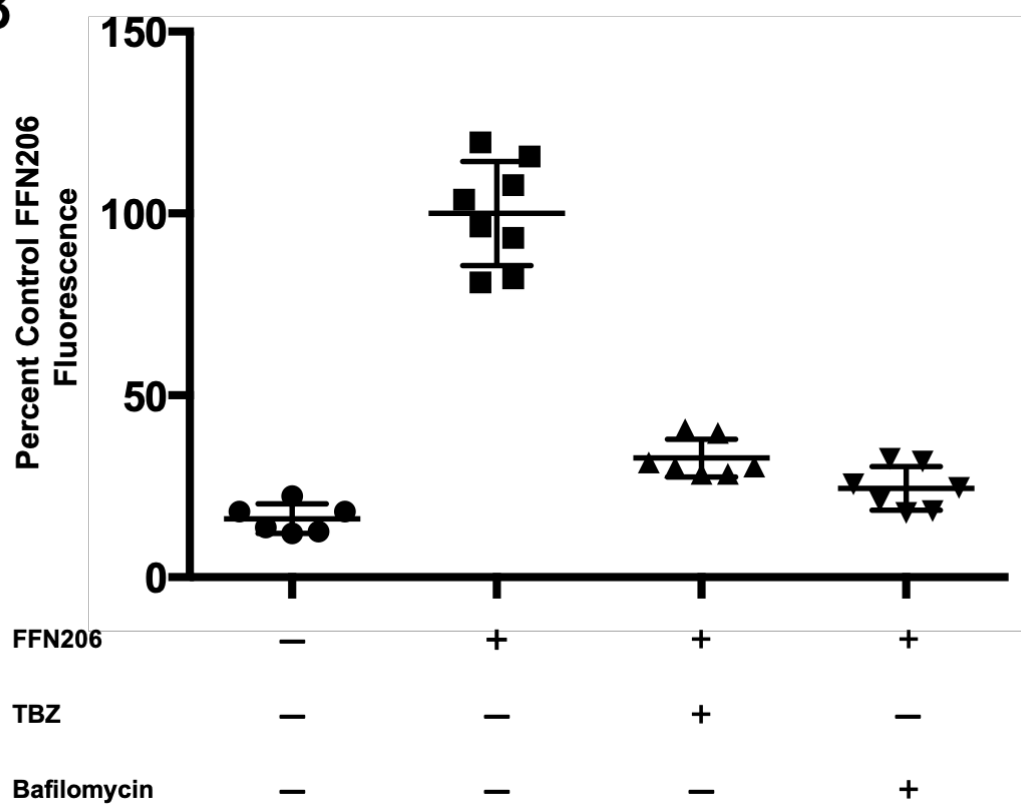
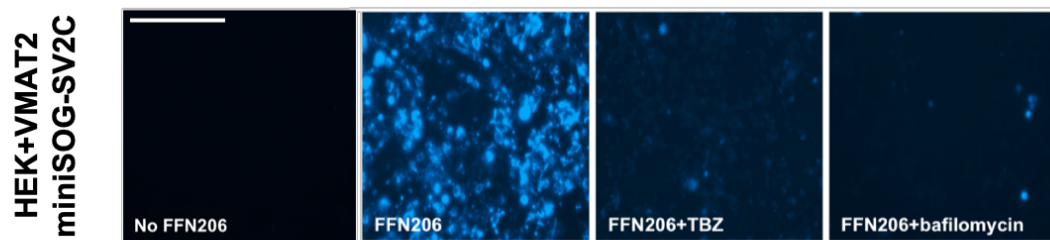
A**B**

Figure 3.2. Validation of a quantifiable vesicular uptake assay under transfection with miniSOG-pcDNA. A) pcDNA3.1 transfection does not affect normal VMAT2 function or vesicle loading. FFN206 loading is dependent on VMAT2 activity and maintenance of the vesicular proton gradient. HEK+VMAT2 cells transiently transfected with pcDNA3.1 and not treated with FFN206 exhibit minimal fluorescence (left image). HEK+VMAT2+pcDNA3.1 cells treated with FFN206 exhibit robust FFN206 fluorescence (second from left image). FFN206 uptake is diminished in HEK+VMAT2+pcDNA3.1 cells when VMAT2 function is inhibited by treatment with 10 μ M tetrabenazine (second from right image) and when the vesicular proton gradient is dissipated by treatment with bafilomycin (right image), indicating that pcDNA3.1 transfection does not interfere with normal FFN206 loading. Imaged by EVOS system at 10x magnification.

B) Quantification of FFN206 fluorescence observed in A. In the absence of FFN206, no fluorescence is observed in HEK+VMAT2+pcDNA3.1 cells. HEK+VMAT2+pcDNA3.1 cells treated with FFN206 exhibit robust fluorescence. FFN206 uptake is diminished in HEK+VMAT2+pcDNA3.1 cells when VMAT2 function is inhibited by treatment with 10 μ M tetrabenazine. FFN206 uptake is diminished in HEK+VMAT2+pcDNA3.1 cells when the vesicular proton gradient is dissipated by treatment with bafilomycin. Graph displayed as mean and standard error of the mean of percent control FFN206 fluorescence (control group: HEK+VMAT2+pcDNA3.1 cells incubated with FFN206). Each point represents one well of cells from a 96-well plate. Scale bar = 400 μ M.

A



B

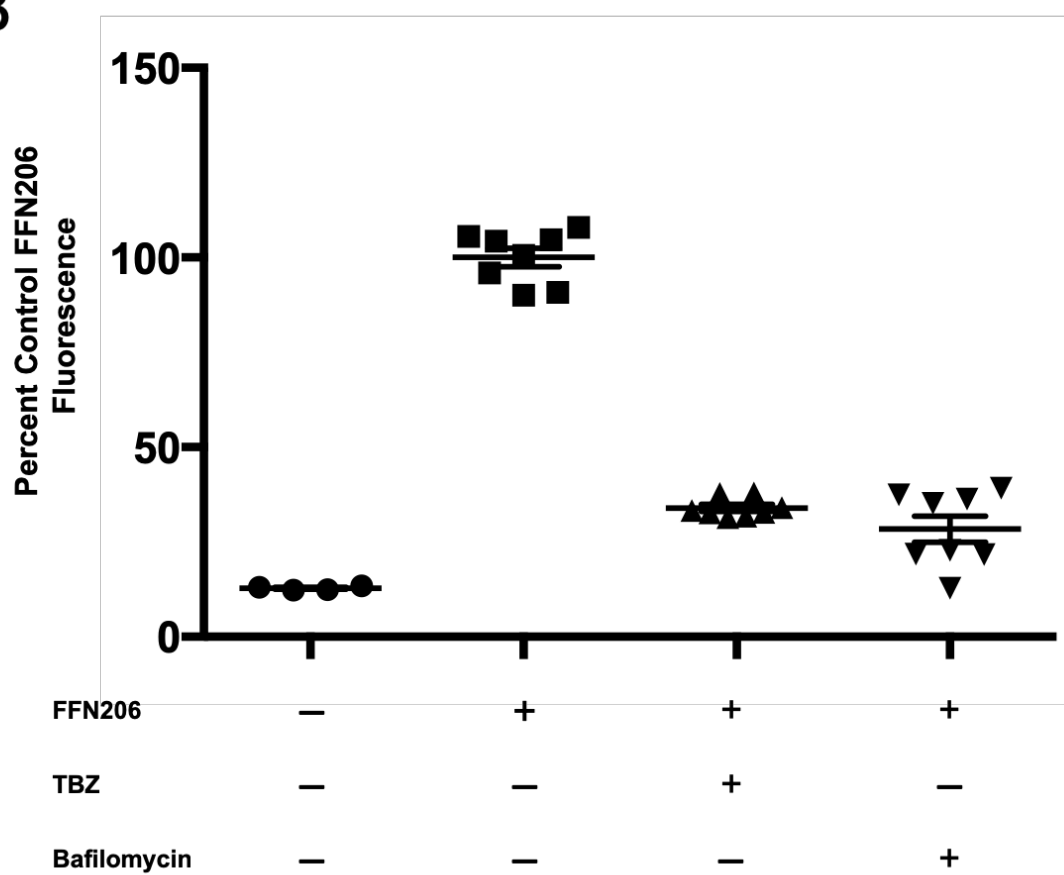


Figure 3.3. Validation of a quantifiable vesicular uptake assay under transfection with miniSOG-SV2C. A) SV2C transfection does not affect normal VMAT2 function or vesicle loading. FFN206 loading is dependent on VMAT2 activity and maintenance of the vesicular proton gradient. HEK+VMAT2 cells transiently transfected with SV2C and not treated with FFN206 exhibit minimal fluorescence (left image). HEK+VMAT2+SV2C cells treated with FFN206 exhibit robust FFN206 fluorescence (second from left image). FFN206 uptake is diminished in HEK+VMAT2+SV2C cells when VMAT2 function is inhibited by treatment with 10 μ M tetrabenazine (second from right image) and when the vesicular proton gradient is dissipated by treatment with bafilomycin (right image), indicating that SV2C transfection does not interfere with normal FFN206 loading. Imaged by EVOS system at 10x magnification. B) Quantification of FFN206 fluorescence observed in A. In the absence of FFN206, no fluorescence is observed in HEK+VMAT2+SV2C cells. HEK+VMAT2+SV2C cells treated with FFN206 exhibit robust fluorescence. FFN206 uptake is diminished in HEK+VMAT2+SV2C cells when VMAT2 function is inhibited by treatment with 10 μ M tetrabenazine. FFN206 uptake is diminished in HEK+VMAT2+SV2C cells when the vesicular proton gradient is dissipated by treatment with bafilomycin. Graph displayed as mean and standard error of the mean of percent control FFN206 fluorescence (control group: HEK+VMAT2+SV2C cells incubated with FFN206). Each point represents one well of cells from a 96-well plate. Scale bar = 400 μ M.

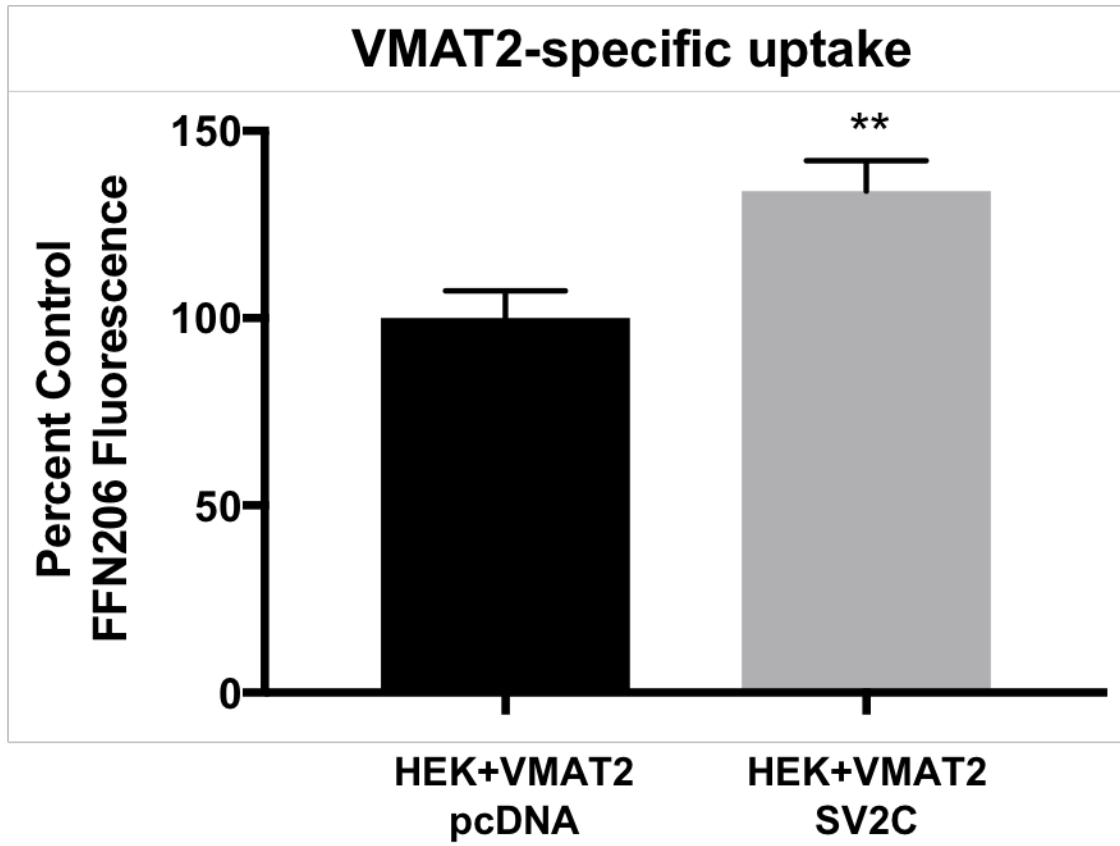
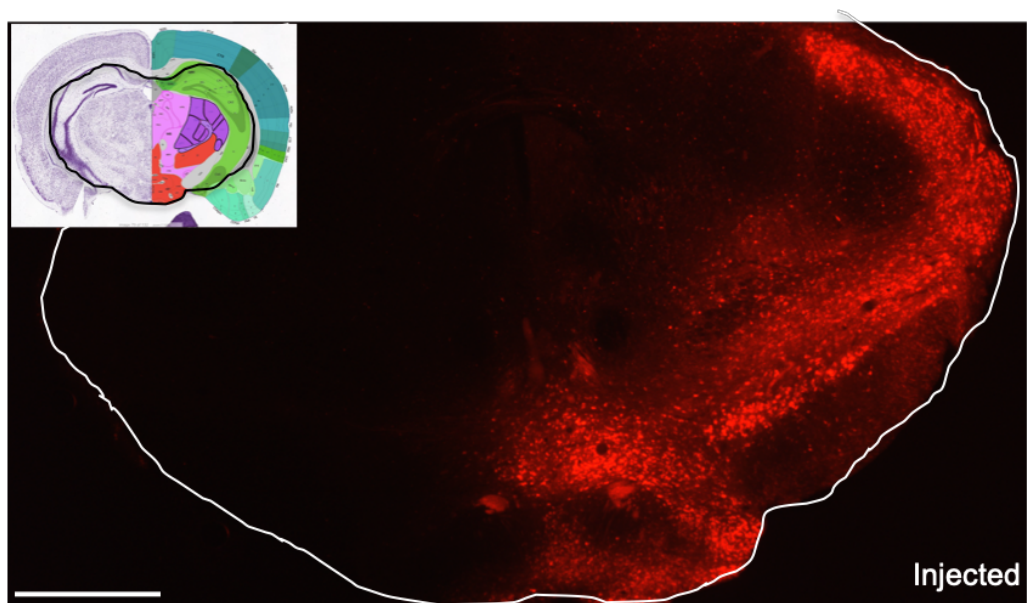


Figure 3.4. In vitro overexpression of SV2C increases vesicle packaging. SV2C transfection increases vesicle loading of FFN206. HEK+VMAT2+SV2C cells treated with FFN206 exhibit significantly increased FFN206 fluorescence as compared to HEK+VMAT2+pcDNA cells treated with FFN206 ($p = 0.0026$). Graph displayed as percent of HEK+VMAT2+pcDNA cell fluorescence with standard error of the mean. Significance was assessed with two-tailed t-test, $\alpha = 0.05$.

A



B

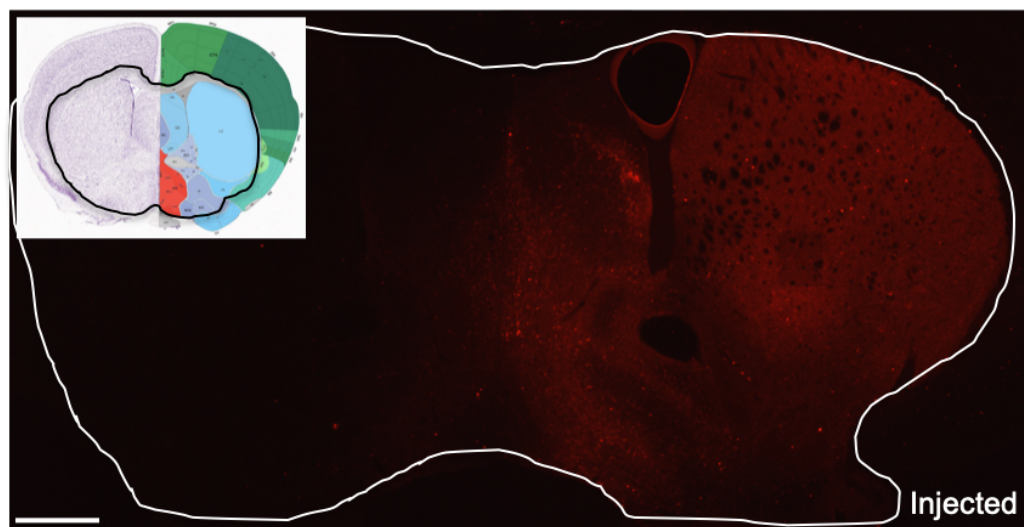
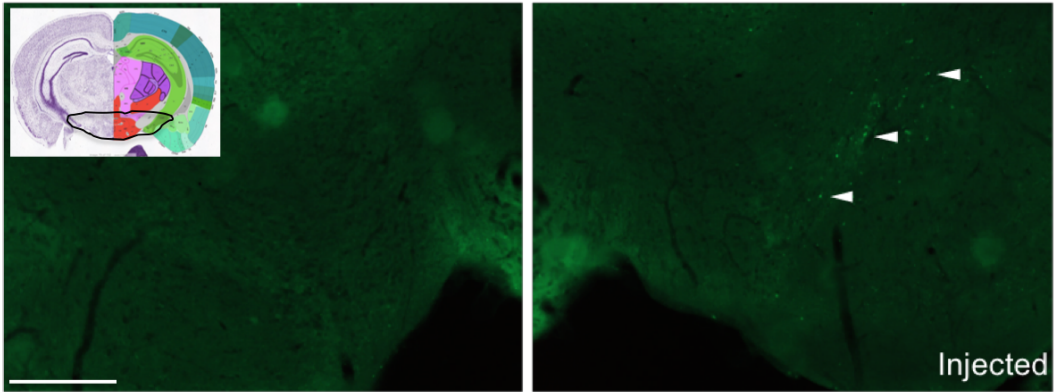


Figure 3.5. Immunofluorescent validation of viral injections of AAV2/9 mCherry. AAV2/9 mCherry was injected into the substantia nigra (AP -3.2 mm, ML -1.2 mm, DV -4.5 mm from surface of the brain) of WT C57BL/6 mice. A) Image of midbrain with robust mCherry fluorescence in the substantia nigra of the injected hemisphere with an absence of fluorescence in the un-injected hemisphere. B) Image of striatum with visible labeling of the injected hemisphere and no labeling in the un-injected hemisphere. Scale bar = 800 microns. Slices are outlined in white to enhance visibility of the fluorescent sections. Thumbnails are derived from the Allen Brain Atlas and represent position of the slice within the midbrain (A) and striatum (B). The part of the brain represented in each fluorescent image is outlined in black. The cortex is not visible in A or B.

A



B

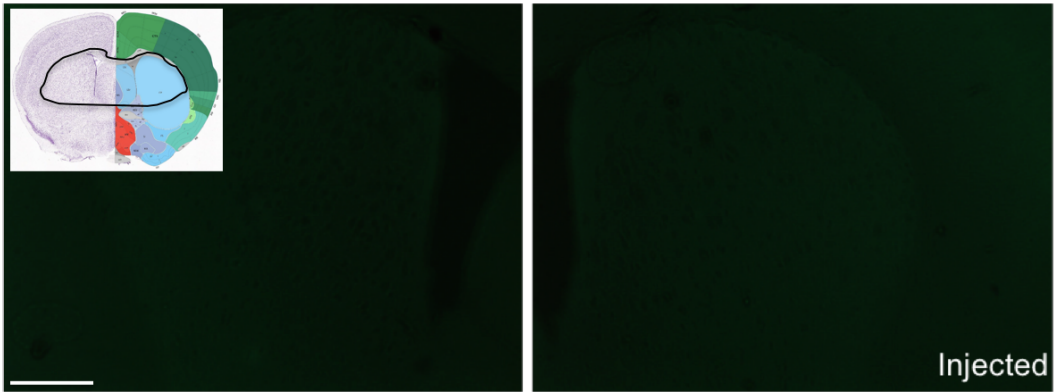


Figure 3.6. Immunofluorescent validation of viral injections of AAV2/9 miniSOG-SV2C. AAV2/9 miniSOG-SV2C was injected into the substantia nigra (AP -3.2 , ML -1.2 , DV -4.5 from surface of the brain) of WT C57BL/6 mice. A) Image of midbrain with visible miniSOG-SV2C fluorescence in the substantia nigra of the injected hemisphere with an absence of SV2C fluorescence in the un-injected hemisphere. Arrows denote SV2C-expressing cell bodies in the midbrain of the injected hemisphere. B) Image of striatum with no visible difference in labeling between the injected and un-injected hemispheres. Scale bar = 700 microns. Thumbnails are derived from the Allen Brain Atlas and represent position of the slice within the midbrain (A) and striatum (B). The part of the brain represented in each fluorescent image is outlined in black.

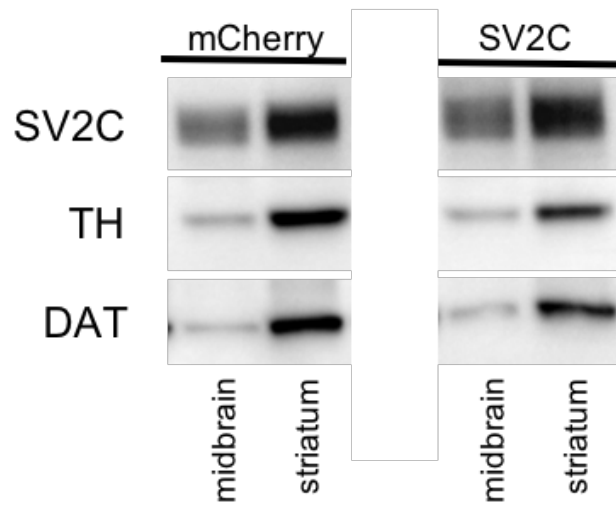


Figure 3.7. Overexpression of miniSOG-SV2C does not alter expression of other dopaminergic proteins. AAV2/9 mCherry or AAV2/9 miniSOG-SV2C was injected into the substantia nigra (AP -3.2 mm, ML -1.2 mm, DV -4.5 mm from surface of the brain) of WT C57BL/6 mice (n = 2 per group). Immunoblot probing for expression of SV2C, tyrosine hydroxylase (TH), and the dopamine transporter (DAT) in isolated midbrain and striatum of mCherry-injected and SV2C-injected mice.

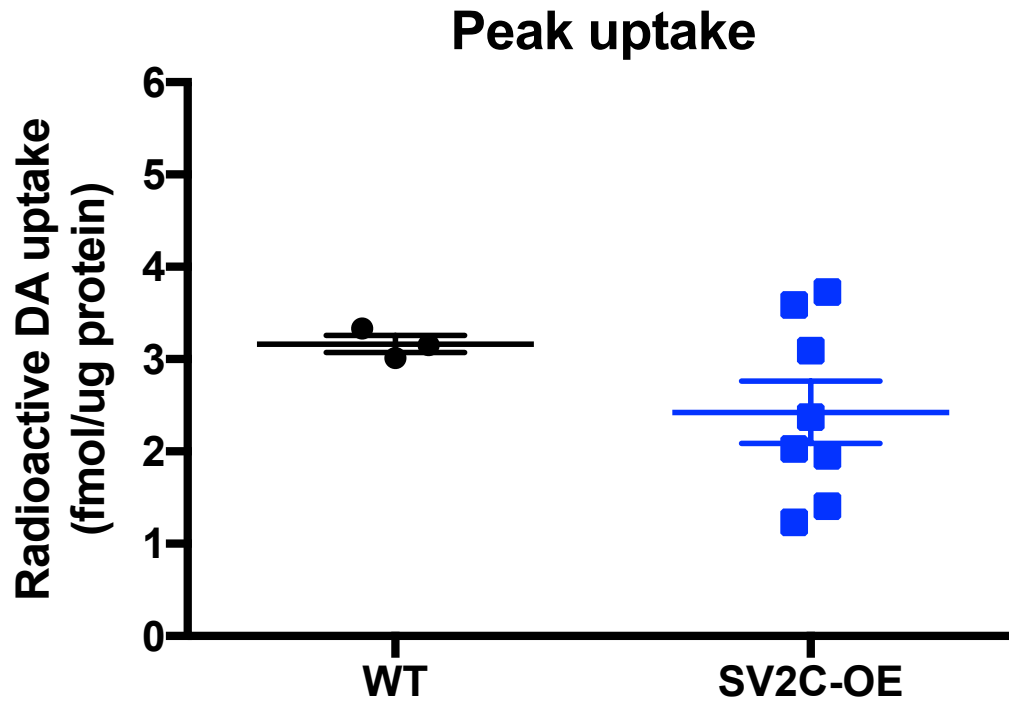


Figure 3.8. SV2C overexpression does not increase peak dopamine uptake. A) Striatal vesicles from mice injected with mCherry (WT, n = 3) and from mice injected with SV2C (SV2C-OE, n = 8) were isolated through differential centrifugation and incubated with radioactive dopamine for three minutes, after which time vesicle loading was arrested by filtration. Peak VMAT2-specific radioactive dopamine uptake was normalized according to protein concentration and a radioactive dopamine standard. There was no difference in peak dopamine uptake between WT and SV2C-OE vesicles ($p = 0.2270$, unpaired two-tailed t-test, $\alpha = 0.05$), though SV2C-OE vesicles exhibited greater variance in dopamine uptake than WT vesicles. Each dot represents one sample, with three replicate samples per animal.

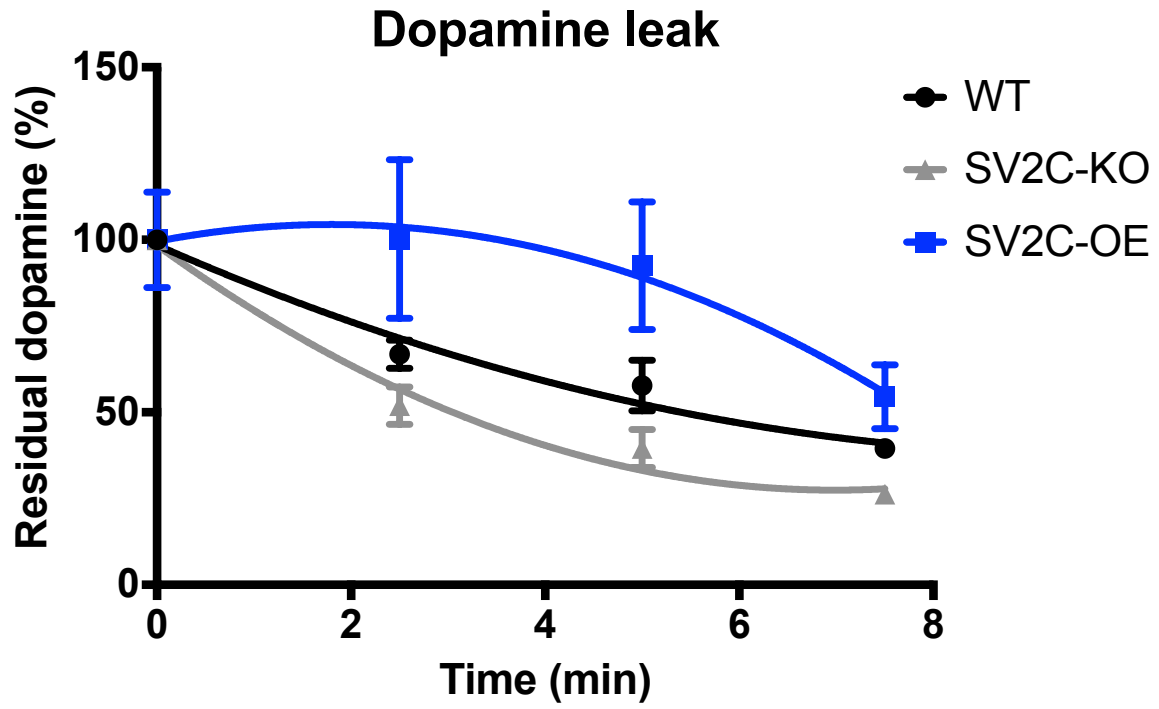


Figure 3.9. SV2C overexpression results in a trend toward increased vesicular retention of dopamine over time. Isolated vesicles from un-injected WT mice and WT mice injected with mCherry (both collapsed into the WT group WT n = 6-7), SV2C-OE (n = 3), and mice with a pan-neuronal deletion of SV2C (SV2C-KO, n = 3-4) were incubated with radioactive dopamine for three minutes before vesicle loading was arrested by addition of tetrabenazine. Samples were then incubated on ice for either 2.5, 5, or 7.5 minutes before leak was arrested through filtration. Dopamine leak is reported as percent of peak radioactive dopamine uptake (0 minutes of leak). SV2C-OE mice exhibited a strong trend toward decreased dopamine leak, or increased retention of dopamine, as compared to WT mice at the 2.5, 5, and 7.5 minute time points (2.5 min.: $p = 0.0559$, 5 min.: $p = 0.0734$, 7.5 min.: $p = 0.0559$). SV2C-KO mice exhibited a general trend toward increased dopamine leak, or decreased retention of dopamine, as compared to WT mice (2.5 min.: $p = 0.4044$, 5 min.: $p = 0.3898$, 7.5 min.: $p = 0.0610$). Graphs represented as mean with standard error of the mean, fitted with a non-linear second order polynomial best-fit line. Significance was assessed with one-way ANOVA at each time point with Dunnett's multiple comparisons test, $\alpha = 0.05$.

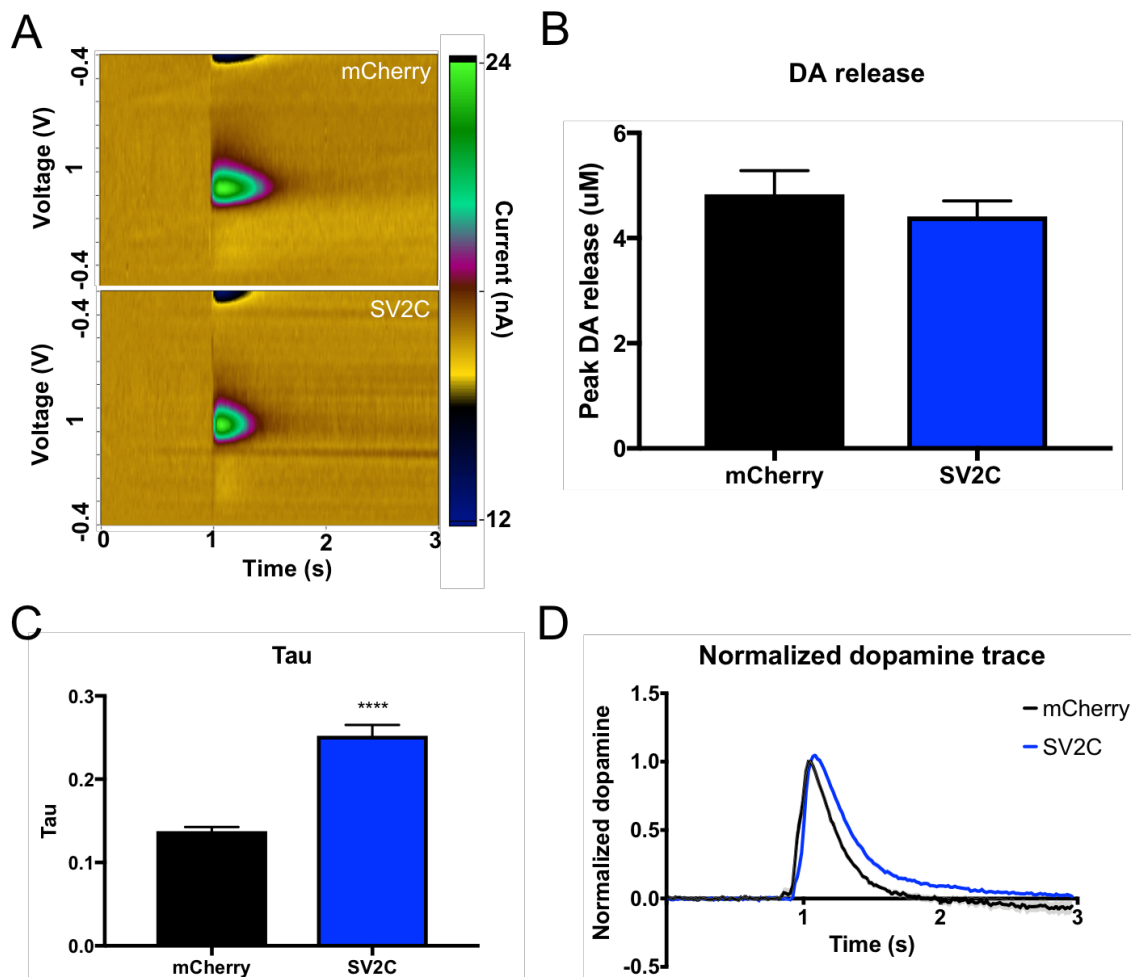


Figure 3.10. SV2C overexpression does not affect the amount of dopamine released, but decreases the rate of dopamine clearance. Dopamine release stimulated by a single electrical pulse in the dorsal striatum of mice injected with mCherry (n = 3) or SV2C (n = 8) was measured using fast scan cyclic voltammetry. There is no difference in peak dopamine release in mCherry-injected and SV2C-injected mice as shown by representative color plots (A) and quantified over all recording sites (B). C) DAT-mediated dopamine clearance rate is diminished in SV2C-injected mice, as evidenced by increased tau in mice overexpressing SV2C. D) Comparative dopamine traces depicting dopamine release and clearance over three seconds in mCherry-injected and SV2C-injected mice. Dopamine traces are normalized to peak dopamine release. Graphs represented as mean with standard error of the mean. Significance was assessed with two-tailed t-test, alpha = 0.05.

Chapter 4- Discussion, future directions, and concluding remarks

Summary of findings

The goals of this dissertation were to 1) develop a series of *in vitro* techniques to examine VMAT2-mediated dopamine transport and 2) characterize the effects of overexpression of SV2C in the dopamine system *in vitro* and *in vivo* with the overarching aim of determining the role of SV2C in the dopamine system.

I first used the fluorescent false neurotransmitter 206 (FFN206) to investigate VMAT2 function and the dynamics of vesicle loading at high resolution and in real-time, and I optimized a 96-well plate assay with a dynamic range that allowed for detection of pharmacological, environmental, and genetic perturbations to VMAT2-mediated vesicular uptake. This assay is also amenable to high throughput screening. I examined VMAT2 function and the dynamics of vesicle loading under physiological conditions, during treatment with pharmacological inhibitors of VMAT2, and during treatment with a range of environmental toxicants. The fluorescent assays developed here allowed for monoamine transport to be measured spatially and temporally with an ease and at a resolution that were previously inaccessible. We show TIRF-level resolution of FFN206 loading and real-time VMAT2-mediated uptake, and recorded a dynamic process of vesicle loading, leak, and retention in real-time that mimicked the dynamic equilibrium seen in monoamine vesicles. We also observed a significant reduction in VMAT2 function after treatment with reserpine, tetrabenazine, methamphetamine, and methylphenidate, and a modest reduction in VMAT2 function after short-term exposure to high concentrations of rotenone, paraquat, unichlor, PFOS, Paroil, Aroclor 1260, and HBCDD, though inhibition of VMAT2 is unlikely to contribute to the toxicity of these compounds at physiologically and environmentally relevant concentrations. The methods of assessing vesicle function developed here can be used to further assess how other pharmacological compounds and environmental toxicants exert their effects at the level of the

vesicle and can elucidate how exposure to such compounds and other genetic modifications contributes to the progression of monoaminergic diseases such as PD.

After investigating vesicle dynamics in a system not expressing SV2s, I sought to examine the role that SV2C plays in dopamine vesicle dynamics and to identify how SV2C affects dopamine handling. To that end, I overexpressed SV2C *in vitro* and show localization of SV2C to vesicle-like compartments in a cell system. Further, overexpression of SV2C led to increased uptake of a dopamine analog, FFN206. I then stereotactically overexpressed SV2C *in vivo* and characterized the effect of this overexpression on dopamine vesicle packaging, retention, and release in C57BL/6 mice. SV2C was overexpressed in midbrain neurons in the region of the substantia nigra and this overexpression enhanced the retention of dopamine in the vesicle and prolonged the presence of dopamine in the synaptic cleft following electrically-stimulated dopamine release. Overall, these findings identify SV2C as a mediator of dopamine vesicle packaging, retention, and release.

Working hypothesis of the mechanism of action of SV2C

Secretory granules, such as those in mast cells and chromaffin cells, contain a gel matrix (Kajiwara and Ross-Murphy 1992; Kwon *et al.*, 1991; Tanaka *et al.*, 1982). More recently, synaptic vesicles have also been posited to contain a gel matrix (Mendoza-Torreblanca *et al.*, 2013; Reigada *et al.*, 2003). This idea has been met with skepticism because the core of synaptic vesicles is clear when observed under an electron microscope; however, electron tomography-derived reconstructions indicate that the synaptic vesicle lumen is occupied by a bilateral assembly of macromolecules with four arms radiating out from a central focal point (Harlow *et al.*, 2013). It has been proposed that SV2 is the mainstay of this intraluminal assembly found in all synaptic vesicles (Harlow *et al.*, 2013; Szule *et al.*, 2015). Further, this luminal assembly has been proposed

to act as a smart gel matrix within the vesicle that regulates the loading of neurotransmitter into vesicles, the quantity of neurotransmitter released upon vesicle fusion, and the rate of neurotransmitter release, as neurotransmitter bound within the gel matrix requires ion-exchange in order to be released (Nowack *et al.*, 2010; Reigada *et al.*, 2003; Vautrin 2009). It must also be noted that while there is evidence for the presence of a gel matrix within synaptic vesicles, the presence of a gel matrix specifically within dopaminergic vesicles has not been examined.

Here, I report that expressing SV2C in HEK+VMAT2 cells results in an increase in vesicle packaging. Furthermore, overexpressing SV2C in C57BL/6 mice results in increased retention of dopamine over time and a reduced rate of dopamine clearance from the synaptic cleft. I suggest that these data align with the finding that SV2s are the main component of the synaptic vesicle gel matrix and I propose that SV2C specifically contributes to the density of the gel matrix within dopaminergic synaptic vesicles such that increasing SV2C expression will increase the density of the synaptic gel matrix and thus alter dopamine handling and release. SV2C contains five predicted glycosylation sites on its intravesicular loop, compared to the three conserved sites on SV2A and SV2B (Bajjalieh *et al.*, 1994; Janz and Sudhof 1999). The presence of additional glycosylation sites on SV2C suggests that increased copy numbers of SV2C on the vesicle can result in formation of a denser gel matrix, while decreased copy numbers of SV2C can result in formation of a smaller gel matrix (Figure 4.1). This dense gel matrix does not appear to increase the peak amount of dopamine loaded into the vesicle, as we observed no difference in dopamine uptake or release in SV2C-injected mice. Instead, I propose that this dense gel matrix acts to shift the distribution of dopamine within the vesicle and alter the rate at which dopamine is retained in the vesicle and released from the vesicle upon vesicle fusion.

The increase in FFN206 fluorescence in cells containing SV2C is consistent with this proposed working hypothesis because the addition of SV2C into a cell system not expressing SV2s

would lead to the formation of a denser gel matrix that allows for a greater amount of FFN206 to be absorbed. The increased retention of vesicular dopamine over time and the decrease in the rate of dopamine clearance resulting from overexpression of SV2C in mice further aligns with this working hypothesis. The denser gel matrix formed by additional SV2C would increase the amount of dopamine bound and the bound neurotransmitter would require ion exchange in order for dopamine to be released; this ion exchange process would slow the reuptake of dopamine into the presynaptic terminal, thus resulting in the decreased rate of dopamine clearance observed here.

To put numerical context into this speculative hypothesis, I will describe a WT dopamine vesicle, a SV2C-OE dopamine vesicle, and a SV2C-KO dopamine vesicle. The percentages used in the following examples are based on the proposed relative distribution of free-floating and bound neurotransmitter in WT vesicles described by Reigada and colleagues (Reigada *et al.*, 2003). The percentages proposed for the SV2C-OE and SV2C-KO vesicles are purely speculative, though they are based on the data reported here and on the work performed by the Reigada group.

Consider that when dopamine is loaded into a wildtype vesicle, 10% of the dopamine remains free-floating within the vesicle lumen and 90% of the dopamine is trapped within the gel matrix formed by the glycosylated intravesicular loops of the SV2 proteins. Upon exocytosis and full fusion of the wildtype vesicle with the plasma membrane, the free-floating dopamine formerly within the vesicle diffuses away from the plasma membrane to interact with post-synaptic receptors, to be reabsorbed through DAT, or to be broken down by COMT or MAO in the synaptic cleft, while the remaining dopamine molecules trapped within the matrix must undergo ion exchange in order to be dissociated from the SV2 proteins and to diffuse away from the plasma membrane. Upon vesicle fusion, all dopamine molecules, free-floating and matrix-bound, are able to be oxidized and thus detected via FSCV (Figure 4.2). The loss of the dopamine signal

(represented by τ) is dependent on how quickly the dopamine molecules are dissociated from the gel matrix and reabsorbed via DAT into the presynaptic terminal.

Alternatively, as dopamine is loaded into an SV2C-overexpressing vesicle, I propose that a denser gel matrix is formed by the additional SV2C protein expressed and this denser matrix traps a larger fraction (95%) of the dopamine within the glycosylated intravesicular loops of, SV2C while only 5% of the dopamine remains free-floating within the vesicle. I do not expect that overexpression of SV2C protein changes the overall number of SV2 proteins on the vesicle, but instead changes the number of each type of SV2 isoform on the vesicle. For example, if a WT vesicle contains five SV2 proteins, 40% may be SV2A (two SV2A proteins), 40% may be SV2B (two SV2B proteins), and 20% may be SV2C (one SV2C protein). I propose that an SV2C-OE vesicle may be comprised of 20% SV2A (one SV2A protein), 20% SV2B (one SV2B protein), and 60% SV2C (three SV2C proteins). Upon exocytosis and full fusion of the SV2C-overexpressing vesicular membrane with the plasma membrane, the small fraction of dopamine molecules that were free-floating within the vesicle lumen diffuse away from the plasma membrane to interact with post-synaptic receptors, to be reabsorbed through DAT, or to be broken down by COMT or MAO in the synaptic cleft, while the remaining dopamine molecules that were trapped within the gel matrix must undergo ion exchange in order to be dissociated from the SV2 proteins. As in the WT vesicle described above, all dopamine molecules, free-floating and matrix-bound, are able to be oxidized and thus detected via FSCV upon vesicle fusion (Figure 4.3). Because a greater fraction of dopamine molecules would be matrix-bound in this model of SV2C overexpressing vesicles, it will take a greater amount of time for all of the matrix-bound dopamine to dissociate and the dopamine signal to dissipate, thus resulting in the longer τ we observed in the SV2C-OE vesicles. In this way, the denser intravesicular gel matrix in SV2C-OE vesicles would slow the

kinetics of dopamine release by altering the rate of dopamine off-loading instead of altering the amount of dopamine present within the vesicle.

Vesicles isolated from SV2C-KO mice do not express SV2C, though they are still expected to contain five copies of SV2 protein. I propose that the loss of SV2C results in the formation of a less dense glycomatrix, as SV2A and SV2B contain three glycosylation sites while SV2C contains five glycosylation sites. The loss of SV2C would reduce the number of glycosylation sites present within the vesicle lumen. SV2C-KO mice also have reduced total dopamine levels as compared to WT mice (Dunn *et al.*, 2017b). In these vesicles, I propose that 20% of the dopamine remains free-floating within the vesicle lumen and 80% of the dopamine is trapped within the gel matrix formed by the glycosylated intravesicular loops of the SV2 proteins. Upon exocytosis and full fusion of the wildtype vesicle with the plasma membrane, the free-floating dopamine formerly within the vesicle diffuses away from the plasma membrane to interact with post-synaptic receptors, to be reabsorbed through DAT, or to be broken down by COMT or MAO in the synaptic cleft, while the remaining dopamine molecules trapped within the matrix must undergo ion exchange in order to be dissociated from the SV2 proteins and to diffuse away from the plasma membrane. Upon vesicle fusion, all dopamine molecules, free-floating and matrix-bound, are able to be oxidized and thus detected via FSCV (Figure 4.4). Because only 80% of the dopamine molecules are matrix-bound in this model of SV2C-KO vesicles, it will take a shorter amount of time for the matrix-bound dopamine to dissociate and the dopamine signal to dissipate, thus resulting in the reduced tau we observed in SV2C-KO vesicles (Dunn *et al.*, 2017b). In this way, SV2C expression mediates the kinetics of dopamine release such that loss of SV2C results in faster dopamine off-loading due to less dopamine molecules being bound in a less dense gel matrix, while overexpression of SV2C results in slower dopamine off-loading due to more

dopamine molecules being bound in a denser gel matrix. Table 4.1 summarizes this speculation of SV2 expression and dopamine handling in WT, SV2C-OE, and SV2C-KO vesicles.

Discussion of unexpected results

Though overexpression of SV2C in the midbrain was strong, there was a lack of overt overexpression of SV2C in the striatum that may have resulted from technical challenges in visualizing SV2C in nerve terminals or from the failure of SV2C translated in the cell body to be effectively trafficked to the nerve terminal. We utilized miniSOG-tagged SV2C to virally overexpress SV2C both *in vitro* and *in vivo*. The localization of fluorescently-tagged SV2C to terminals dispersed throughout the striatum made visualization of striatal SV2C overexpression challenging. We may have observed greater SV2C fluorescence and staining at higher magnification; however, increasing magnification in fluorescent IHC decreased the signal to noise ratio, thus drowning the SV2C signal in background fluorescence. Further, we examined SV2C expression using DAB-IHC (images not shown here) and increasing magnification of DAB-IHC does not allow for resolution of discrete terminal-level staining. Our lack of striatal SV2C overexpression may alternatively be the result of SV2C not being properly trafficked to nerve terminals. SV2C overexpression was high at the site of injection in the substantia nigra, indicating that we were able to successfully inject and express SV2C in midbrain cell bodies, though the lack of SV2C staining in the striatum can indicate that SV2C was not overexpressed in the nerve terminal. We observed an altered vesicular phenotype in mice overexpressing SV2C, as evidenced by the increased retention of vesicular dopamine over time and the decrease in the rate of dopamine clearance in SV2C-OE mice. If this phenotype does not result from overexpression of SV2C on the vesicle, then overexpression of SV2C in the cell body may have led to an alteration in the

expression of other proteins on the vesicle, such as VMAT2 or the proton pump. In this way, overexpression of SV2C in the cell body could still result in vesicle-level perturbations.

Overexpression of SV2C resulted in inconsistent outcomes in cells and mice, with SV2C overexpression in cells resulting in an increase in vesicle packaging and SV2C overexpression in mice resulting in no difference in the peak amount of dopamine packaged or released from the vesicle. We must consider the differential natures of the *in vitro* and *in vivo* expression systems: by transfecting SV2C *in vitro*, we added SV2C into a system that did not contain SV2C or any other SV2s. Conversely, by injecting SV2C *in vivo*, we added SV2C into a system that already contained SV2C and other SV2s. I propose that adding SV2C in cells produced a more drastic effect on vesicle packaging because the cells did not previously contain any SV2s. Adding SV2C into mice produced a less drastic effect on vesicle packaging because SV2s were already expressed in this system and the expression of additional SV2C shifted the ratio of SV2s expressed without significantly altering the amount of dopamine packaged.

Future directions

To date, there have been few studies published that examine how SV2C mediates dopamine vesicle handling. The work presented in this dissertation has made strides towards elucidating the function of SV2C in non-pathological conditions, though many questions remain.

Bettering visualization and overexpression of SV2C in vivo. In this dissertation, I was able to visualize the localization of transfected SV2C to the vesicle-like compartments in HEK cells; however, a similar level of visualization of SV2C localization was not achieved *in vivo*. High magnification imaging of SV2C overexpression should be achieved through electron microscopy (EM). Our use of miniSOG-tagged SV2C to produce overexpression easily lends itself to EM applications, though we attempted to visualize SV2C overexpression with EM with little success.

As SV2C has never been visualized with EM, such high magnification imaging of SV2C expression and/or SV2C overexpression should be performed.

Uncovering mechanisms of SV2C. The findings presented here align with the speculative hypothesis that the intraluminal loops of SV2C form an intravesicular gel matrix that mediates dopamine packaging into the vesicle and the rate of dopamine release from the vesicle. However, much research remains in order to determine whether this hypothesis reflects the true mechanism of action of SV2C. One area to be further researched pertains to the involvement of the glycosylated intravesicular loop in the mechanism of SV2C. Previous studies indicate that glycosylation mediates normal SV2 function: mutation of the glycosylation sites of SV2A disrupts normal protein folding and trafficking (Chang and Sudhof 2009) and glycosylation mediates the binding of SV2C to botulinum neurotoxin A (Mahrhold *et al.*, 2016; Yao *et al.*, 2016). In order to test the hypothesis that the intravesicular loop of SV2C modulates both the uptake of dopamine into vesicles and the long-term storage of dopamine within the vesicle, the intravesicular loop of SV2C must be manipulated and the resulting effects on dopamine uptake and retention recorded. The intravesicular loop of SV2C contains five predicted glycosylation sites. Our lab previously generated DNA constructs containing mutations at each of the five predicted glycosylation sites on the intravesicular loop of SV2C. These constructs can be transfected into VMAT2-expressing cells and dopamine uptake can be assessed using our fluorescent assay of vesicular dopamine transport. These constructs can also be injected into SV2C-KO mice and dopamine uptake can be assessed using radioactive dopamine uptake. We have previously recorded the amount of radioactive dopamine that can be packaged into vesicles isolated from SV2C-KO mice and from SV2C-WT mice, thus producing a range of SV2C-mediated dopamine uptake. Injecting each SV2C glycomutant construct into SV2C-KO mice will produce levels of dopamine uptake that

falls between that of SV2C-KO mice and SV2C-WT mice and will allow for assessment of the contribution of each glycosylation site to dopamine packaging.

In order to further prove whether this working hypothesis represents the mechanism of SV2C, the function of DAT and TH need to be further examined. Though there was no measured difference in DAT or TH expression in SV2C-OE mice, a lack of alteration in expression does not discount the potential for an alteration in function of DAT and TH in the SV2C-OE mice. Radioactive DAT binding and HPLC will allow for the function of DAT to be assessed and for dopamine production (resulting from TH function) and dopamine turnover to be measured. The total number of vesicles released also needs to be accounted for; it is possible that overexpression of SV2C alters the number of vesicles released or the rate at which vesicles are released. Measuring membrane capacitance after stimulating vesicle release would allow for the number of vesicles exocytosed as well as the rate of vesicle endocytosis to be determined.

Uncovering mechanisms of SV2C in pathological conditions. In the appendix of this dissertation, I investigated the role of SV2C in dopaminergic neurotoxicity related to alpha-synuclein pathogenesis. My findings indicate that there is an interaction between alpha-synuclein and SV2C that mediates dopaminergic toxicity, though the exact nature of this interaction is still unclear. Both alpha-synuclein and SV2C have a unique relationship with dopamine and dopaminergic neurons. Alpha-synuclein modulates the trafficking of DAT to the synaptic terminal and influences its activity (Butler *et al.*, 2015; Lee *et al.*, 2001). Dopamine also inhibits the formation of alpha-synuclein fibrils; breaks down existing fibrils (Fischer and Matera 2015; Mor *et al.*, 2017); stabilizes the toxic oligomers of alpha-synuclein; and induces the formation of these toxic oligomers (Fischer and Matera 2015). SV2C expression is enriched in the dopaminergic neurons located in the substantia nigra pars compacta and in the ventral tegmental area, with 70%

of dopamine neurons expressing SV2C (Dardou *et al.*, 2011; Dardou *et al.*, 2013; Dunn *et al.*, 2017b; Janz and Sudhof 1999).

The interaction between SV2C and alpha-synuclein may involve formation of a physical protein complex connecting SV2C and alpha-synuclein, or SV2C and alpha-synuclein may both be involved in similar, but non-physically overlapping processes occurring in the presynaptic terminal. We have previously shown that SV2C co-immunoprecipitates with alpha-synuclein, suggesting the presence of a physical protein complex connecting SV2C and alpha-synuclein (Dunn *et al.*, 2017b). The formation of this SV2C—alpha-synuclein complex may serve to stabilize the non-toxic conformation of alpha-synuclein, thus reducing neurotoxicity. Alternately, SV2C and alpha-synuclein may both be involved in similar, but non-physically overlapping processes occurring in the presynaptic terminal. Both alpha-synuclein and SV2s are associated with SNARE complex formation, with mutations in alpha-synuclein leading to alterations in SNARE protein associations (Burre *et al.*, 2010; Garcia-Reitböck *et al.*, 2010) and deletion of SV2A resulting in decreased SNARE complex formation (Xu and Bajjalieh 2001). SV2s also bind to and traffic with synaptotagmin, a SNARE protein present on the vesicular membrane (Nowack *et al.*, 2010; Schivell *et al.*, 2005; Yao *et al.*, 2010). Both proteins are also associated with vesicular trafficking (Diao *et al.*, 2013; Iezzi *et al.*, 2005; Miraglia *et al.*, 2018; Nemani *et al.*, 2010; Wang *et al.*, 2014). Because both SV2C and alpha-synuclein are involved in several overlapping processes in the presynaptic terminal, a “multi-hit” hypothesis may come into play. In this vein, if both SV2C and alpha-synuclein are involved in the same vesicle fusion and trafficking processes, then the loss of normal SV2C or alpha-synuclein function in the presence of normal alpha-synuclein or SV2C function, respectively, would lead to altered vesicle handling and cytotoxicity. However, the loss of function of both SV2C and alpha-synuclein would lead to

enhanced impairment in vesicular handling beyond the loss of function that would be expected based on the loss of two non-interacting proteins, thus resulting in greatly increased neurotoxicity.

To determine whether SV2C and alpha-synuclein physically interact, Forster resonance energy transfer (FRET) and bioluminescence resonance energy transfer (BRET) imaging assays should be performed on populations of cells overexpressing SV2C and alpha-synuclein. This will allow for the examination of protein-protein interactions in real-time, and will elucidate when SV2C and alpha-synuclein interact during the vesicle handling process. More research should also be done examining which form of alpha-synuclein interacts with SV2C. While we observed a reduction in total alpha-synuclein expression in A53T-OE mice overexpressing SV2C, it is unclear whether this reduction results from a decrease in phosphorylated, monomeric, or multimeric alpha-synuclein expression. Furthermore, I have investigated the relationship between A53T-OE mice and SV2C expression; however, the interaction between WT alpha-synuclein and SV2C may differ from the interaction between the A53T mutant of alpha-synuclein and SV2C. Therefore, the interaction between WT alpha-synuclein and SV2C should be characterized both *in vitro* and *in vivo* through the use of cells and mice overexpressing WT alpha-synuclein.

Conclusion

Vesicular dysfunction in the dopamine system contributes to the progression of PD. SV2C was recently identified as a modulator of dopamine neurotransmission, its expression is disrupted in human PD, and its genetic deletion results in the development of motor symptoms of PD and enhanced dopaminergic neurodegeneration. Despite these associations, little was known about the mechanism of SV2C and its role in dopamine neurotransmission. Results from this dissertation identify SV2C as a mediator of dopamine vesicle packaging, retention, and release. More work

remains to fully uncover the mechanism of SV2C in mediating dopamine handling and dopamine neuron vulnerability in PD.

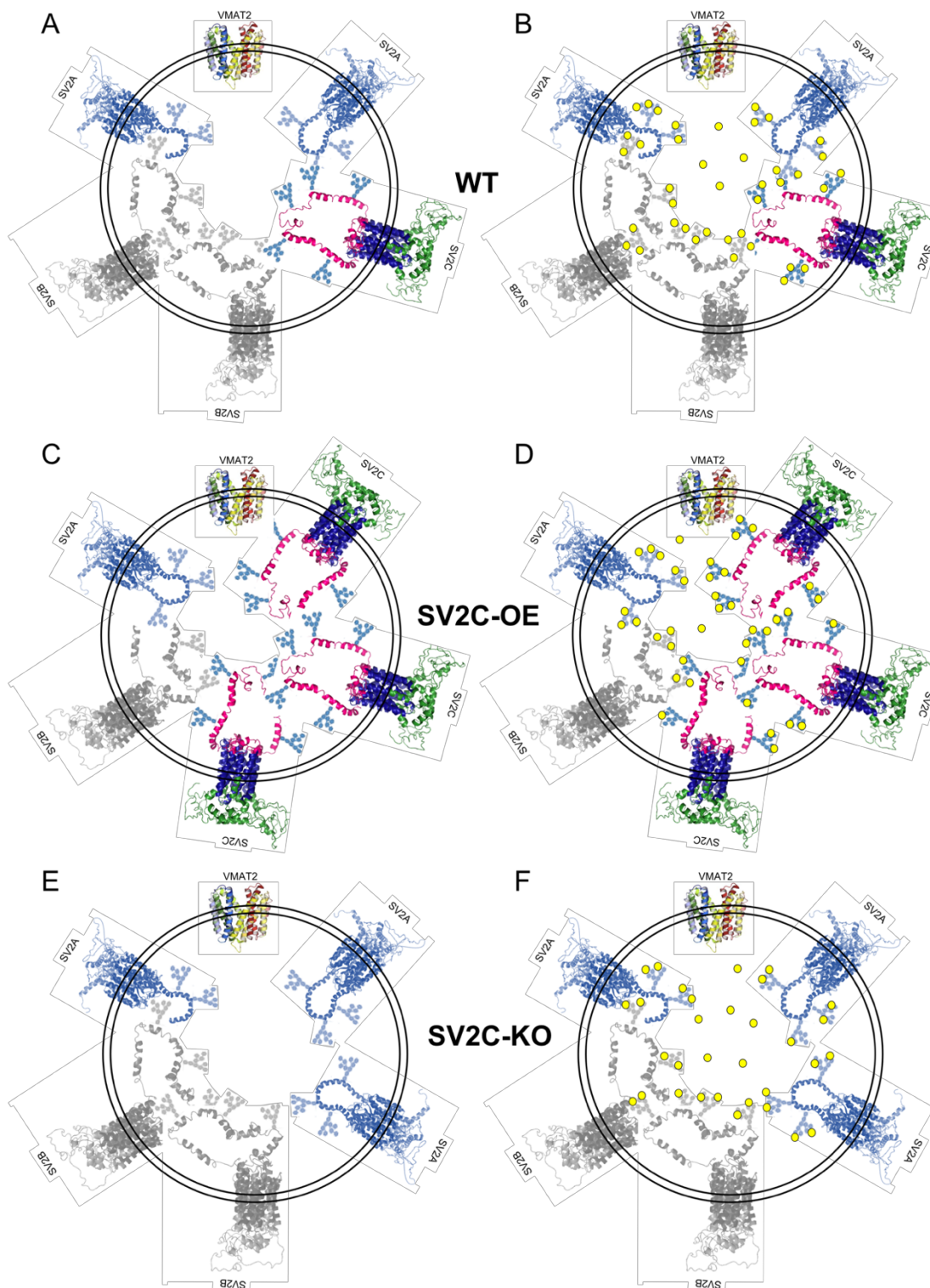


Figure 4.1. Distribution of dopamine molecules in wildtype, SV2C-overexpressing, and SV2C-KO synaptic vesicles. A) Wildtype synaptic vesicles contain five copies of SV2 protein. The vesicle shown here is expressing one VMAT2 molecule (located at the top of the vesicle) as well as two SV2A proteins (blue), two SV2B proteins (gray), and one SV2C protein (green, blue, and pink). B) Representation of distribution of dopamine molecules (yellow dots) within a wildtype vesicle. This hypothetical representation of a wildtype dopamine vesicle contains 40 molecules of dopamine. Out of 40 dopamine molecules, four (10%) are free-floating within the cytosol and 36 (90%) are bound up in the glycosylated intravesicular loops of the SV2 proteins. C) We do not expect that over-expression of SV2C protein changes the overall number of SV2 proteins on the vesicle, but instead changes the number of each SV2 isoform on the vesicle. The vesicle shown here is expressing one VMAT2 molecule (located at the top of the vesicle) as well as one SV2A molecule (blue), one SV2B molecule (gray), and three SV2C molecules (green, blue, and pink). D) Representation of distribution of dopamine molecules (yellow dots) within a SV2C-overexpressing vesicle. This hypothetical representation of a SV2C-overexpressing dopamine vesicle contains 40 molecules of dopamine. Out of 40 dopamine molecules, two (5%) are free-floating within the cytosol and 38 (95%) are bound up in the glycosylated intravesicular loops of the SV2 proteins. E) SV2C-KO vesicles do not express SV2C, though they are still expected to contain five copies of SV2 protein. The vesicle shown here is expressing one VMAT2 molecule (located at the top of the vesicle) as well as three SV2A proteins (blue) and two SV2B proteins (gray). F) Representation of distribution of dopamine molecules (yellow dots) within a SV2C-KO vesicle. SV2C-KO mice express a reduction in total dopamine content. This hypothetical representation of a SV2C-KO dopamine vesicle contains 32 molecules of dopamine. Out of 32 total dopamine molecules (20% reduction from WT), six (20%) are free-floating within the cytosol and 26 (80%) are bound up in the glycosylated intravesicular loops of the SV2 proteins.

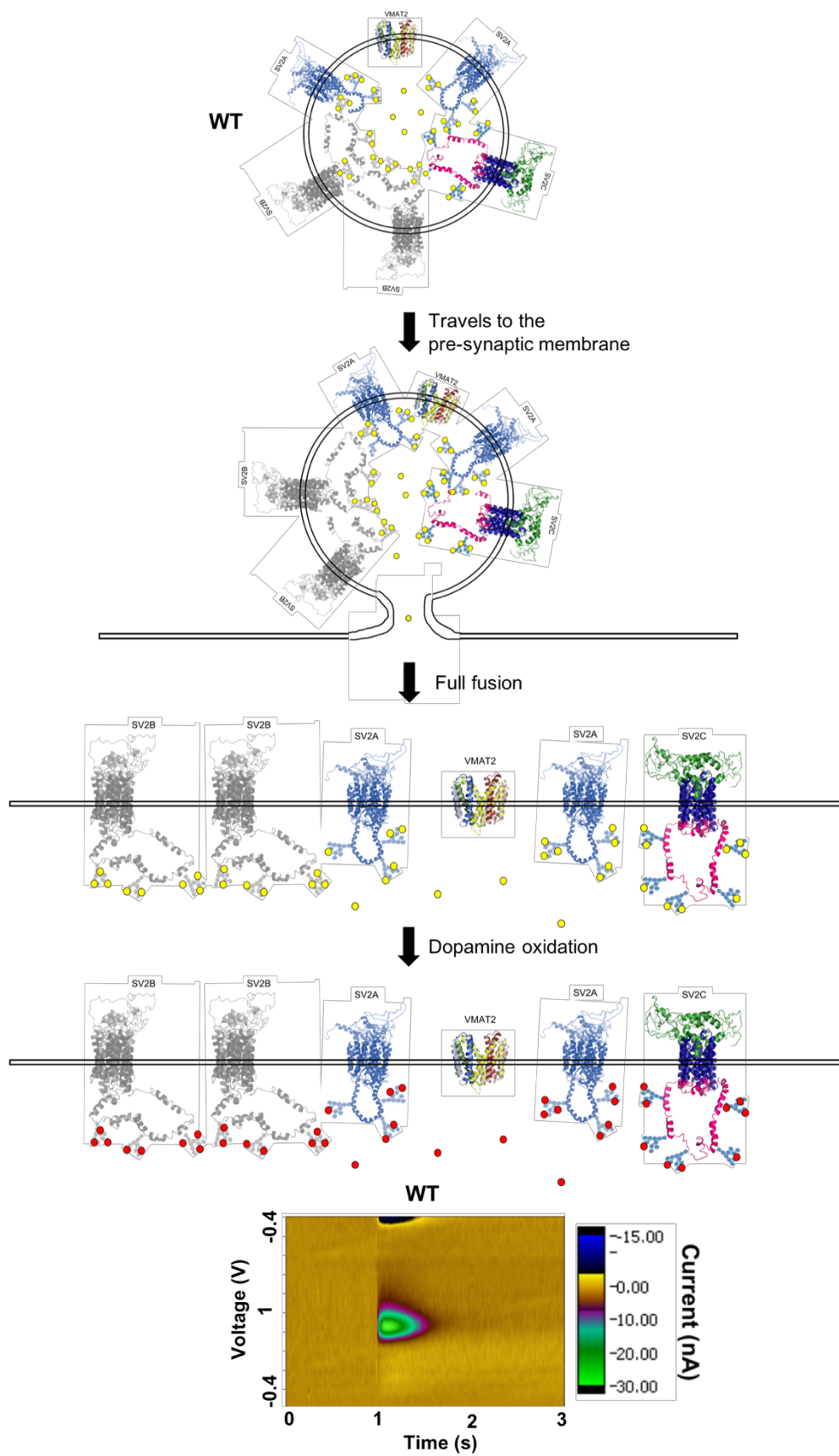


Figure 4.2. Dopamine release in wildtype synaptic vesicles. Dopamine release in a wildtype synaptic vesicle after full fusion exocytosis. The vesicle shown at the top is expressing one VMAT2 molecule (located at the top of the vesicle) as well as two SV2A proteins (blue), two SV2B proteins (gray), and one SV2C protein (green, blue, and pink) and is loaded with dopamine molecules (yellow dots). This hypothetical representation of a wildtype dopamine vesicle contains 40 molecules of dopamine. Out of 40 dopamine molecules, four (10%) are free-floating within the cytosol and 36 (90%) are bound up in the glycosylated intravesicular loops of the SV2 proteins. After the vesicle travels to the presynaptic membrane, forms a fusion pore (second image), and there is a full collapse of the vesicle membrane into the plasma membrane (third image), the intravesicular lumen becomes exposed to the extracellular space. This allows the four previously free-floating dopamine molecules to diffuse away from the plasma membrane, while the 36 remaining dopamine molecules continue to be bound to the glycosylated loops of the SV2 proteins until they dissociate from the glycosylated moieties through ion-exchange. All dopamine molecules are exposed to the extracellular space after full fusion and are able to be oxidized and detected by FSCV (oxidation potential is represented by the color change in the dopamine molecules from yellow to red).

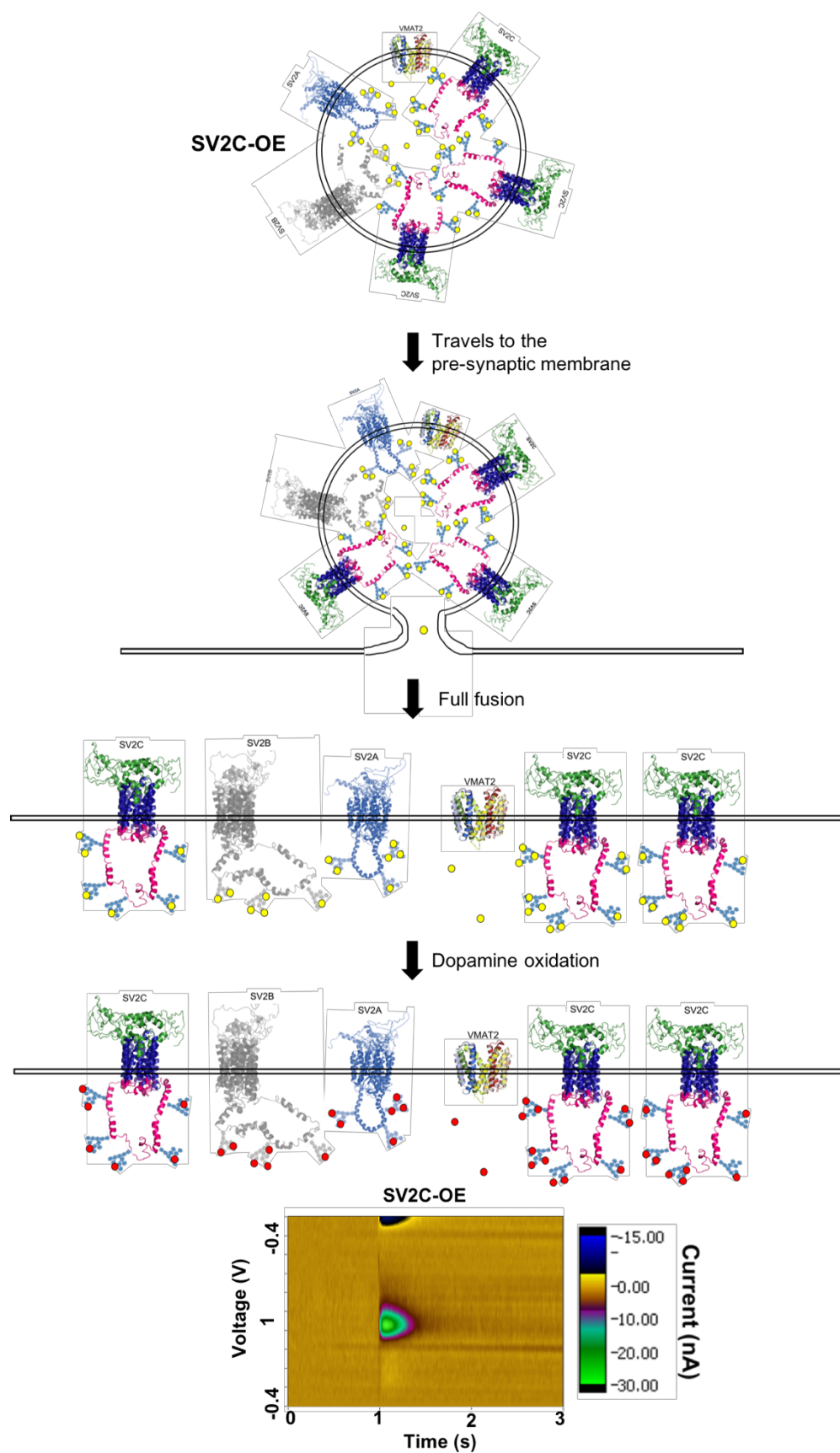


Figure 4.3. Dopamine release in SV2C-overexpressing synaptic vesicles. Dopamine release in a SV2C-overexpressing synaptic vesicle after full fusion exocytosis. The vesicle shown at the top is expressing one VMAT2 molecule (located at the top of the vesicle) as well as one SV2A molecule (blue), one SV2B molecule (gray), and three SV2C molecules (green, blue, and pink) and is loaded with dopamine molecules (yellow dots). This hypothetical representation of a SV2C-overexpressing dopamine vesicle contains 40 molecules of dopamine. Out of 40 dopamine molecules, two (5%) are free-floating within the cytosol and 38 (95%) are bound up in the glycosylated intravesicular loops of the SV2 proteins. After the vesicle travels to the presynaptic membrane, forms a fusion pore (second image), and there is a full collapse of the vesicle membrane into the plasma membrane (third image), the intravesicular lumen becomes exposed to the extracellular space. This allows the two previously free-floating dopamine molecules to diffuse away from the plasma membrane, while the 38 remaining dopamine molecules continue to be bound to the glycosylated loops of the SV2 proteins until they dissociate from the glycosylated moieties through ion-exchange. All dopamine molecules are exposed to the extracellular space after full fusion and are able to be oxidized and detected by FSCV (oxidation potential is represented by the color change in the dopamine molecules from yellow to red).

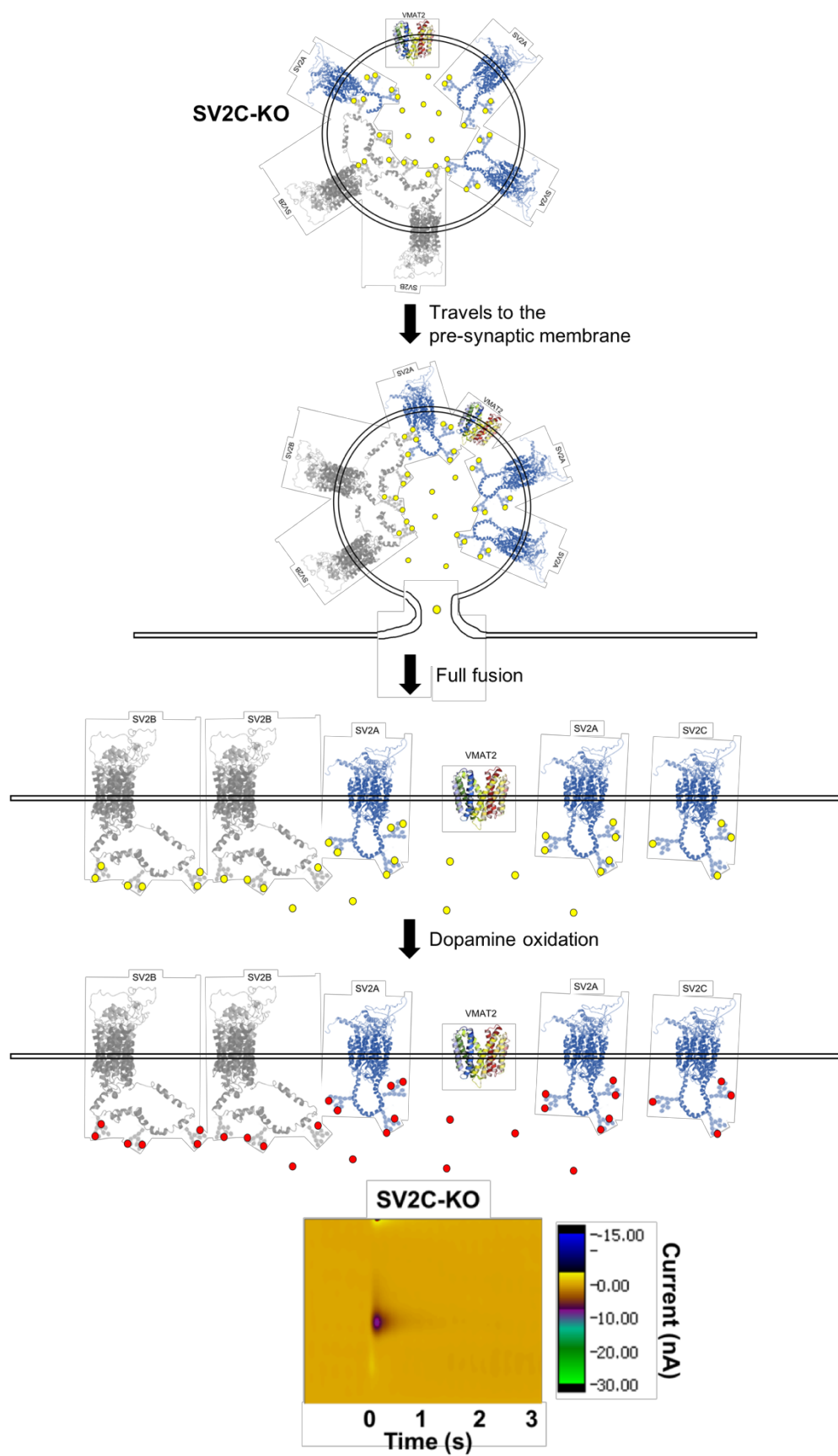


Figure 4.4. Dopamine release in SV2C-KO vesicles. Dopamine release in a SV2C-KO synaptic vesicle after full fusion exocytosis. The vesicle shown at the top is expressing one VMAT2 molecule (located at the top of the vesicle) as well as three SV2A molecules (blue) and two SV2B molecules (gray) and is loaded with dopamine molecules (yellow dots). SV2C deletion produces a reduction in total dopamine content; therefore, the vesicle depicted here contains 20% less dopamine than the WT and SV2C-OE vesicles depicted in the previous figures. This hypothetical representation of a SV2C-KO dopamine vesicle contains 32 molecules of dopamine. Out of 32 dopamine molecules, six (20%) are free-floating within the cytosol and 26 (80%) are bound up in the glycosylated intravesicular loops of the SV2 proteins. After the vesicle travels to the presynaptic membrane, forms a fusion pore (second image), and there is a full collapse of the vesicle membrane into the plasma membrane (third image), the intravesicular lumen becomes exposed to the extracellular space. This allows the six previously free-floating dopamine molecules to diffuse away from the plasma membrane, while the 26 remaining dopamine molecules continue to be bound to the glycosylated loops of the SV2 proteins until they dissociate from the glycosylated moieties through ion-exchange. All dopamine molecules are exposed to the extracellular space after full fusion and are able to be oxidized and detected by FSCV (oxidation potential is represented by the color change in the dopamine molecules from yellow to red).

	WT	SV2C-OE	SV2C-KO
# of SV2s	5	5	5
# of SV2Cs	1	3	0
# of glycosylation sites	17	21	12
Amount of dopamine	40 molecules	40 molecules	32 molecules
Amount of free dopamine	10% (4 molecules)	5% (2 molecules)	20% (6 molecules)
% oxidizable upon release	100%	100%	100%

Table 4.1. SV2 expression and dopamine handling across genotypes.

References

Abeliovich A, Schmitz Y, Farinas I, Choi-Lundberg D, Ho WH, Castillo PE, Shinsky N, Verdugo JM, Armanini M, Ryan A, Hynes M, Phillips H, Sulzer D, Rosenthal A. Mice lacking alpha-synuclein display functional deficits in the nigrostriatal dopamine system. *Neuron*. 2000;25(1):239-252. PubMed PMID: 10707987.

Alter SP, Lenzi GM, Bernstein AI, Miller GW. Vesicular integrity in parkinson's disease. *Current neurology and neuroscience reports*. 2013;13(7):362. doi: 10.1007/s11910-013-0362-3. PubMed PMID: 23690026; PMCID: PMC4019229.

Alter SP, Stout KA, Lohr KM, Taylor TN, Shepherd KR, Wang M, Guillot TS, Miller GW. Reduced vesicular monoamine transport disrupts serotonin signaling but does not cause serotonergic degeneration. *Exp Neurol*. 2016;275 Pt 1:17-24. doi: 10.1016/j.expneurol.2015.09.016. PubMed PMID: 26428905; PMCID: PMC4793730.

Altmann V, Schumacher-Schuh AF, Rieck M, Callegari-Jacques SM, Rieder CR, Hutz MH. Influence of genetic, biological and pharmacological factors on levodopa dose in parkinson's disease. *Pharmacogenomics*. 2016. doi: 10.2217/pgs.15.183. PubMed PMID: 27019953.

Ascherio A, Chen H, Weisskopf MG, O'Reilly E, McCullough ML, Calle EE, Schwarzschild MA, Thun MJ. Pesticide exposure and risk for parkinson's disease. *Ann Neurol*. 2006;60(2):197-203. doi: 10.1002/ana.20904. PubMed PMID: 16802290.

Bajjalieh SM, Frantz GD, Weimann JM, McConnell SK, Scheller RH. Differential expression of synaptic vesicle protein 2 (sv2) isoforms. *J Neurosci*. 1994;14(9):5223-5235. PubMed PMID: 8083732.

Baldwin MR, Barbieri JT. Association of botulinum neurotoxin serotypes a and b with synaptic vesicle protein complexes. *Biochemistry*. 2007;46(11):3200-3210. doi: 10.1021/bi602396x. PubMed PMID: 17311420.

Baldwin MR, Barbieri JT. Association of botulinum neurotoxins with synaptic vesicle protein complexes. *Toxicon*. 2009;54(5):570-574. doi: 10.1016/j.toxicon.2009.01.040. PubMed PMID: 19362106; PMCID: PMC2730980.

Bemis JC, Seegal RF. Pcb-induced inhibition of the vesicular monoamine transporter predicts reductions in synaptosomal dopamine content. *Toxicol Sci*. 2004;80(2):288-295. doi: 10.1093/toxsci/kfh153. PubMed PMID: 15115888.

Bennett MK, Calakos N, Kreiner T, Scheller RH. Synaptic vesicle membrane proteins interact to form a multimeric complex. *J Cell Biol*. 1992;116(3):761-775. PubMed PMID: 1730776; PMCID: PMC2289316.

Bernstein AI, Stout KA, Miller GW. A fluorescent-based assay for live cell, spatially resolved assessment of vesicular monoamine transporter 2-mediated neurotransmitter transport. *J Neurosci Methods*. 2012;209(2):357-366. doi: 10.1016/j.jneumeth.2012.06.002. PubMed PMID: 22698664; PMCID: PMC3429701.

Bombardier JP, Munson M. Three steps forward, two steps back: Mechanistic insights into the assembly and disassembly of the snare complex. *Curr Opin Chem Biol*. 2015;29:66-71. doi: 10.1016/j.cbpa.2015.10.003. PubMed PMID: 26498108; PMCID: PMC4623305.

Bove J, Perier C. Neurotoxin-based models of parkinson's disease. *Neuroscience*. 2012;211:51-76. doi: 10.1016/j.neuroscience.2011.10.057. PubMed PMID: 22108613.

Bradner JM, Suragh TA, Wilson WW, Lazo CR, Stout KA, Kim HM, Wang MZ, Walker DI, Pennell KD, Richardson JR, Miller GW, Caudle WM. Exposure to the polybrominated diphenyl ether mixture de-71 damages the nigrostriatal dopamine system: Role of dopamine handling in neurotoxicity. *Exp Neurol*. 2013;241:138-147. doi: 10.1016/j.expneurol.2012.12.013. PubMed PMID: 23287494; PMCID: PMC3600580.

Brighina L, Riva C, Bertola F, Saracchi E, Fermi S, Goldwurm S, Ferrarese C. Analysis of vesicular monoamine transporter 2 polymorphisms in parkinson's disease. *Neurobiol Aging*. 2013;34(6):1712.e1719-1713. doi: 10.1016/j.neurobiolaging.2012.12.020. PubMed PMID: 23369548; PMCID: PMC3605583.

Brusa L, Orlacchio A, Stefani A, Galati S, Pierantozzi M, Iani C, Mercuri NB. Tetrabenazine improves levodopa-induced peak-dose dyskinesias in patients with parkinson's disease. *Funct Neurol*. 2013;28(2):101-105. doi: 10.11138/FNeur/2013.28.2.101. PubMed PMID: 24125559; PMCID: PMC3812731.

Burke WJ, Li SW, Chung HD, Ruggiero DA, Kristal BS, Johnson EM, Lampe P, Kumar VB, Franko M, Williams EA, Zahm DS. Neurotoxicity of mao metabolites of catecholamine neurotransmitters: Role in neurodegenerative diseases. *Neurotoxicology*. 2004;25(1-2):101-115. doi: 10.1016/s0161-813x(03)00090-1. PubMed PMID: 14697885.

Burre J, Sharma M, Tsetsenis T, Buchman V, Etherton MR, Sudhof TC. Alpha-synuclein promotes snare-complex assembly in vivo and in vitro. *Science (New York, NY)*. 2010;329(5999):1663-1667. doi: 10.1126/science.1195227. PubMed PMID: 20798282; PMCID: PMC3235365.

Butler B, Saha K, Rana T, Becker JP, Sambo D, Davari P, Goodwin JS, Khoshbouei H. Dopamine transporter activity is modulated by alpha-synuclein. *The Journal of biological chemistry*.

2015;290(49):29542-29554. doi: 10.1074/jbc.M115.691592. PubMed PMID: 26442590; PMCID: PMC4705954.

Cannon JR, Geghman KD, Tapias V, Sew T, Dail MK, Li C, Greenamyre JT. Expression of human e46k-mutated alpha-synuclein in bac-transgenic rats replicates early-stage parkinson's disease features and enhances vulnerability to mitochondrial impairment. *Exp Neurol*. 2013;240:44-56. doi: 10.1016/j.expneurol.2012.11.007. PubMed PMID: 23153578; PMCID: PMC3552027.

Cannon JR, Greenamyre JT. Gene-environment interactions in parkinson's disease: Specific evidence in humans and mammalian models. *Neurobiol Dis*. 2013;57:38-46. doi: 10.1016/j.nbd.2012.06.025. PubMed PMID: 22776331; PMCID: PMC3815566.

Caudle WM, Richardson JR, Delea KC, Guillot TS, Wang M, Pennell KD, Miller GW. Polychlorinated biphenyl-induced reduction of dopamine transporter expression as a precursor to parkinson's disease-associated dopamine toxicity. *Toxicol Sci*. 2006;92(2):490-499. doi: 10.1093/toxsci/kfl018. PubMed PMID: 16702228.

Caudle WM, Richardson JR, Wang MZ, Taylor TN, Guillot TS, McCormack AL, Colebrooke RE, Di Monte DA, Emson PC, Miller GW. Reduced vesicular storage of dopamine causes progressive nigrostriatal neurodegeneration. *J Neurosci*. 2007;27(30):8138-8148. doi: 10.1523/JNEUROSCI.0319-07.2007. PubMed PMID: 17652604.

Caughey B, Lansbury PT. Protofibrils, pores, fibrils, and neurodegeneration: Separating the responsible protein aggregates from the innocent bystanders. *Annu Rev Neurosci*. 2003;26:267-298. doi: 10.1146/annurev.neuro.26.010302.081142. PubMed PMID: 12704221.

Chang WP, Sudhof TC. Sv2 renders primed synaptic vesicles competent for ca²⁺ -induced exocytosis. *J Neurosci.* 2009;29(4):883-897. doi: 10.1523/jneurosci.4521-08.2009. PubMed PMID: 19176798; PMCID: PMC2693337.

Chartier-Harlin MC, Kachergus J, Roumier C, Mouroux V, Douay X, Lincoln S, Levecque C, Larvor L, Andrieux J, Hulihan M, Waucquier N, Defebvre L, Amouyel P, Farrer M, Destee A. Alpha-synuclein locus duplication as a cause of familial parkinson's disease. *Lancet.* 2004;364(9440):1167-1169. doi: 10.1016/s0140-6736(04)17103-1. PubMed PMID: 15451224.

Chen CX, Huang SY, Zhang L, Liu YJ. Synaptophysin enhances the neuroprotection of vmat2 in mpp⁺-induced toxicity in mn9d cells. *Neurobiol Dis.* 2005;19(3):419-426. doi: 10.1016/j.nbd.2005.01.014. PubMed PMID: 16023584.

Chen JF, Xu K, Petzer JP, Staal R, Xu YH, Beilstein M, Sonsalla PK, Castagnoli K, Castagnoli N, Jr., Schwarzschild MA. Neuroprotection by caffeine and a(2a) adenosine receptor inactivation in a model of parkinson's disease. *J Neurosci.* 2001;21(10):Rc143. PubMed PMID: 11319241.

Chen L, Ding Y, Cagniard B, Van Laar AD, Mortimer A, Chi W, Hastings TG, Kang UJ, Zhuang X. Unregulated cytosolic dopamine causes neurodegeneration associated with oxidative stress in mice. *J Neurosci.* 2008;28(2):425-433. doi: 10.1523/jneurosci.3602-07.2008. PubMed PMID: 18184785.

Collier TJ, Kanaan NM, Kordower JH. Ageing as a primary risk factor for parkinson's disease: Evidence from studies of non-human primates. *Nature reviews Neuroscience.* 2011;12(6):359-366. doi: 10.1038/nrn3039. PubMed PMID: 21587290; PMCID: PMC3387674.

Conway KA, Rochet JC, Bieganski RM, Lansbury PT, Jr. Kinetic stabilization of the alpha-synuclein protofibril by a dopamine-alpha-synuclein adduct. *Science (New York, NY)*. 2001;294(5545):1346-1349. doi: 10.1126/science.1063522. PubMed PMID: 11701929.

Custer KL, Austin NS, Sullivan JM, Bajjalieh SM. Synaptic vesicle protein 2 enhances release probability at quiescent synapses. *J Neurosci*. 2006;26(4):1303-1313. doi: 10.1523/jneurosci.2699-05.2006. PubMed PMID: 16436618.

Dardou D, Dassesse D, Cuvelier L, Deprez T, De Ryck M, Schiffmann SN. Distribution of sv2c mrna and protein expression in the mouse brain with a particular emphasis on the basal ganglia system. *Brain Res*. 2011;1367:130-145. doi: 10.1016/j.brainres.2010.09.063. PubMed PMID: 20869353.

Dardou D, Monlezun S, Foerch P, Courade JP, Cuvelier L, De Ryck M, Schiffmann SN. A role for sv2c in basal ganglia functions. *Brain research*. 2013;1507:61-73. doi: 10.1016/j.brainres.2013.02.041. PubMed PMID: 23458503.

Denker A, Rizzoli SO. Synaptic vesicle pools: An update. *Front Synaptic Neurosci*. 2010;2:135. doi: 10.3389/fnsyn.2010.00135. PubMed PMID: 21423521; PMCID: PMC3059705.

Diao J, Burre J, Vivona S, Cipriano DJ, Sharma M, Kyoung M, Sudhof TC, Brunger AT. Native alpha-synuclein induces clustering of synaptic-vesicle mimics via binding to phospholipids and synaptobrevin-2/vamp2. *eLife*. 2013;2:e00592. doi: 10.7554/eLife.00592. PubMed PMID: 23638301; PMCID: PMC3639508.

Driver JA, Logroscino G, Gaziano JM, Kurth T. Incidence and remaining lifetime risk of parkinson disease in advanced age. *Neurology*. 2009;72(5):432-438. doi: 10.1212/01.wnl.0000341769.50075.bb. PubMed PMID: 19188574; PMCID: PMC2676726.

Dunn AR, Hoffman CA, Stout KA, Ozawa M, Dhamsania RK, Miller GW. Immunochemical analysis of the expression of sv2c in mouse, macaque and human brain. *Brain research*. 2017a. doi: 10.1016/j.brainres.2017.12.029. PubMed PMID: 29274878; PMCID: PMC6013333.

Dunn AR, Stout KA, Ozawa M, Lohr KM, Hoffman CA, Bernstein AI, Li Y, Wang M, Sgobio C, Sastry N, Cai H, Caudle WM, Miller GW. Synaptic vesicle glycoprotein 2c (sv2c) modulates dopamine release and is disrupted in parkinson disease. *Proceedings of the National Academy of Sciences of the United States of America*. 2017b. doi: 10.1073/pnas.1616892114. PubMed PMID: 28246328.

Elbaz A, Clavel J, Rathouz PJ, Moisan F, Galanaud JP, Delemotte B, Alperovitch A, Tzourio C. Professional exposure to pesticides and parkinson disease. *Ann Neurol*. 2009;66(4):494-504. doi: 10.1002/ana.21717. PubMed PMID: 19847896.

Feany MB, Lee S, Edwards RH, Buckley KM. The synaptic vesicle protein sv2 is a novel type of transmembrane transporter. *Cell*. 1992;70(5):861-867. PubMed PMID: 1355409.

Fischer AF, Matera KM. Stabilization of alpha-synuclein oligomers in vitro by the neurotransmitters, dopamine and norepinephrine: The effect of oxidized catecholamines. *Neurochem Res*. 2015;40(7):1341-1349. doi: 10.1007/s11064-015-1597-y. PubMed PMID: 25956992.

Floor E, Grad O, Leeman SE. Synaptic vesicles containing substance p purified by chromatography on controlled pore glass. *Neuroscience*. 1982;7(7):1647-1655. doi: [https://doi.org/10.1016/0306-4522\(82\)90023-9](https://doi.org/10.1016/0306-4522(82)90023-9).

Fon EA, Poethos EN, Sun BC, Killeen N, Sulzer D, Edwards RH. Vesicular transport regulates monoamine storage and release but is not essential for amphetamine action. *Neuron*. 1997;19(6):1271-1283. PubMed PMID: 9427250.

Fredenburg RA, Rospigliosi C, Meray RK, Kessler JC, Lashuel HA, Eliezer D, Lansbury PT, Jr. The impact of the e46k mutation on the properties of alpha-synuclein in its monomeric and oligomeric states. *Biochemistry*. 2007;46(24):7107-7118. doi: 10.1021/bi7000246. PubMed PMID: 17530780.

Freire C, Koifman S. Pesticide exposure and parkinson's disease: Epidemiological evidence of association. *Neurotoxicology*. 2012;33(5):947-971. doi: 10.1016/j.neuro.2012.05.011. PubMed PMID: 22627180.

Fumagalli F, Gainetdinov RR, Wang YM, Valenzano KJ, Miller GW, Caron MG. Increased methamphetamine neurotoxicity in heterozygous vesicular monoamine transporter 2 knock-out mice. *J Neurosci*. 1999;19(7):2424-2431. PubMed PMID: 10087057.

Gainetdinov RR, Fumagalli F, Wang YM, Jones SR, Levey AI, Miller GW, Caron MG. Increased mptp neurotoxicity in vesicular monoamine transporter 2 heterozygote knockout mice. *J Neurochem*. 1998;70(5):1973-1978. PubMed PMID: 9572281.

Garcia-Reitböck P, Anichtchik O, Bellucci A, Iovino M, Ballini C, Fineberg E, Ghetti B, Della Corte L, Spano P, Tofaris GK, Goedert M, Spillantini MG. Snare protein redistribution and synaptic failure in a transgenic mouse model of parkinson's disease. *Brain : a journal of neurology*. 2010;133(Pt 7):2032-2044. doi: 10.1093/brain/awq132. PubMed PMID: 20534649; PMCID: PMC2892942.

Genskow KR, Bradner JM, Hossain MM, Richardson JR, Michael Caudle W. Selective damage to dopaminergic transporters following exposure to the brominated flame retardant, hbcdd. *Neurotoxicol Teratol.* 2015. doi: 10.1016/j.ntt.2015.06.003. PubMed PMID: 26073293.

Ghiglieri V, Calabrese V, Calabresi P. Alpha-synuclein: From early synaptic dysfunction to neurodegeneration. *Front Neurol.* 2018;9:295. doi: 10.3389/fneur.2018.00295. PubMed PMID: 29780350; PMCID: PMC5945838.

Glatt CE, Wahner AD, White DJ, Ruiz-Linares A, Ritz B. Gain-of-function haplotypes in the vesicular monoamine transporter promoter are protective for parkinson disease in women. *Human molecular genetics.* 2006;15(2):299-305. doi: 10.1093/hmg/ddi445. PubMed PMID: 16339215; PMCID: PMC3643966.

Godwin-Austen RB, Lee PN, Marmot MG, Stern GM. Smoking and parkinson's disease. *J Neurol Neurosurg Psychiatry.* 1982;45(7):577-581. PubMed PMID: 7119826; PMCID: PMC491470.

Goldberg MS, Lansbury PT, Jr. Is there a cause-and-effect relationship between alpha-synuclein fibrillization and parkinson's disease? *Nature cell biology.* 2000;2(7):E115-119. doi: 10.1038/35017124. PubMed PMID: 10878819.

Goldman SM. Environmental toxins and parkinson's disease. *Annu Rev Pharmacol Toxicol.* 2014;54:141-164. doi: 10.1146/annurev-pharmtox-011613-135937. PubMed PMID: 24050700.

Graham DG, Tiffany SM, Bell WR, Jr., Gutknecht WF. Autoxidation versus covalent binding of quinones as the mechanism of toxicity of dopamine, 6-hydroxydopamine, and related compounds toward c1300 neuroblastoma cells in vitro. *Mol Pharmacol.* 1978;14(4):644-653. PubMed PMID: 567274.

Grandinetti A, Morens DM, Reed D, MacEachern D. Prospective study of cigarette smoking and the risk of developing idiopathic parkinson's disease. *Am J Epidemiol.* 1994;139(12):1129-1138. PubMed PMID: 8209872.

Gubernator NG, Zhang H, Staal RG, Mosharov EV, Pereira DB, Yue M, Balsanek V, Vadola PA, Mukherjee B, Edwards RH, Sulzer D, Sames D. Fluorescent false neurotransmitters visualize dopamine release from individual presynaptic terminals. *Science (New York, NY).* 2009;324(5933):1441-1444. doi: 10.1126/science.1172278. PubMed PMID: 19423778.

Guillot TS, Miller GW. Protective actions of the vesicular monoamine transporter 2 (vmat2) in monoaminergic neurons. *Mol Neurobiol.* 2009;39(2):149-170. doi: 10.1007/s12035-009-8059-y. PubMed PMID: 19259829.

Guillot TS, Shepherd KR, Richardson JR, Wang MZ, Li Y, Emson PC, Miller GW. Reduced vesicular storage of dopamine exacerbates methamphetamine-induced neurodegeneration and astrogliosis. *J Neurochem.* 2008;106(5):2205-2217. doi: 10.1111/j.1471-4159.2008.05568.x. PubMed PMID: 18643795; PMCID: PMC4086661.

Harlow ML, Ress D, Stoschek A, Marshall RM, McMahan UJ. The architecture of active zone material at the frog's neuromuscular junction. *Nature.* 2001;409(6819):479-484. doi: 10.1038/35054000. PubMed PMID: 11206537.

Harlow ML, Szule JA, Xu J, Jung JH, Marshall RM, McMahan UJ. Alignment of synaptic vesicle macromolecules with the macromolecules in active zone material that direct vesicle docking. *PloS one.* 2013;8(7):e69410. doi: 10.1371/journal.pone.0069410. PubMed PMID: 23894473; PMCID: PMC3718691.

Hatcher-Martin JM, Gearing M, Steenland K, Levey AI, Miller GW, Pennell KD. Association between polychlorinated biphenyls and parkinson's disease neuropathology. *Neurotoxicology*. 2012;33(5):1298-1304. doi: 10.1016/j.neuro.2012.08.002. PubMed PMID: 22906799; PMCID: PMC3470755.

Hernan MA, Takkouche B, Caamano-Isorna F, Gestal-Otero JJ. A meta-analysis of coffee drinking, cigarette smoking, and the risk of parkinson's disease. *Ann Neurol*. 2002;52(3):276-284. doi: 10.1002/ana.10277. PubMed PMID: 12205639.

Hernan MA, Zhang SM, Rueda-deCastro AM, Colditz GA, Speizer FE, Ascherio A. Cigarette smoking and the incidence of parkinson's disease in two prospective studies. *Ann Neurol*. 2001;50(6):780-786. PubMed PMID: 11761476.

Hill-Burns EM, Singh N, Ganguly P, Hamza TH, Montimurro J, Kay DM, Yearout D, Sheehan P, Frodey K, McLear JA, Feany MB, Hanes SD, Wolfgang WJ, Zabetian CP, Factor SA, Payami H. A genetic basis for the variable effect of smoking/nicotine on parkinson's disease. *Pharmacogenomics J*. 2013;13(6):530-537. doi: 10.1038/tpj.2012.38. PubMed PMID: 23032990; PMCID: PMC3538110.

Hu G, Henke A, Karpowicz RJ, Jr., Sonders MS, Farrimond F, Edwards R, Sulzer D, Sames D. New fluorescent substrate enables quantitative and high-throughput examination of vesicular monoamine transporter 2 (vmat2). *ACS Chem Biol*. 2013;8(9):1947-1954. doi: 10.1021/cb400259n. PubMed PMID: 23859623; PMCID: PMC4557792.

Huang LZ, Parameswaran N, Bordia T, Michael McIntosh J, Quik M. Nicotine is neuroprotective when administered before but not after nigrostriatal damage in rats and monkeys. *J Neurochem*.

2009;109(3):826-837. doi: 10.1111/j.1471-4159.2009.06011.x. PubMed PMID: 19250334; PMCID: PMC2677631.

Iezzi M, Theander S, Janz R, Loze C, Wollheim CB. Sv2a and sv2c are not vesicular ca²⁺ transporters but control glucose-evoked granule recruitment. *J Cell Sci.* 2005;118(Pt 23):5647-5660. doi: 10.1242/jcs.02658. PubMed PMID: 16306227.

Iwai A, Masliah E, Yoshimoto M, Ge N, Flanagan L, de Silva HA, Kittel A, Saitoh T. The precursor protein of non-a beta component of alzheimer's disease amyloid is a presynaptic protein of the central nervous system. *Neuron.* 1995;14(2):467-475. PubMed PMID: 7857654.

Janz R, Goda Y, Geppert M, Missler M, Sudhof TC. Sv2a and sv2b function as redundant ca²⁺ regulators in neurotransmitter release. *Neuron.* 1999;24(4):1003-1016. PubMed PMID: 10624962.

Janz R, Sudhof TC. Sv2c is a synaptic vesicle protein with an unusually restricted localization: Anatomy of a synaptic vesicle protein family. *Neuroscience.* 1999;94(4):1279-1290. PubMed PMID: 10625067.

Jung JH, Szule JA, Marshall RM, McMahan UJ. Variable priming of a docked synaptic vesicle. *Proc Natl Acad Sci U S A.* 2016;113(8):E1098-1107. doi: 10.1073/pnas.1523054113. PubMed PMID: 26858418; PMCID: PMC4776491.

Kajiwara K, Ross-Murphy SB. Synthetic gels on the move. *Nature.* 1992;355:208. doi: 10.1038/355208a0.

Kiyoi T, Liu S, Sahid MNA, Shudou M, Maeyama K, Mogi M. High-throughput screening system for dynamic monitoring of exocytotic vesicle trafficking in mast cells. *PloS one.*

2018;13(6):e0198785. doi: 10.1371/journal.pone.0198785. PubMed PMID: 29883480; PMCID: PMC5993286.

Kumar P, Guha S, Diederichsen U. Snare protein analog-mediated membrane fusion. *Journal of peptide science : an official publication of the European Peptide Society*. 2015;21(8):621-629. doi: 10.1002/psc.2773. PubMed PMID: 25858776.

Kwon IC, Bae YH, Kim SW. Electrically erodible polymer gel for controlled release of drugs. *Nature*. 1991;354(6351):291-293. doi: 10.1038/354291a0. PubMed PMID: 1956379.

Langston JW, Ballard P, Tetrud JW, Irwin I. Chronic parkinsonism in humans due to a product of meperidine-analog synthesis. *Science (New York, NY)*. 1983;219(4587):979-980. PubMed PMID: 6823561.

Lau T, Proissl V, Ziegler J, Schloss P. Visualization of neurotransmitter uptake and release in serotonergic neurons. *J Neurosci Methods*. 2015;241:10-17. doi: 10.1016/j.jneumeth.2014.12.009. PubMed PMID: 25528111.

Lee A, Gilbert RM. Epidemiology of parkinson disease. *Neurol Clin*. 2016;34(4):955-965. doi: 10.1016/j.ncl.2016.06.012. PubMed PMID: 27720003.

Lee FJ, Liu F, Pristupa ZB, Niznik HB. Direct binding and functional coupling of alpha-synuclein to the dopamine transporters accelerate dopamine-induced apoptosis. *FASEB J*. 2001;15(6):916-926. PubMed PMID: 11292651.

Li J, Zhu M, Manning-Bog AB, Di Monte DA, Fink AL. Dopamine and l-dopa disaggregate amyloid fibrils: Implications for parkinson's and alzheimer's disease. *FASEB J*. 2004;18(9):962-964. doi: 10.1096/fj.03-0770fje. PubMed PMID: 15059976.

Lin X, Parisiadou L, Sgobio C, Liu G, Yu J, Sun L, Shim H, Gu XL, Luo J, Long CX, Ding J, Mateo Y, Sullivan PH, Wu LG, Goldstein DS, Lovinger D, Cai H. Conditional expression of parkinson's disease-related mutant alpha-synuclein in the midbrain dopaminergic neurons causes progressive neurodegeneration and degradation of transcription factor nuclear receptor related 1. *J Neurosci.* 2012;32(27):9248-9264. doi: 10.1523/jneurosci.1731-12.2012. PubMed PMID: 22764233; PMCID: PMC3417246.

Liu FT, Chen Y, Yang YJ, Yang L, Yu M, Zhao J, Wu JJ, Huang F, Liu W, Ding ZT, Wang J. Involvement of mortalin/grp75/mthsp70 in the mitochondrial impairments induced by a53t mutant alpha-synuclein. *Brain research.* 2015;1604:52-61. doi: 10.1016/j.brainres.2015.01.050. PubMed PMID: 25665531.

Liu Y, Edwards RH. The role of vesicular transport proteins in synaptic transmission and neural degeneration. *Annu Rev Neurosci.* 1997;20:125-156. doi: 10.1146/annurev.neuro.20.1.125. PubMed PMID: 9056710.

Liu Y, Peter D, Roghani A, Schuldiner S, Prive GG, Eisenberg D, Brecha N, Edwards RH. A cdna that suppresses mpp+ toxicity encodes a vesicular amine transporter. *Cell.* 1992;70(4):539-551. PubMed PMID: 1505023.

Lohr KM, Bernstein AI, Stout KA, Dunn AR, Lazo CR, Alter SP, Wang M, Li Y, Fan X, Hess EJ, Yi H, Vecchio LM, Goldstein DS, Guillot TS, Salahpour A, Miller GW. Increased vesicular monoamine transporter enhances dopamine release and opposes parkinson disease-related neurodegeneration in vivo. *Proceedings of the National Academy of Sciences of the United States of America.* 2014;111(27):9977-9982. doi: 10.1073/pnas.1402134111. PubMed PMID: 24979780; PMCID: PMC4103325.

Lohr KM, Chen M, Hoffman CA, McDaniel MJ, Stout KA, Dunn AR, Wang M, Bernstein A, Miller GW. Vesicular monoamine transporter 2 (vmat2) level regulates mptp vulnerability and clearance of excess dopamine in mouse striatal terminals. *Toxicol Sci.* 2016. doi: 10.1093/toxsci/kfw106. PubMed PMID: 27287315.

Lohr KM, Stout KA, Dunn AR, Wang M, Salahpour A, Guillot TS, Miller GW. Increased vesicular monoamine transporter 2 (vmat2; slc18a2) protects against methamphetamine toxicity. *ACS Chem Neurosci.* 2015. doi: 10.1021/acschemneuro.5b00010. PubMed PMID: 25746685.

Lubbe S, Morris HR. Recent advances in parkinson's disease genetics. *J Neurol.* 2014;261(2):259-266. doi: 10.1007/s00415-013-7003-2. PubMed PMID: 23798000.

Lynch BA, Lambeng N, Nocka K, Kensel-Hammes P, Bajjalieh SM, Matagne A, Fuks B. The synaptic vesicle protein sv2a is the binding site for the antiepileptic drug levetiracetam. *Proceedings of the National Academy of Sciences of the United States of America.* 2004;101(26):9861-9866. doi: 10.1073/pnas.0308208101. PubMed PMID: 15210974; PMCID: PMC470764.

Mahrhold S, Bergstrom T, Stern D, Dorner BG, Astot C, Rummel A. Only the complex n559-glycan in sv2c mediates high affinity binding to botulinum neurotoxin serotype a1. *Biochem J.* 2016. doi: 10.1042/bcj20160439. PubMed PMID: 27313224.

Mahrhold S, Rummel A, Bigalke H, Davletov B, Binz T. The synaptic vesicle protein 2c mediates the uptake of botulinum neurotoxin a into phrenic nerves. *FEBS letters.* 2006;580(8):2011-2014. doi: 10.1016/j.febslet.2006.02.074. PubMed PMID: 16545378.

Marder K, Levy G, Louis ED, Mejia-Santana H, Cote L, Andrews H, Harris J, Waters C, Ford B, Frucht S, Fahn S, Ottman R. Familial aggregation of early- and late-onset parkinson's disease. *Ann Neurol*. 2003;54(4):507-513. doi: 10.1002/ana.10711. PubMed PMID: 14520664.

Mendoza-Torreblanca JG, Vanoye-Carlo A, Phillips-Farfan BV, Carmona-Aparicio L, Gomez-Lira G. Synaptic vesicle protein 2a: Basic facts and role in synaptic function. *Eur J Neurosci*. 2013;38(11):3529-3539. doi: 10.1111/ejn.12360. PubMed PMID: 24102679.

Miller GW, Kirby ML, Levey AI, Bloomquist JR. Heptachlor alters expression and function of dopamine transporters. *Neurotoxicology*. 1999;20(4):631-637. PubMed PMID: 10499361.

Miraglia F, Ricci A, Rota L, Colla E. Subcellular localization of alpha-synuclein aggregates and their interaction with membranes. *Neural regeneration research*. 2018;13(7):1136-1144. doi: 10.4103/1673-5374.235013. PubMed PMID: 30028312; PMCID: PMC6065224.

Mooslehner KA, Chan PM, Xu W, Liu L, Smadja C, Humby T, Allen ND, Wilkinson LS, Emson PC. Mice with very low expression of the vesicular monoamine transporter 2 gene survive into adulthood: Potential mouse model for parkinsonism. *Mol Cell Biol*. 2001;21(16):5321-5331. doi: 10.1128/mcb.21.16.5321-5331.2001. PubMed PMID: 11463816; PMCID: PMC87256.

Mor DE, Tsika E, Mazzulli JR, Gould NS, Kim H, Daniels MJ, Doshi S, Gupta P, Grossman JL, Tan VX, Kalb RG, Caldwell KA, Caldwell GA, Wolfe JH, Ischiropoulos H. Dopamine induces soluble alpha-synuclein oligomers and nigrostriatal degeneration. *Nat Neurosci*. 2017;20(11):1560-1568. doi: 10.1038/nn.4641. PubMed PMID: 28920936; PMCID: PMC5893155.

Mutch SA, Kensel-Hammes P, Gadd JC, Fujimoto BS, Allen RW, Schiro PG, Lorenz RM, Kuyper CL, Kuo JS, Bajjalieh SM, Chiu DT. Protein quantification at the single vesicle level reveals that

a subset of synaptic vesicle proteins are trafficked with high precision. *J Neurosci.* 2011;31(4):1461-1470. doi: 10.1523/jneurosci.3805-10.2011. PubMed PMID: 21273430; PMCID: PMC3078718.

Nemani VM, Lu W, Berge V, Nakamura K, Onoa B, Lee MK, Chaudhry FA, Nicoll RA, Edwards RH. Increased expression of alpha-synuclein reduces neurotransmitter release by inhibiting synaptic vesicle recluster after endocytosis. *Neuron.* 2010;65(1):66-79. doi: 10.1016/j.neuron.2009.12.023. PubMed PMID: 20152114; PMCID: PMC3119527.

Nistico R, Mehdawy B, Piccirilli S, Mercuri N. Paraquat- and rotenone-induced models of parkinson's disease. *Int J Immunopathol Pharmacol.* 2011;24(2):313-322. doi: 10.1177/039463201102400205. PubMed PMID: 21658306.

Nowack A, Yao J, Custer KL, Bajjalieh SM. Sv2 regulates neurotransmitter release via multiple mechanisms. *American journal of physiology Cell physiology.* 2010;299(5):C960-967. doi: 10.1152/ajpcell.00259.2010. PubMed PMID: 20702688; PMCID: PMC2980308.

Nur S, Adams CE. Chlorpromazine versus reserpine for schizophrenia. *Cochrane Database Syst Rev.* 2016;4:Cd012122. doi: 10.1002/14651858.CD012122.pub2. PubMed PMID: 27124109.

Parain K, Hapdey C, Rousselet E, Marchand V, Dumery B, Hirsch EC. Cigarette smoke and nicotine protect dopaminergic neurons against the 1-methyl-4-phenyl-1,2,3,6-tetrahydropyridine parkinsonian toxin. *Brain research.* 2003;984(1-2):224-232. PubMed PMID: 12932857.

Parkinson J. *An essay on the shaking palsy.* London: Sherwood, Neely, and Jones; 1817.

Pereira DB, Schmitz Y, Meszaros J, Merchant P, Hu G, Li S, Henke A, Lizardi-Ortiz JE, Karpowicz RJ, Jr., Morgenstern TJ, Sonders MS, Kanter E, Rodriguez PC, Mosharov EV, Sames

D, Sulzer D. Fluorescent false neurotransmitter reveals functionally silent dopamine vesicle clusters in the striatum. *Nat Neurosci.* 2016;19(4):578-586. doi: 10.1038/nn.4252. PubMed PMID: 26900925; PMCID: PMC4853199.

Pifl C, Rajput A, Reither H, Blesa J, Cavada C, Obeso JA, Rajput AH, Hornykiewicz O. Is parkinson's disease a vesicular dopamine storage disorder? Evidence from a study in isolated synaptic vesicles of human and nonhuman primate striatum. *J Neurosci.* 2014;34(24):8210-8218. doi: 10.1523/jneurosci.5456-13.2014. PubMed PMID: 24920625.

Polymeropoulos MH, Lavedan C, Leroy E, Ide SE, Dehejia A, Dutra A, Pike B, Root H, Rubenstein J, Boyer R, Stenroos ES, Chandrasekharappa S, Athanassiadou A, Papapetropoulos T, Johnson WG, Lazzarini AM, Duvoisin RC, Di Iorio G, Golbe LI, Nussbaum RL. Mutation in the alpha-synuclein gene identified in families with parkinson's disease. *Science (New York, NY).* 1997;276(5321):2045-2047. PubMed PMID: 9197268.

Porta M, Sassi M, Cavallazzi M, Fornari M, Brambilla A, Servello D. Tourette's syndrome and role of tetrabenazine: Review and personal experience. *Clin Drug Investig.* 2008;28(7):443-459. PubMed PMID: 18544005.

Postuma RB, Lang AE, Munhoz RP, Charland K, Pelletier A, Moscovich M, Filla L, Zanatta D, Rios Romenets S, Altman R, Chuang R, Shah B. Caffeine for treatment of parkinson disease: A randomized controlled trial. *Neurology.* 2012;79(7):651-658. doi: 10.1212/WNL.0b013e318263570d. PubMed PMID: 22855866; PMCID: PMC3414662.

Rahamimoff R, Fernandez JM. Pre- and postfusion regulation of transmitter release. *Neuron.* 1997;18(1):17-27. PubMed PMID: 9010202.

Ramachandiran S, Hansen JM, Jones DP, Richardson JR, Miller GW. Divergent mechanisms of paraquat, mpp+, and rotenone toxicity: Oxidation of thioredoxin and caspase-3 activation. *Toxicol Sci.* 2007;95(1):163-171. doi: 10.1093/toxsci/kfl125. PubMed PMID: 17018646.

Rana AQ, Ahmed US, Chaudry ZM, Vasani S. Parkinson's disease: A review of non-motor symptoms. *Expert Rev Neurother.* 2015;15(5):549-562. doi: 10.1586/14737175.2015.1038244. PubMed PMID: 25936847.

Reeve A, Simcox E, Turnbull D. Ageing and parkinson's disease: Why is advancing age the biggest risk factor? *Ageing research reviews.* 2014;14:19-30. doi: 10.1016/j.arr.2014.01.004. PubMed PMID: 24503004; PMCID: PMC3989046.

Reigada D, Diez-Perez I, Gorostiza P, Verdaguer A, Gomez de Aranda I, Pineda O, Vilarrasa J, Marsal J, Blasi J, Aleu J, Solsona C. Control of neurotransmitter release by an internal gel matrix in synaptic vesicles. *Proceedings of the National Academy of Sciences of the United States of America.* 2003;100(6):3485-3490. doi: 10.1073/pnas.0336914100. PubMed PMID: 12629223; PMCID: PMC152319.

Reimsnider S, Manfredsson FP, Muzyczka N, Mandel RJ. Time course of transgene expression after intrastriatal pseudotyped raav2/1, raav2/2, raav2/5, and raav2/8 transduction in the rat. *Mol Ther.* 2007;15(8):1504-1511. doi: 10.1038/sj.mt.6300227. PubMed PMID: 17565350.

Richardson JR, Caudle WM, Wang M, Dean ED, Pennell KD, Miller GW. Developmental exposure to the pesticide dieldrin alters the dopamine system and increases neurotoxicity in an animal model of parkinson's disease. *FASEB J.* 2006;20(10):1695-1697. doi: 10.1096/fj.06-5864fje. PubMed PMID: 16809432.

Richardson JR, Miller GW. Acute exposure to aroclor 1016 or 1260 differentially affects dopamine transporter and vesicular monoamine transporter 2 levels. *Toxicol Lett.* 2004;148(1-2):29-40. doi: 10.1016/j.toxlet.2003.12.006. PubMed PMID: 15019086.

Rilstone JJ, Alkhatir RA, Minassian BA. Brain dopamine-serotonin vesicular transport disease and its treatment. *N Engl J Med.* 2013;368(6):543-550. doi: 10.1056/NEJMoa1207281. PubMed PMID: 23363473.

Rizzoli SO. Synaptic vesicle recycling: Steps and principles. *EMBO J.* 2014;33(8):788-822. doi: 10.1002/emboj.201386357. PubMed PMID: 24596248; PMCID: PMC4194108.

Rodriguez PC, Pereira DB, Borgkvist A, Wong MY, Barnard C, Sonders MS, Zhang H, Sames D, Sulzer D. Fluorescent dopamine tracer resolves individual dopaminergic synapses and their activity in the brain. *Proceedings of the National Academy of Sciences of the United States of America.* 2013;110(3):870-875. doi: 10.1073/pnas.1213569110. PubMed PMID: 23277566; PMCID: PMC3549135.

Rosenmund C, Stevens CF. Definition of the readily releasable pool of vesicles at hippocampal synapses. *Neuron.* 1996;16(6):1197-1207. PubMed PMID: 8663996.

Ross OA, Braithwaite AT, Skipper LM, Kachergus J, Hulihan MM, Middleton FA, Nishioka K, Fuchs J, Gasser T, Maraganore DM, Adler CH, Larvor L, Chartier-Harlin MC, Nilsson C, Langston JW, Gwinn K, Hattori N, Farrer MJ. Genomic investigation of alpha-synuclein multiplication and parkinsonism. *Ann Neurol.* 2008;63(6):743-750. doi: 10.1002/ana.21380. PubMed PMID: 18571778; PMCID: PMC3850281.

Salgado R, Lopez-Doval S, Pereiro N, Lafuente A. Perfluorooctane sulfonate (pfos) exposure could modify the dopaminergic system in several limbic brain regions. *Toxicol Lett.* 2016;240(1):226-235. doi: 10.1016/j.toxlet.2015.10.023. PubMed PMID: 26529483.

Schivell AE, Mochida S, Kensel-Hammes P, Custer KL, Bajjalieh SM. Sv2a and sv2c contain a unique synaptotagmin-binding site. *Molecular and cellular neurosciences.* 2005;29(1):56-64. doi: 10.1016/j.mcn.2004.12.011. PubMed PMID: 15866046.

Scott LJ. Tetrabenazine: For chorea associated with huntington's disease. *CNS drugs.* 2011;25(12):1073-1085. doi: 10.2165/11208330-000000000-00000. PubMed PMID: 22133328.

Semchuk KM, Love EJ, Lee RG. Parkinson's disease and exposure to agricultural work and pesticide chemicals. *Neurology.* 1992;42(7):1328-1335. PubMed PMID: 1620342.

Serpell LC, Berriman J, Jakes R, Goedert M, Crowther RA. Fiber diffraction of synthetic alpha-synuclein filaments shows amyloid-like cross-beta conformation. *Proceedings of the National Academy of Sciences of the United States of America.* 2000;97(9):4897-4902. PubMed PMID: 10781096; PMCID: PMC18329.

Sherer TB, Richardson JR, Testa CM, Seo BB, Panov AV, Yagi T, Matsuno-Yagi A, Miller GW, Greenamyre JT. Mechanism of toxicity of pesticides acting at complex i: Relevance to environmental etiologies of parkinson's disease. *J Neurochem.* 2007;100(6):1469-1479. doi: 10.1111/j.1471-4159.2006.04333.x. PubMed PMID: 17241123.

Shu X, Lev-Ram V, Deerinck TJ, Qi Y, Ramko EB, Davidson MW, Jin Y, Ellisman MH, Tsien RY. A genetically encoded tag for correlated light and electron microscopy of intact cells, tissues, and organisms. *PLoS Biol.* 2011;9(4):e1001041. doi: 10.1371/journal.pbio.1001041. PubMed PMID: 21483721; PMCID: PMC3071375.

Shulman JM, De Jager PL, Feany MB. Parkinson's disease: Genetics and pathogenesis. *Annu Rev Pathol.* 2011;6:193-222. doi: 10.1146/annurev-pathol-011110-130242. PubMed PMID: 21034221.

Singh K, Singh S, Singhal NK, Sharma A, Parmar D, Singh MP. Nicotine- and caffeine-mediated changes in gene expression patterns of mptp-lesioned mouse striatum: Implications in neuroprotection mechanism. *Chem Biol Interact.* 2010;185(2):81-93. doi: 10.1016/j.cbi.2010.03.015. PubMed PMID: 20230807.

Skarnes WC, Rosen B, West AP, Koutourakis M, Bushell W, Iyer V, Mujica AO, Thomas M, Harrow J, Cox T, Jackson D, Severin J, Biggs P, Fu J, Nefedov M, de Jong PJ, Stewart AF, Bradley A. A conditional knockout resource for the genome-wide study of mouse gene function. *Nature.* 2011;474(7351):337-342. doi: 10.1038/nature10163. PubMed PMID: 21677750; PMCID: PMC3572410.

Spillantini MG, Schmidt ML, Lee VM, Trojanowski JQ, Jakes R, Goedert M. Alpha-synuclein in lewy bodies. *Nature.* 1997;388(6645):839-840. doi: 10.1038/42166. PubMed PMID: 9278044.

Staal RG, Sonsalla PK. Inhibition of brain vesicular monoamine transporter (vmat2) enhances 1-methyl-4-phenylpyridinium neurotoxicity in vivo in rat striata. *J Pharmacol Exp Ther.* 2000;293(2):336-342. PubMed PMID: 10773000.

Stefanis L, Larsen KE, Rideout HJ, Sulzer D, Greene LA. Expression of a53t mutant but not wild-type alpha-synuclein in pc12 cells induces alterations of the ubiquitin-dependent degradation system, loss of dopamine release, and autophagic cell death. *J Neurosci.* 2001;21(24):9549-9560. PubMed PMID: 11739566.

Szule JA, Jung JH, McMahan UJ. The structure and function of 'active zone material' at synapses. *Philos Trans R Soc Lond B Biol Sci.* 2015;370(1672). doi: 10.1098/rstb.2014.0189. PubMed PMID: 26009768; PMCID: PMC4455758.

Takahashi N, Miner LL, Sora I, Ujike H, Revay RS, Kostic V, Jackson-Lewis V, Przedborski S, Uhl GR. *Vmat2* knockout mice: Heterozygotes display reduced amphetamine-conditioned reward, enhanced amphetamine locomotion, and enhanced mptp toxicity. *Proc Natl Acad Sci U S A.* 1997;94(18):9938-9943. PubMed PMID: 9275230; PMCID: PMC23302.

Takami C, Eguchi K, Hori T, Takahashi T. Impact of vesicular glutamate leakage on synaptic transmission at the calyx of held. *J Physiol.* 2017;595(4):1263-1271. doi: 10.1113/jp273467. PubMed PMID: 27801501; PMCID: PMC5309358.

Takamori S, Holt M, Stenius K, Lemke EA, Grønborg M, Riedel D, Urlaub H, Schenck S, Brügger B, Ringler P, Müller SA, Rammner B, Gräter F, Hub JS, De Groot BL, Mieskes G, Moriyama Y, Klingauf J, Grubmüller H, Heuser J, Wieland F, Jahn R. Molecular anatomy of a trafficking organelle. *Cell.* 2006;127(4):831-846. doi: 10.1016/j.cell.2006.10.030. PubMed PMID: 17110340.

Tanaka T, Nishio I, Sun ST, Ueno-Nishio S. Collapse of gels in an electric field. *Science (New York, NY).* 1982;218(4571):467-469. doi: 10.1126/science.218.4571.467. PubMed PMID: 17808541.

Tanner CM, Kamel F, Ross GW, Hoppin JA, Goldman SM, Korell M, Marras C, Bhudhikanok GS, Kasten M, Chade AR, Comyns K, Richards MB, Meng C, Priestley B, Fernandez HH, Cambi F, Umbach DM, Blair A, Sandler DP, Langston JW. Rotenone, paraquat, and parkinson's disease. *Environ Health Perspect.* 2011;119(6):866-872. doi: 10.1289/ehp.1002839. PubMed PMID: 21269927; PMCID: PMC3114824.

Taylor TN, Caudle WM, Miller GW. Vmat2-deficient mice display nigral and extranigral pathology and motor and nonmotor symptoms of parkinson's disease. *Parkinsons Dis.* 2011;2011:124165. doi: 10.4061/2011/124165. PubMed PMID: 21403896; PMCID: PMC3043293.

Taylor TN, Caudle WM, Shepherd KR, Noorian A, Jackson CR, Iuvone PM, Weinshenker D, Greene JG, Miller GW. Nonmotor symptoms of parkinson's disease revealed in an animal model with reduced monoamine storage capacity. *J Neurosci.* 2009;29(25):8103-8113. doi: 10.1523/jneurosci.1495-09.2009. PubMed PMID: 19553450; PMCID: PMC2813143.

Theillet FX, Binolfi A, Bekei B, Martorana A, Rose HM, Stuver M, Verzini S, Lorenz D, van Rossum M, Goldfarb D, Selenko P. Structural disorder of monomeric alpha-synuclein persists in mammalian cells. *Nature.* 2016;530(7588):45-50. doi: 10.1038/nature16531. PubMed PMID: 26808899.

Thomas P, Smart TG. Hek293 cell line: A vehicle for the expression of recombinant proteins. *J Pharmacol Toxicol Methods.* 2005;51(3):187-200. doi: 10.1016/j.vascn.2004.08.014. PubMed PMID: 15862464.

Vautrin J. Sv2 frustrating exocytosis at the semi-diffusor synapse. *Synapse (New York, NY).* 2009;63(4):319-338. doi: 10.1002/syn.20610. PubMed PMID: 19140166.

Volles MJ, Lansbury PT, Jr. Zeroing in on the pathogenic form of alpha-synuclein and its mechanism of neurotoxicity in parkinson's disease. *Biochemistry.* 2003;42(26):7871-7878. doi: 10.1021/bi030086j. PubMed PMID: 12834338.

Wan QF, Zhou ZY, Thakur P, Vila A, Sherry DM, Janz R, Heidelberger R. Sv2 acts via presynaptic calcium to regulate neurotransmitter release. *Neuron*. 2010;66(6):884-895. doi: 10.1016/j.neuron.2010.05.010. PubMed PMID: 20620874; PMCID: PMC2913707.

Wang L, Das U, Scott DA, Tang Y, McLean PJ, Roy S. Alpha-synuclein multimers cluster synaptic vesicles and attenuate recycling. *Curr Biol*. 2014;24(19):2319-2326. doi: 10.1016/j.cub.2014.08.027. PubMed PMID: 25264250; PMCID: PMC4190006.

Wang YM, Gainetdinov RR, Fumagalli F, Xu F, Jones SR, Bock CB, Miller GW, Wightman RM, Caron MG. Knockout of the vesicular monoamine transporter 2 gene results in neonatal death and supersensitivity to cocaine and amphetamine. *Neuron*. 1997;19(6):1285-1296. PubMed PMID: 9427251.

Winner B, Jappelli R, Maji SK, Desplats PA, Boyer L, Aigner S, Hetzer C, Loher T, Vilar M, Campioni S, Tzitzilonis C, Soragni A, Jessberger S, Mira H, Consiglio A, Pham E, Masliah E, Gage FH, Riek R. In vivo demonstration that alpha-synuclein oligomers are toxic. *Proceedings of the National Academy of Sciences of the United States of America*. 2011;108(10):4194-4199. doi: 10.1073/pnas.1100976108. PubMed PMID: 21325059; PMCID: PMC3053976.

Wu M, Kang X, Wang Q, Zhou C, Mohan C, Peng A. Regulator of g protein signaling-1 modulates paraquat-induced oxidative stress and longevity via the insulin like signaling pathway in *Caenorhabditis elegans*. *Toxicol Lett*. 2017;273:97-105. doi: 10.1016/j.toxlet.2017.03.027. PubMed PMID: 28366735.

Xu T, Bajjalieh SM. Sv2 modulates the size of the readily releasable pool of secretory vesicles. *Nature Cell Biology*. 2001;3(8):691-698. doi: 10.1038/35087000. PubMed PMID: 11483953.

Xu-Friedman MA, Harris KM, Regehr WG. Three-dimensional comparison of ultrastructural characteristics at depressing and facilitating synapses onto cerebellar purkinje cells. *J Neurosci.* 2001;21(17):6666-6672. PubMed PMID: 11517256.

Yao G, Zhang S, Mahrhold S, Lam KH, Stern D, Bagramyan K, Perry K, Kalkum M, Rummel A, Dong M, Jin R. N-linked glycosylation of sv2 is required for binding and uptake of botulinum neurotoxin a. *Nat Struct Mol Biol.* 2016. doi: 10.1038/nsmb.3245. PubMed PMID: 27294781.

Yao J, Nowack A, Kensel-Hammes P, Gardner RG, Bajjalieh SM. Cotrafficking of sv2 and synaptotagmin at the synapse. *J Neurosci.* 2010;30(16):5569-5578. doi: 10.1523/jneurosci.4781-09.2010. PubMed PMID: 20410110; PMCID: PMC2866018.

Zhang H, Gubernator NG, Yue M, Staal RG, Mosharov EV, Pereira D, Balsanek V, Vadola PA, Mukherjee B, Edwards RH, Sulzer D, Sames D. Dopamine release at individual presynaptic terminals visualized with ffns. *Journal of visualized experiments : JoVE.* 2009(30). doi: 10.3791/1562. PubMed PMID: 19721412; PMCID: PMC3253714.

Zhang JH, Chung TD, Oldenburg KR. A simple statistical parameter for use in evaluation and validation of high throughput screening assays. *Journal of biomolecular screening.* 1999;4(2):67-73. PubMed PMID: 10838414.

Appendix I- SV2C expression mediates alpha-synuclein pathology

Abstract

Dopamine vesicle function is impaired in patients with Parkinson's disease (PD) and mutations in numerous vesicular proteins have been associated with PD development. One such protein is alpha-synuclein, which facilitates vesicular trafficking, recycling, clustering, and docking. Mice overexpressing A53T mutant alpha-synuclein (A53T-OE) exhibit dopaminergic neurodegeneration, motor deficits, and decreased dopamine release. The synaptic vesicle glycoprotein 2 C (SV2C) also positively modulates dopamine vesicle function and mice with a genetic deletion of SV2C exhibit decreased dopamine release and motor deficits. There is also a connection between SV2C and alpha-synuclein, with A53T-OE mice exhibiting abnormal expression of SV2C in the striatum. Here, we further explore the interaction between SV2C, alpha-synuclein, and dopamine neuron vulnerability by using A53T-OE mice, SV2C knockout (SV2C-KO) mice, and viral vectors to determine the effect of SV2C expression on alpha-synuclein pathogenesis and neurotoxicity. We injected A53T-OE mice with AAV2/9 mCherry or AAV2/9 miniSOG-SV2C vector in the substantia nigra and show that SV2C overexpression resulted in a decrease in total alpha-synuclein expression. We then injected SV2C-KO and SV2C-WT mice with AAV2/9 mCherry or AAV2/9 human alpha-synuclein vector in the substantia nigra and show that alpha-synuclein injection resulted in overexpression of alpha-synuclein and enhanced dopamine cell loss in SV2C-KO mice. While preliminary, these results indicate that SV2C expression affects dopamine neuron vulnerability and alpha-synuclein pathogenesis.

Introduction

Parkinson's disease (PD) is characterized by the degeneration of dopaminergic neurons in the substantia nigra pars compacta and affects over 1% of the population over age 60, making aging the greatest risk factor for developing PD (Collier *et al.*, 2011; Driver *et al.*, 2009). Dysfunctional dopamine handling is also fundamental to the disease, as mutations in the gene encoding VMAT2 lead to infantile parkinsonism (Rilstone *et al.*, 2013), increased expression of VMAT2 is associated with decreased risk for PD (Brighina *et al.*, 2013; Glatt *et al.*, 2006), and dopamine vesicle function is impaired in patients with PD (Pifl *et al.*, 2014).

Mutations and alterations in the expression of several vesicular-associated proteins, such as alpha-synuclein and the synaptic vesicular glycoprotein 2 C (SV2C), have been linked to PD. Alpha-synuclein is the main protein component in Lewy bodies, cytoplasmic neuronal aggregates associated with PD pathology and other related dementias (Spillantini *et al.*, 1997). Alpha-synuclein has been associated with neurotransmitter release and synaptic plasticity, as it facilitates vesicular trafficking, recycling, clustering, and docking (Diao *et al.*, 2013; Miraglia *et al.*, 2018; Nemani *et al.*, 2010; Wang *et al.*, 2014). Mutations in alpha-synuclein have been correlated to PD risk (Ross *et al.*, 2008), early onset of PD (Polymeropoulos *et al.*, 1997), and altered dopamine neurotransmitter metabolism (Cannon *et al.*, 2013). The A53T mutation of alpha-synuclein is the most frequent and best characterized mutation of alpha-synuclein (Miraglia *et al.*, 2018), and a strain of mice overexpressing A53T mutant alpha-synuclein in midbrain dopaminergic neurons under the Pitx3 promoter (A53T-OE mice) exhibit dopaminergic neurodegeneration, motor deficits, and decreased dopamine release (Lin *et al.*, 2012).

SV2s have also been implicated in several aspects of vesicular function and one variant in the SV2 family, SV2C, was recently identified as a genetic mediator of one of the most robust environmental modulators of PD risk: nicotine/smoking use, which is strongly protective against

PD (Hill-Burns *et al.*, 2013). Further, mice with a genetic deletion of SV2C mirror the motor disturbances and deficits in gait seen in human PD patients, displaying decreased total locomotor activity and a reduction in stride length (Dunn *et al.*, 2017b). Several lines of evidence also suggest a connection between SV2C and alpha-synuclein: there is aggregated SV2C in mice that overexpress the A53T variant of alpha-synuclein and immunoprecipitation of SV2C pulls down alpha-synuclein (Dunn *et al.*, 2017b).

Our lab has recently produced a line of mice lacking SV2C (SV2C-KO) that exhibit reduced striatal dopamine content, decreased stimulated dopamine release in the dorsal striatum, and increased expression of higher molecular weight forms of alpha-synuclein (Dunn *et al.*, 2017b). Here, we further explore the interaction between SV2C, alpha-synuclein, and dopamine neuron vulnerability by using A53T-OE mice, SV2C-KO mice, and viral vectors to determine the effect of SV2C expression on alpha-synuclein pathogenesis and neurotoxicity. We hypothesized that SV2C expression mediated dopamine neuron vulnerability such that increased expression of SV2C would confer protection from alpha-synuclein toxicity and decreased expression of SV2C would result in an exacerbated response to alpha-synuclein toxicity. To determine whether alpha-synuclein toxicity was diminished with enhanced SV2C expression, we injected A53T-OE and A53T-WT mice with AAV2/9 mCherry or AAV2/9 miniSOG-SV2C vector in the substantia nigra and show that stereotactic injection of SV2C resulted in SV2C overexpression and a decrease in total alpha-synuclein expression. To determine whether alpha-synuclein toxicity was exacerbated in SV2C-KO mice, we injected a small cohort of SV2C-KO and SV2C-WT mice with AAV2/9 mCherry or AAV2/9 human alpha-synuclein vector in the substantia nigra and show that stereotactic injection of alpha-synuclein resulted in alpha-synuclein overexpression and enhanced dopamine cell loss in SV2C-KO mice. While preliminary, these results indicate that SV2C expression mediates dopamine neuron vulnerability and alpha-synuclein pathogenesis.

Materials and Methods

Mice. Male and female mice overexpressing the A53T alpha-synuclein missense mutation in nigrostriatal dopamine cells under the *Pitx3* promoter were generated as described previously (A53T-OE) (Lin *et al.*, 2012). A53T-OE mice and their WT littermates were aged to two months before undergoing stereotactic injection. Male and female SV2C-KO mice and their WT littermates were aged to two months before undergoing stereotactic injection. SV2C-KO mice were generated as previously described (Dunn *et al.*, 2017b). Briefly, C57BL/6 embryonic stem cells from the European Conditional Mouse Mutagenesis Program containing the SV2C “knockout-first construct” (Skarnes *et al.*, 2011) were implanted into female C57BL/6 mice. Heterozygous knockout-first (KOF) mice were then bred with FLP homozygous mice (Charles River) to excise the LacZ/neo cassette and restore a functional gene, with exon 2 flanked by loxP sites. Heterozygous SV2C-floxed mice positive for FLP were crossed with nestin-CRE mice (Charles River), then bred to homozygosity to generate global neuronal knockout of SV2C. Mice were separated into individual cages with food and water *ad libitum* one day prior to stereotactic injection or tissue collection for immunohistochemistry. All procedures were carried out in accordance with NIH guidelines and the Institutional Animal Care and Use Committee at Emory University.

Stereotactic injections. Mice were anesthetized with vaporized isoflurane 1-4% (Piramal Healthcare) and placed into a stereotaxic frame with nose cone. Anesthesia was maintained using 1-2% isoflurane for the duration of surgery. An incision was made along the midline of the scalp. Thirty percent hydrogen peroxide was used to clean the skull and to better visualize lambda and bregma and ensure that the head was level. A hole was drilled through the skull above the left substantia nigra and AAV 2/9 vectors were injected at a rate of 0.5 μ L per minute (2 μ L vector; AP -3.2 mm, ML -1.2 mm, DV -4.5 mm from surface of the brain). AAV 2/9 vectors containing

either mCherry or miniSOG-tagged SV2C were injected into A53T-WT and A53T-OE mice. AAV 2/9 vectors containing either mCherry or human alpha-synuclein were injected into SV2C-WT and SV2C-KO mice. All AAV 2/9 vectors were provided by Dr. Fredric Manfredsson. After each injection, the needle (pulled glass needle attached to a Hamilton syringe) was left in place for five minutes and then was slowly withdrawn. The skin was glued back together (3M Vetbond) and neomycin antibiotic ointment (Waterjel) and lidocaine cream (Aspercreme) were placed on the incision. Animals were allowed to recover in their home cage on a heating pad for one-hour post-surgery. Buprenorphine injections were given once within this hour of recovery for post-operative pain relief (Buprenex, McKesson, dose 0.05 mg/kg body weight) and again the morning after surgery. Animals were monitored daily for three days post-surgery and were sacrificed for tissue collection 8 weeks post-surgery.

Immunohistochemistry. Mice were killed by rapid decapitation or transcardial perfusion. Brains were removed and placed in 4% paraformaldehyde for fixation followed by storage in 30% (wt/vol) sucrose. Brains were sectioned to 40 μ m. Endogenous peroxidase was quenched with 3% (vol/vol) H₂O₂, followed by antigen retrieval in citrate buffer (pH 6.0) at 95 °C. Nonspecific antibody binding was blocked with 3% (vol/vol) normal horse serum. Tissue was probed with TH (Millipore) or alpha-synuclein (BD Transduction Laboratories). The primary antibodies were diluted to 1:1000. Biotinylated, HRP-conjugated secondary antibodies (Jackson ImmunoResearch) were diluted to 1:1000, signal was enhanced with an avidin-biotin complex (Vector Laboratories), and was developed with a 3-3' diaminobenzidine (DAB) reaction for ~45s.

Western blotting. Mice were decapitated and tissue was flash-frozen in liquid nitrogen. The frozen tissue was homogenized in homogenization buffer (HB; 4 mM HEPES, 0.32 M sucrose, pH 7.4) and protease inhibitors (1:1000) using an immersion homogenizer (Tissue Tearor) for approximately 15 seconds. This homogenate was centrifuged at 1150 x g for 5 minutes at 4 °C

and the resultant supernatant was centrifuged at 18,407 x g for 45 minutes at 4 °C. The pellet was resuspended in HB plus protease inhibitors and protein content was determined by BCA assay. Samples (9 µg of protein) were subjected to gel electrophoresis on 4-12% bis-tris gels (NuPAGE) before being transferred onto a polyvinylidene difluoride (PVDF) membrane at 4 °C, blocked with 7.5% nonfat dry milk for one hour at room temperature, and incubated with appropriate primary antibody overnight at 4 °C with gentle agitation (mouse anti-alpha-synuclein was purchased from BD Transduction Laboratories; rabbit anti-TH was purchased from Millipore; polyclonal rabbit anti-mSV2C antibodies were designed by our lab and custom-produced by Covance as described previously (Dunn *et al.*, 2017a); mouse anti-actin was purchased from Sigma). The following day, blots were incubated at room temperature for 1 hour with the appropriate secondary antibody (HRP-conjugated). Signal was amplified using chemiluminescence (Thermo) and visualized using a BioRad UV imager. Densitometry was conducted using Image Lab software (Bio Rad).

Results

Injection of SV2C in A53T-OE mice leads to successful protein overexpression and reduction in alpha-synuclein expression. In order to examine the relationship between SV2C expression and alpha-synuclein pathology, we first sought to determine whether adding SV2C into mice overexpressing alpha-synuclein would slow progression of alpha-synuclein pathogenesis. Mice overexpressing A53T mutant alpha-synuclein (A53T-OE) exhibit dopaminergic neurodegeneration, motor deficits, decreased dopamine release, and aggregated SV2C in the striatum (Dunn *et al.*, 2017b; Lin *et al.*, 2012). We implemented a stereotactic injection protocol to inject A53T-OE mice and their WT littermates with AAV2/9 mCherry or AAV2/9 miniSOG-tagged SV2C into the substantia nigra (AP -3.2 mm, ML -1.2 mm, DV -4.5 mm from surface of the brain). We observed overexpression of SV2C in the A53T-OE mice, as represented by an

increase in SV2C-positive cell bodies in the midbrains of SV2C-injected A53T-OE mice (Figure A.1A). SV2C overexpression was also visible in the striatum, where there was a slight increase in SV2C staining in A53T-OE mice injected with SV2C (Figure A.1B). In order to assess whether increased expression of SV2C altered alpha-synuclein pathology, we measured total alpha-synuclein expression in the midbrain and striatum and observed a substantial decrease in alpha-synuclein expression in A53T-OE mice injected with SV2C in both brain regions (Figure A.2). There is a substantial reduction in alpha-synuclein-positive cell bodies in the midbrain (Figure A.2A) and an overall decrease in alpha-synuclein staining in the striatum (Figure A.2B) of A53T-OE mice injected with SV2C compared to mCherry-injected A53T-OE mice. This decrease in alpha-synuclein staining was also confirmed by western blot (Figure A.3).

Injection of alpha-synuclein in SV2C-KO and WT mice leads to successful protein overexpression and severe dopamine cell loss. We then sought to determine whether adding alpha-synuclein into mice with a genetic deletion of SV2C would exacerbate progression of alpha-synuclein pathogenesis. To this end, we injected SV2C-KO mice and their WT littermates with AAV2/9 mCherry or AAV2/9 human alpha-synuclein into the substantia nigra (AP -3.2 mm, ML -1.2 mm, DV -4.5 mm from surface of the brain). Alpha-synuclein injection resulted in an increase in total alpha-synuclein expression in the midbrain (Figure A.4A). An increasing gradient of alpha-synuclein expression is visible when comparing across genotype and injection condition: SV2C-WT mice injected with mCherry have uniform expression of alpha-synuclein across the midbrain with slightly darker staining in the substantia nigra and cortex; SV2C-KO mice injected with mCherry exhibit darker alpha-synuclein staining in the medial region of the substantia nigra; and SV2C-KO mice injected with alpha-synuclein exhibit dark alpha-synuclein staining across the entire ventral section of the midbrain. This gradient of alpha-synuclein expression across genotype and injection condition is less visible in the striatum, with the mCherry-injected SV2C-KO mice

appearing to express the most alpha-synuclein. While these results indicate a successful overexpression of alpha-synuclein, they further indicate that SV2C-KO mice exhibit enhanced expression of alpha-synuclein at baseline, as both mCherry-injected and alpha-synuclein-injected SV2C-KO mice display increased alpha-synuclein staining (Figure A.4B).

After confirming that we were able to successfully overexpress alpha-synuclein, we sought to determine the effect of this overexpression on the nigrostriatal dopamine toxicity. To this end, we measured TH expression in the midbrain and striatum and observed a decrease in TH expression in SV2C-KO mice (Figure A.5). A decreasing gradient of TH expression is visible when comparing the midbrains of SV2C-WT mice injected with mCherry, SV2C-KO mice injected with mCherry, and SV2C-KO mice injected with alpha-synuclein, with alpha-synuclein-injected SV2C-KO mice expressing the least TH. There is some loss of TH-positive cell bodies in the mCherry-injected SV2C-KO mice, and there is a substantial decrease in TH expression in the alpha-synuclein injected SV2C-KO mice (Figure A.5A). This loss in TH expression is less drastic in the striatum, with the mCherry-injected SV2C-WT mice and the mCherry-injected SV2C-KO mice exhibiting similar amounts of TH staining. However, the alpha-synuclein injected SV2C-KO mice have an essentially complete loss of TH staining in the striatum (Figure A.5B).

We also visualized alpha-synuclein and TH expression via western blot on midbrain and striatal tissue isolated from one SV2C-WT mouse injected with mCherry, one SV2C-KO mouse injected with mCherry, and one SV2C-KO mouse injected with alpha-synuclein. The alpha-synuclein overexpression and TH cell loss observed via immunohistochemistry was also observed by western blot (Figure A.6). Injection of alpha-synuclein into the substantia nigra resulted in an increase in alpha-synuclein expression in the midbrain and striatum of the SV2C-KO mouse. Alpha-synuclein expression in the midbrain of mCherry-injected mice is comparable, while alpha-synuclein expression in the striatum of the SV2C-WT mouse injected with mCherry is greater than

that of the SV2C-KO mouse injected with mCherry and is similar to that of the SV2C-KO mouse injected with alpha-synuclein. Injection of alpha-synuclein led to a decrease in TH expression in the midbrain and striatum of the SV2C-KO mouse. The mCherry-injected SV2C-KO mouse expressed less TH than the SV2C-WT mouse in the striatum, and injection of alpha-synuclein into the SV2C-KO mouse further decreased TH expression in the striatum. As expected, SV2C-KO mice do not express SV2C protein in the midbrain or striatum.

Discussion

Here, we used A53T-OE mice, SV2C-KO mice, and viral vectors to determine the effect of SV2C expression on alpha-synuclein pathogenesis and neurotoxicity. We injected A53T-OE mice and their WT littermates with either AAV2/9 mCherry or AAV2/9 miniSOG-tagged SV2C into the substantia nigra and show successful SV2C overexpression as well as a decrease in alpha-synuclein expression in the midbrain and striatum. We then injected SV2C-KO mice and their WT littermates with AAV2/9 mCherry or AAV2/9 human alpha-synuclein into the substantia nigra and show successful alpha-synuclein overexpression and enhanced dopamine cell loss in the midbrain and striatum. These results indicate that SV2C expression affects dopamine neuron vulnerability and mediates alpha-synuclein pathogenesis.

We first overexpressed SV2C in a system already containing increased expression of alpha-synuclein to determine whether adding SV2C into mice overexpressing alpha-synuclein slows progression of alpha-synuclein pathogenesis. We observed overexpression of SV2C in the A53T-OE mice, as represented by an increase in SV2C-positive cell bodies in the midbrains of SV2C-injected A53T-OE mice. In order to assess whether increased expression of SV2C altered alpha-synuclein induced toxicity, we measured total alpha-synuclein expression in the midbrain and striatum. There was a substantial reduction in alpha-synuclein-positive cell bodies in the midbrain

and an overall decrease in alpha-synuclein staining in the striatum of SV2C-injected A53T-OE mice compared to mCherry-injected A53T-OE mice. As overexpression of SV2C resulted in decreased presence of total alpha-synuclein, these findings support an interaction between SV2C and alpha-synuclein, though the nature of this interaction remains to be determined.

We then overexpressed alpha-synuclein in a system containing a genetic deletion of SV2C to determine whether adding alpha-synuclein in the absence of SV2C would enhance progression of alpha-synuclein pathogenesis. An increasing gradient of alpha-synuclein expression is visible when comparing the midbrains of SV2C-WT mice injected with mCherry, SV2C-KO mice injected with mCherry, and SV2C-KO mice injected with alpha-synuclein, with alpha-synuclein-injected SV2C-KO mice expressing the most alpha-synuclein. This gradient of alpha-synuclein expression across genotype and injection condition is less visible in the striatum, with the mCherry-injected SV2C-KO mice appearing to express the most alpha-synuclein. While these results indicate a successful overexpression of alpha-synuclein, they further indicate that SV2C-KO mice exhibit enhanced expression of alpha-synuclein at baseline, as both mCherry-injected and alpha-synuclein-injected SV2C-KO mice display increased alpha-synuclein staining. This evidence corroborates the previous finding that SV2C-KO mice exhibit an increase alpha-synuclein expression (Dunn *et al.*, 2017b).

After confirming that we were able to achieve successful overexpression of alpha-synuclein, we sought to determine the effect of this overexpression on the nigrostriatal dopamine system. To this end, we measured TH expression in the midbrain and striatum of mice injected with mCherry or alpha-synuclein and observed a decrease in TH expression in SV2C-KO mice regardless of injection condition. A decreasing gradient of TH expression was visible when comparing the midbrains of SV2C-WT mice injected with mCherry, SV2C-KO mice injected with mCherry, and SV2C-KO mice injected with alpha-synuclein, with alpha-synuclein-injected

SV2C-KO mice expressing the least TH. This pattern of TH expression in the midbrain does not align with previous work from our lab showing no difference in the expression of SV2A, SV2B, TH, or DAT in SV2C-KO mice vs. WT littermates (Dunn *et al.*, 2017b). The presence of TH cell loss in the mCherry SV2C-KO mice is unlikely to result from the stereotactic injection itself, as SV2C-KO mice injected with mCherry exhibit a loss in TH expression as compared to SV2C-WT mice injected with mCherry. However, SV2C-KO mice may respond more adversely to stereotactic injection than WT mice. Regardless of this potential for exacerbated stereotactic injection-related toxicity in the midbrains of SV2C-KO mice, TH expression in the striatum of SV2C-WT and SV2C-KO mice injected with mCherry is virtually indistinguishable, with slightly darker TH staining in the lateral region of the striatum of SV2C-KO mice. Furthermore, alpha-synuclein injection in the SV2C-KO mice resulted in severe TH cell loss in the midbrain that correlates to an essentially complete loss of TH staining in the striatum of alpha-synuclein injected SV2C-KO mice. This severely exacerbated loss of TH expression in SV2C-KO mice overexpressing alpha-synuclein supports an interaction between alpha-synuclein and SV2C such that impairment of the alpha-synuclein—SV2C complex results in enhanced cell death.

These data are preliminary, as difficulties in breeding the SV2C-KO mice resulted in small sample sizes for each injection condition. Data collection will continue at Columbia University as the SV2C-KO colony is re-established and breeding ensues. After creation of a stable colony, additional surgeries followed by immunohistochemical and western blot analyses will be performed.

Overall, these findings indicate that there is an interaction between alpha-synuclein and SV2C that mediates dopaminergic toxicity, though the nature of this interaction is still unclear. Both alpha-synuclein and SV2C have a unique relationship with dopamine and dopaminergic neurons. Alpha-synuclein modulates the trafficking of DAT to the synaptic terminal and

influences its activity (Butler *et al.*, 2015; Lee *et al.*, 2001). Dopamine also inhibits the formation of alpha-synuclein fibrils; breaks down existing fibrils (Fischer and Matera 2015; Mor *et al.*, 2017); stabilizes the toxic oligomers of alpha-synuclein; and induces the formation of these toxic oligomers (Fischer and Matera 2015). SV2C expression is enriched in the dopaminergic neurons located in the substantia nigra pars compacta and in the ventral tegmental area, with 70% of dopamine neurons expressing SV2C (Dardou *et al.*, 2011; Dardou *et al.*, 2013; Dunn *et al.*, 2017b; Janz and Sudhof 1999).

The interaction between SV2C and alpha-synuclein may involve formation of a physical protein complex connecting SV2C and alpha-synuclein, or SV2C and alpha-synuclein may both be involved in similar, but non-physically overlapping processes occurring in the presynaptic terminal. We have previously shown that SV2C co-immunoprecipitates with alpha-synuclein, suggesting the presence of a physical protein complex connecting SV2C and alpha-synuclein (Dunn *et al.*, 2017b). The formation of this SV2C—alpha-synuclein complex may serve to stabilize the non-toxic conformation of alpha-synuclein, thus reducing neurotoxicity. Alternately, SV2C and alpha-synuclein may both be involved in similar, but non-physically overlapping processes occurring in the presynaptic terminal. Both alpha-synuclein and SV2s are associated with SNARE complex formation, with mutations in alpha-synuclein leading to alterations in SNARE protein associations (Burre *et al.*, 2010; Garcia-Reitböck *et al.*, 2010) and deletion of SV2A resulting in decreased SNARE complex formation (Xu and Bajjalieh 2001). SV2s also bind to and traffic with synaptotagmin, a SNARE protein present on the vesicular membrane (Nowack *et al.*, 2010; Schivell *et al.*, 2005; Yao *et al.*, 2010). Both proteins are also associated with vesicular trafficking (Diao *et al.*, 2013; Iezzi *et al.*, 2005; Miraglia *et al.*, 2018; Nemani *et al.*, 2010; Wang *et al.*, 2014). Because both SV2C and alpha-synuclein are involved in several overlapping processes in the presynaptic terminal, a “multi-hit” hypothesis may come into play. In this vein,

if both SV2C and alpha-synuclein are involved in the same vesicle fusion and trafficking processes, then the loss of normal SV2C or alpha-synuclein function in the presence of normal alpha-synuclein or SV2C function, respectively, would lead to altered vesicle handling and cytotoxicity. However, the loss of function of both SV2C and alpha-synuclein would lead to enhanced impairment in vesicular handling beyond the loss of function that would be expected based on the loss of two non-interacting proteins, thus resulting in greatly increased neurotoxicity.

Overall, we have shown here that SV2C expression affects alpha-synuclein expression and pathogenesis such that increased SV2C expression decreases alpha-synuclein expression and decreased alpha-synuclein expression in the presence of SV2C deletion results in enhanced dopamine cell death. Though these findings must be repeated and expanded upon with larger sample sizes per injection condition and more research is required to fully elucidate the nature of the relationship between SV2C and alpha-synuclein, this work represents a step toward uncovering the interaction of these two proteins and their dual role in PD development.

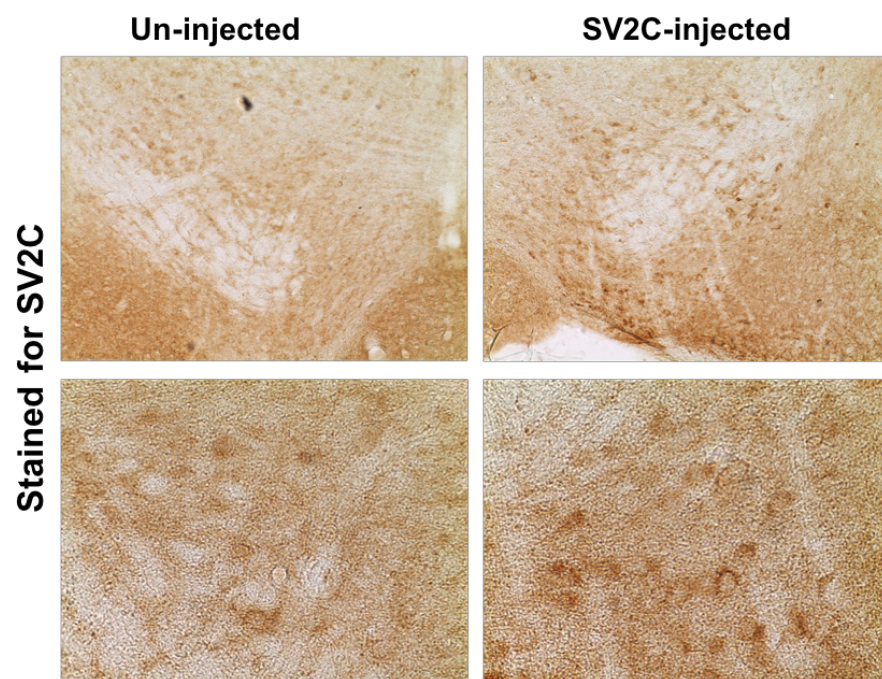
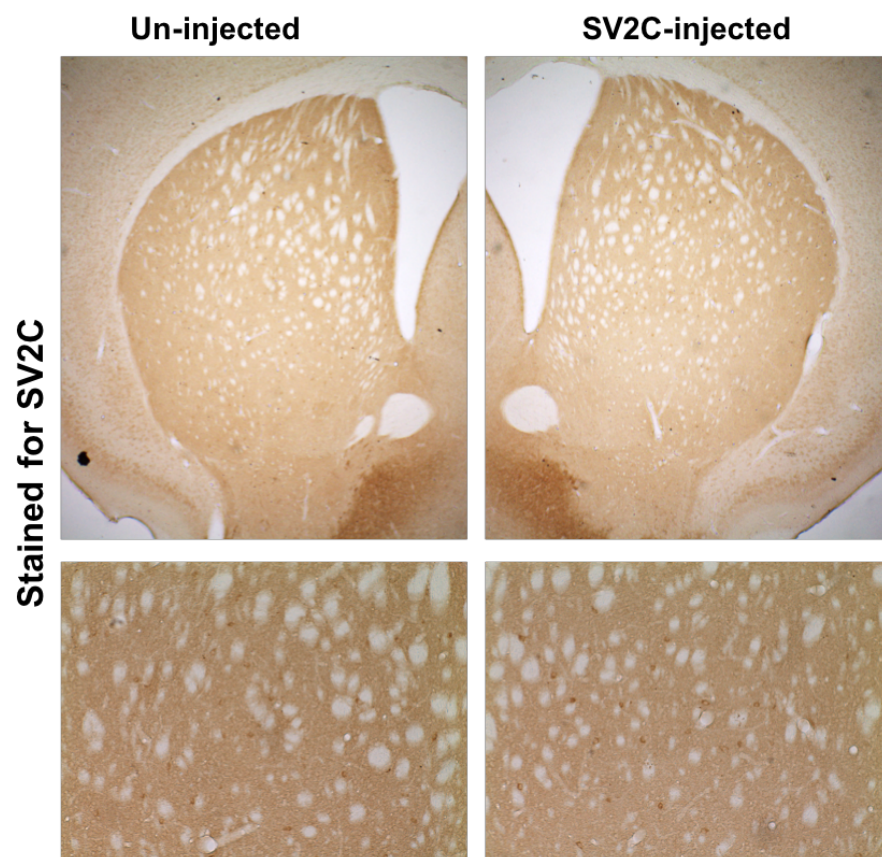
A**B**

Figure A.1. Overexpression of SV2C in A53T-OE mice. AAV2/9 mCherry or AAV2/9 miniSOG-SV2C was injected into the substantia nigra (AP -3.2 mm, ML -1.2 mm, DV -4.5 mm from surface of the brain) of A53T-OE mice. A) Representative images from midbrain of mCherry injected and SV2C injected mice, stained for SV2C. Top: 10x, bottom: 40x. B) Representative images from striatum of mCherry injected and SV2C injected mice, stained for SV2C. Top: 2.5x, bottom: 10x. Bottom panels are high magnification insets from top panels.

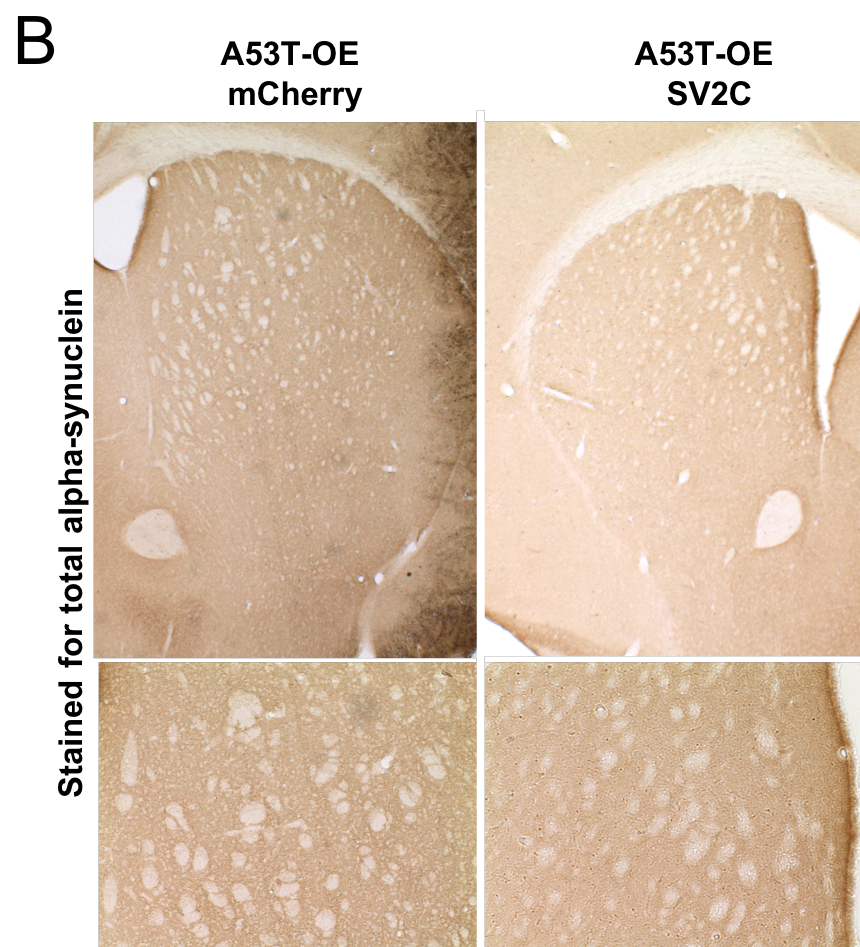
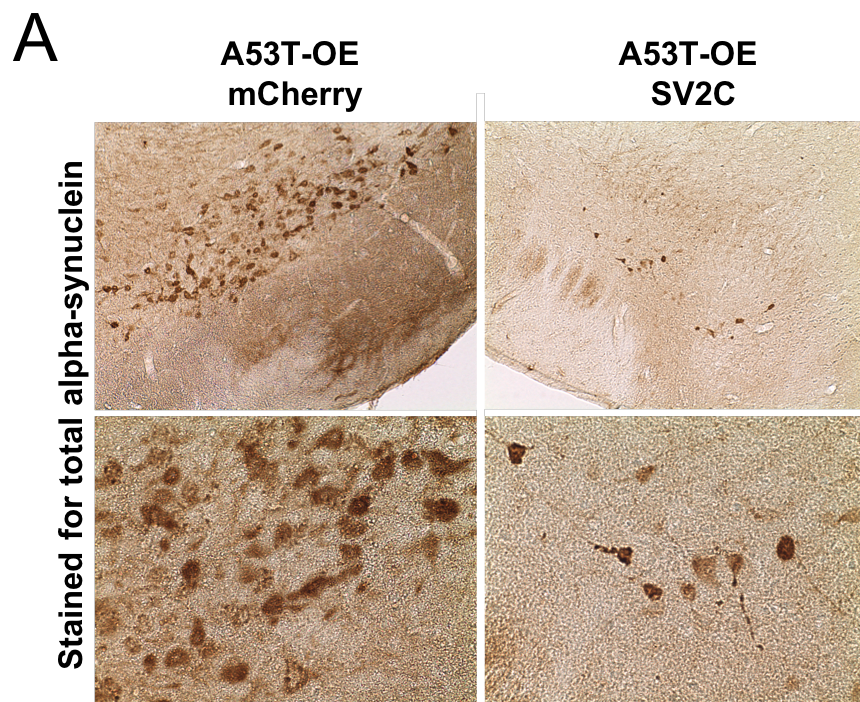


Figure A.2. Overexpression of SV2C in A53T-OE mice reduces expression of total alpha-synuclein. AAV2/9 mCherry or AAV2/9 miniSOG-SV2C was injected into the substantia nigra (AP -3.2 mm, ML -1.2 mm, DV -4.5 mm from surface of the brain) of A53T-OE mice and their WT littermates. A) Representative images from midbrain of mCherry injected A53T-OE and SV2C injected A53T-OE mice, stained for alpha-synuclein. Top: 10x, bottom: 40x. B) Representative images from striatum of mCherry injected A53T-OE and SV2C injected A53T-OE mice, stained for alpha-synuclein. Top: 2.5x, bottom: 10x. Bottom panels are high magnification insets from top panels.

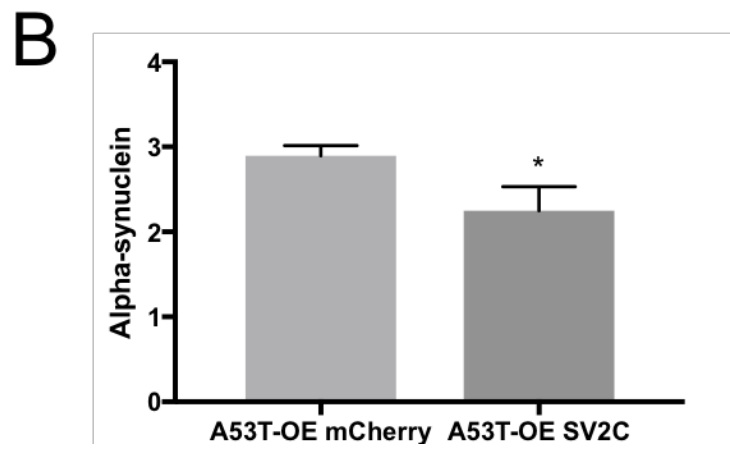
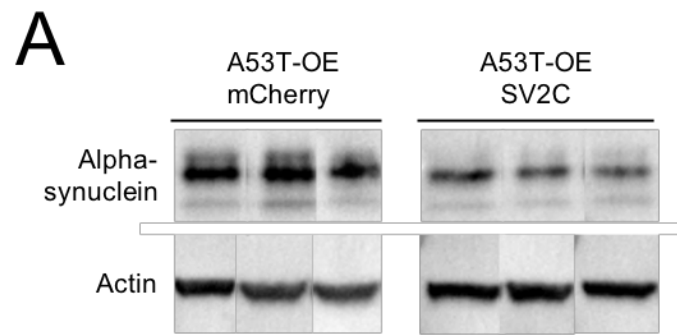


Figure A.3. SV2C overexpression in A53T-OE mice decreases expression of total alpha-synuclein. A) Representative immunoblot probing for expression of total alpha-synuclein and actin in whole half brain of A53T-OE mice injected with mCherry or SV2C. B) SV2C-injected A53T-OE mice have a significant reduction in total alpha-synuclein expression ($p = 0.0401$) as compared to mCherry injected A53T-OE mice. Graph represents mean protein expression with standard error of the mean as measured by semi-quantitative immunoblot. Significance was assessed with unpaired one-tailed t-test, $\alpha = 0.05$.

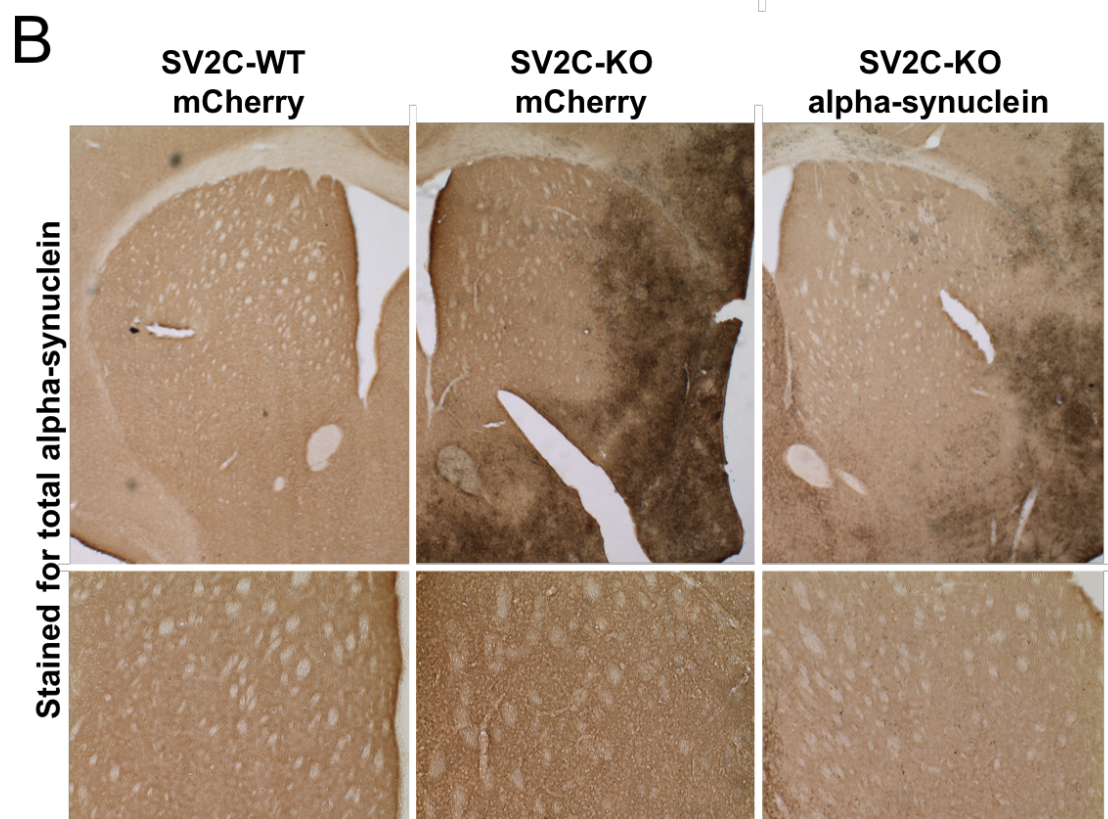
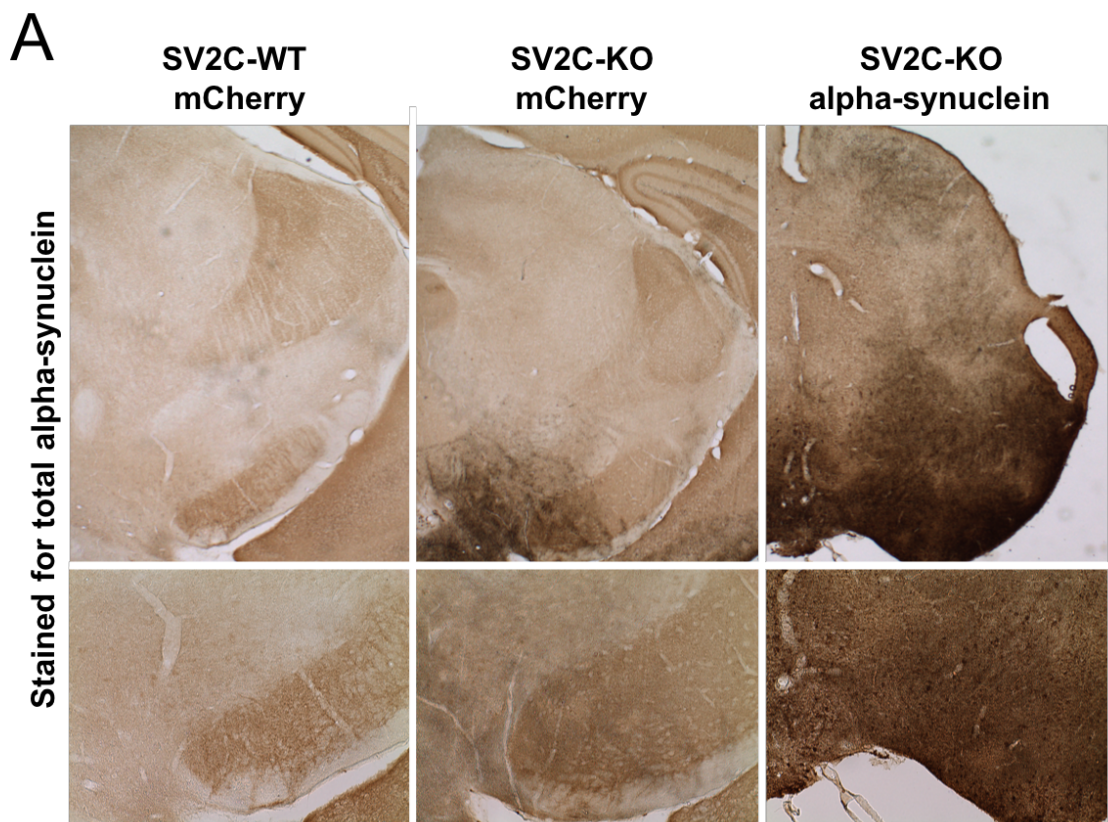


Figure A.4. Overexpression of alpha-synuclein in SV2C-KO and SV2C-WT mice. AAV2/9 mCherry or AAV2/9 alpha-synuclein was injected into the substantia nigra (AP -3.2 mm, ML -1.2 mm, DV -4.5 mm from surface of the brain) of SV2C-KO mice and their WT littermates. A) Images from midbrain of mCherry injected WT, mCherry injected SV2C-KO, and alpha-synuclein injected SV2C-KO mice, stained for alpha-synuclein. Top: 2.5x, bottom: 10x. B) Images from striatum of mCherry injected WT, mCherry injected SV2C-KO, and alpha-synuclein injected SV2C-KO mice, stained for alpha-synuclein. Top: 2.5x, bottom: 10x. Bottom panels are high magnification insets from top panels.

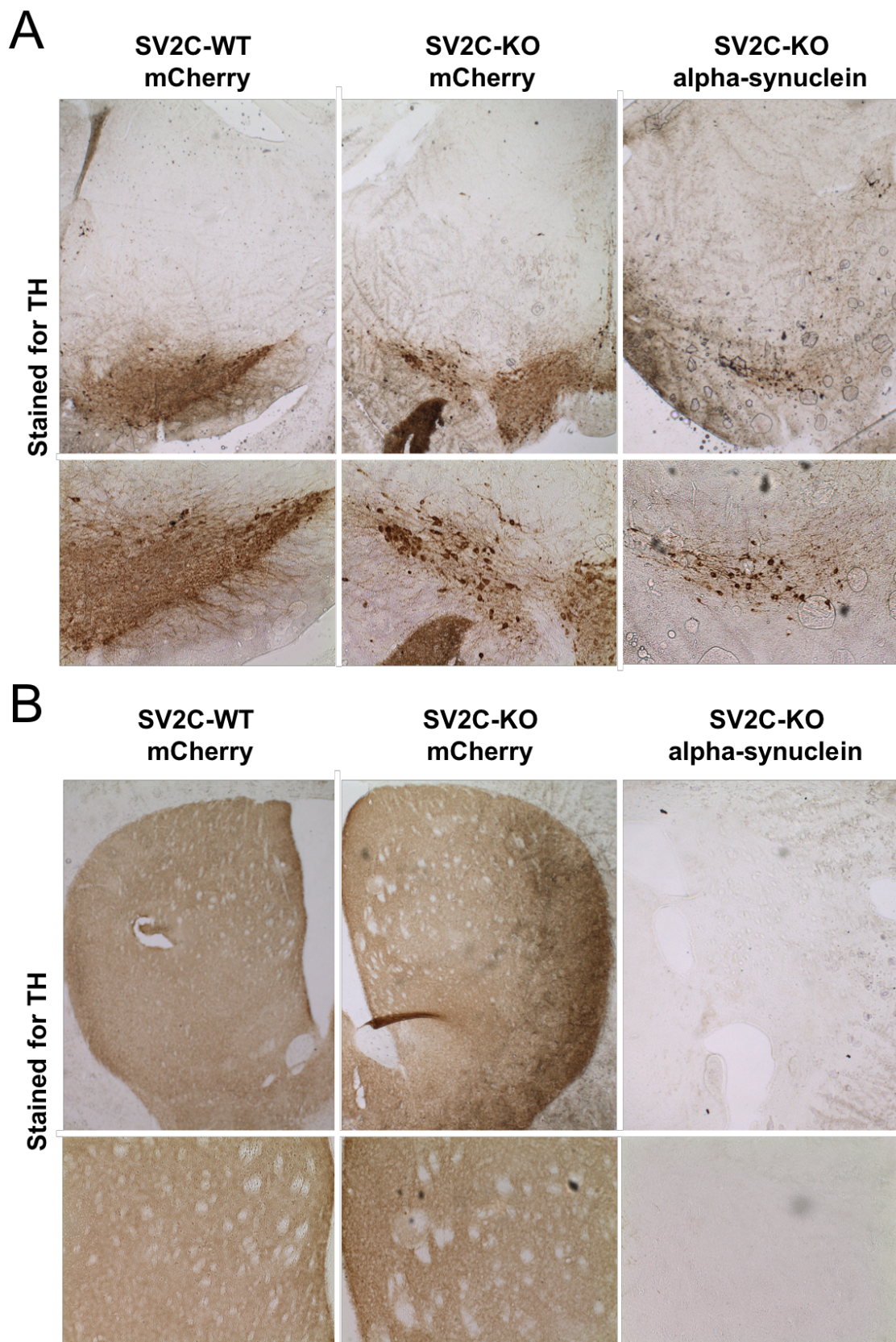


Figure A.5. Overexpression of alpha-synuclein causes reduction in TH expression in SV2C-KO and SV2C-WT mice. AAV2/9 mCherry or AAV2/9 alpha-synuclein was injected into the substantia nigra (AP -3.2 mm, ML -1.2 mm, DV -4.5 mm from surface of the brain) of SV2C-KO mice and their WT littermates. A) Images from midbrain of mCherry injected WT, mCherry injected SV2C-KO, and alpha-synuclein injected SV2C-KO mice, stained for tyrosine hydroxylase (TH). Top: 2.5x, bottom: 10x. B) Images from striatum of mCherry injected WT, mCherry injected SV2C-KO, and alpha-synuclein injected SV2C-KO mice, stained for TH. Top: 2.5x, bottom: 10x. Bottom panels are high magnification insets from top panels.

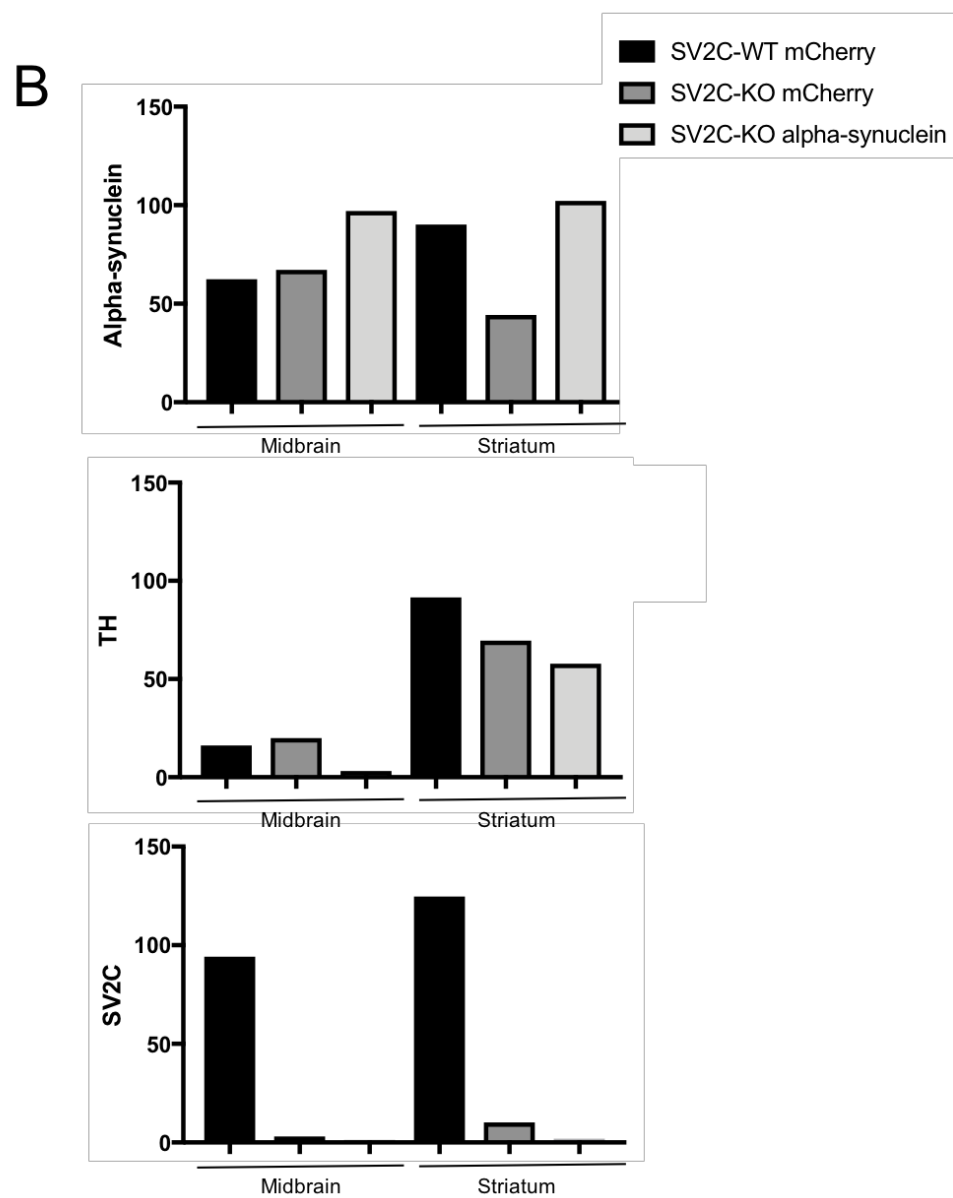
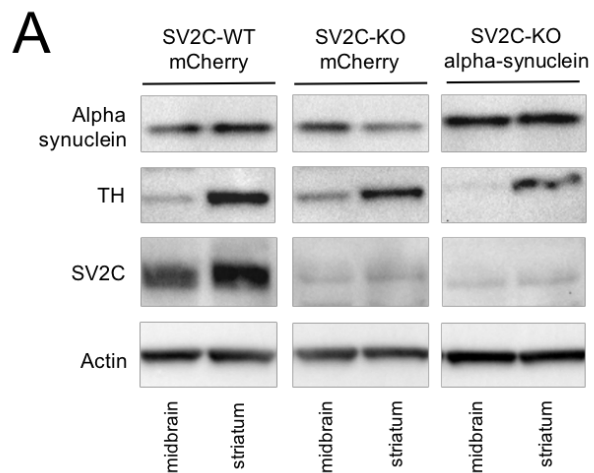


Figure A.6. Quantification of protein expression resulting from overexpression of alpha-synuclein. AAV2/9 mCherry or AAV2/9 alpha-synuclein was injected into the substantia nigra (AP -3.2 mm, ML -1.2 mm, DV -4.5 mm from surface of the brain) of SV2C-KO mice and their WT littermates (n=1 per group). A) Immunoblot probing for expression of alpha-synuclein, tyrosine hydroxylase (TH), SV2C, and actin in isolated midbrain and striatum of a mCherry injected WT, a mCherry injected SV2C-KO, and an alpha-synuclein injected SV2C-KO mouse. B) Injection of alpha-synuclein into the substantia nigra resulted in an increase in alpha-synuclein expression in the midbrain and striatum of the SV2C-KO mouse (light gray bar). Injection of alpha-synuclein led to a decrease in TH expression in the midbrain and striatum of the SV2C-KO mouse (light gray bar). SV2C-KO mice do not express SV2C protein in the midbrain or striatum. Graphs represent protein expression as measured by semi-quantitative immunoblot. As there is only one mouse represented per group, no statistical analyses were performed.